





















CCI Land Cover

ALGORITHM THEORETICAL BASIS DOCUMENT

PRE-PROCESSING

YEAR 2 - 1.0

DOCUMENT REF: CCI-LC-ATBDv2

DELIVERABLE REF: D2.2

VERSION: 1.0

CREATION DATE: 2014-07-31

LAST MODIFIED: 2016-05-02

This page is intentionally blank.

Document Signature Table

	NAME	FUNCTION	COMPANY	SIGNATURE	DATE
PREPARED	Kirches G.		BC		
PREPARED	Militzer J.		BC		
PREPARED	Boettcher M.		BC		
PREPARED	Brockmann C.		BC		
VERIFIED	Defourny P.	Science leader	UCL		
APPROVED					

Document Change Record

VERSION	DATE	DESCRIPTION	APPROVED
0.1	2015-10-22	First draft version, based on Year 1 document (version 1.2)	
1.0	2016-05-02	First version of Year 2, to be submitted to ESA before AR2	

Document Change Record (from Year 1 to Year 2)

RID	SECTION	COMMENTS
-	Acronyms List	Links are waived due to their maintenance costs.
-	Reference Document list	Links are waived due to their maintenance costs.
-	2.1	Update related the processing chain of Phase II
-	2.2	Update related the products of Phase II
-	3	New section regarding the quality control of the input products
-	4.1	Update related the products of Phase II
-	4.2	Update related the products of Phase II
-	4.3	Update related the PROBA-V products
-	4.4	Update related the products of Phase II
-	4.5	Update related the products of Phase II particularly with regard to the AVHRR products
-	4.6	Update related the products of Phase II

Document Diffusion List

ORGANISATION	NAME	QUANTITY
ESA	O. Arino, F. Ramoino	

© UCL-Geomatics 2016
This document is the property of the LAND_COVER_CCI partnership, no part of it shall be reproduced or transmitted without the express prior written authorization of UCL-Geomatics (Belgium).

SYMBOLS AND ACRONYMS

AATSR : Advance Along Track Scanning Radiometer

ATSR : Along Track Scanning Radiometer

ACRI-ST : ACRI subsidiaries

A/D converter : Analog-to-Digital-Converter

AMF : Air Mass Factor

AMORGOS : Accurate MERIS Ortho Rectified Geo-location Operational Software

ANN : Artificial Neural Network

AOD : Aerosol Optical Depth

AOT : Aerosol Optical Thickness

ASAR : Advanced Synthetic Aperture Radar

ATBD : Algorithm Theoretical Basis Document

AVHRR : Advanced Very High Resolution Radiometer

BC : Brockmann Consult GmbH

BDC : Bi-directional compositing algorithm

BEAM : Basic ENVISAT Tool for AATSR & MERIS

BELMANIP : Benchmark Land Multi-site Analysis and Inter-comparison of Products

BISE : Best Index Slope Extraction

BOA : Bottom-Of-Atmosphere

BRDF : Bidirectional Reflectance Distribution Function

BRF : Bidirectional Reflectance Factor

C3AT : Channel 3b Reflectance Test over land

CBH : Cloud Base Height

CCD : Charge-Coupled Device

CCI : Climate Change Initiative

CCI-LC : CCI Land Cover

CESBIO : Center for the Study of the Biosphere from Space

CFI : Customer Furnished Item

CEOS : Committee on Earth Observation Satellites

CLAVR : Clouds from AVHRR

CMC : Climate Modelling Community

CoastColour : ESA DUE project

© UCL-Geomatics 2016
This document is the property of the LAND_COVER_CCI partnership, no part of it shall be reproduced or transmitted without the express prior written authorization of UCL-Geomatics (Belgium).

CTH : Cloud Top Height

CWV : Water Vapour Column Content

CYC : Hagolle Algorithm

DARD : Data Access Requirements Document

DBT2 : Database for Task 2

DEM : Digital Elevation Model

DJF : Design Justification File

DOM : Dark Object Method

DOY : Day of year

DPM : Detailed Processing Model

ECV : Essential Climate Variable

EEA : European Environment Agency

ELEV : Elevation

ENVISAT : Environnement Satellite

EO : Earth Observation

ERA Interim : Global atmospheric reanalysis from 1979

ERS : European Remote Sensing Satellite

ESA : European Space Agency

ECV : Essential Climate Variable

EUMETSAT : European Meteorological Satellites Agency

f_{APAR} : Fraction of Absorbed Photosynthetically Active Radiation

FMFT : Four Minus Five Test

$FMFT_{adap}$: Four Minus Five Test adapted

FOV : Field Of View

FR : Full Resolution

FRS : Full Resolution Swath

FSG : Full Swath Geo-corrected

GCOS : Global Climate Observing System

GlobAlbedo : ESA DUE project

GlobCover : ESA DUE project

GMES : Global Monitoring for Environment and Security

GOME : Global Ozone Monitoring Experiment

HDF : Hierarchical Data Format

HOT : Haze Optimized Transform

© UCL-Geomatics 2016
This document is the property of the LAND_COVER_CCI partnership, no part of it shall be reproduced or transmitted without the express prior written authorization of UCL-Geomatics (Belgium).

HSV	: Hue Saturation Value colour space
IdePix	: Pixel Identification
IDEAS+	: Instrument Data quality Evaluation and Analysis Service Plus
IKONOS	: Commercial Earth Observation Satellite
IODD	: Input and Output Data Description
KO	: Kick-Off
L0, L1, L2, L3	: Level 0, Level 1, Level 2, Level 3
LAI	: Leaf Area Index
LARS	: Land Aerosol Remote Sensing
LC	: Land Cover
LC-condition	: Land Cover condition
LC-maps	: Land Cover maps
LUT	: Look-Up Table
MAX	: Maximum
MC	: Mean Compositing
MDSI	: MERIS Differential Snow Index
MERIS	: Medium Resolution Imaging Spectrometer
MIN	: Minimum
MIR	: Mid-wavelength InfraRed
LUT	: Look-Up Table
MODIS	: Moderate Resolution Imaging Spectroradiometer
MOMO	: Matrix-Operator-Model
MSI	: Multi-Spectral Imager
NaN	: Not a Number
n.a.	: not applicable
NDII	: Normalized Difference Ice Index
NDVI	: Normalized Difference Vegetation Index
NDSI	: Normalized Difference Snow Index
NIR	: Near InfraRed
NN	: Neuronal Net
NOAA	: National Oceanic and Atmospheric Administration
NRT	: Near Real Time
OLCI	: Ocean and Land Colour Instrument
OZO	: Ozone Column Content

© UCL-Geomatics 2016
This document is the property of the LAND_COVER_CCI partnership, no part of it shall be reproduced or transmitted without the express prior written authorization of UCL-Geomatics (Belgium).

PCA	: Principal Component Analysis
PG	: Projects Guidelines
PROBA	: Project for On-Board Autonomy
PROBA-V	: PROBA Vegetation
PROSPECT	: Model of Leaf Optical Properties Spectra
PSD	: Product Specification Document
PUG	: Product User Guide
PVASR	: Product Validation and Algorithm Selection Report
PVP	: Product Validation Plan
PVIR	: Product Validation and Intercomparison Report
RAA	: Relative Azimuth Angle
RD	: Reference Dataset
RGB	: Red Green Blue colour space
RGCT	: Reflectance Gross Contrast Test
RMS	: Root Mean Square
RR	: Reduced Resolution
RRCT	: Reflectance Ratio Contrast Test
RRG	: AMORGOS- Processed MERIS RR
RTC	: Radiative Transfer Code
RTE	: Radiative Transfer Equation
S-2	: GMES SENTINEL-2
S-3	: GMES SENTINEL-3
SAIL	: Scattering by Arbitrary Inclined Leaves (SAIL) 1D radiative transfer model
SAR	: Synthetic Aperture Radar
SCIAMACHY	: Scanning Imaging Spectrometer for Atmospheric CHartographY
SDR	: Surface Directional Reflectance
SLSTR	: Sea and Land Surface Temperature Radiometer
SMAC	: Simplified Method for Atmospheric Correction
SoW	: Statement of Work
SPOT	: Satellite Pour l'Observation de la Terre
SPOT-VGT	: SPOT-VEGETATION
SPOT VGT P	: SPOT VGT P Product (physical product)
SPOT VGT S1	: SPOT VGT S1 Product (daily surface product)
SR	: Surface Reflectance

© UCL-Geomatics 2016
This document is the property of the LAND_COVER_CCI partnership, no part of it shall be reproduced or transmitted without the express prior written authorization of UCL-Geomatics (Belgium).

SRTM : Shuttle Radar Topography Mission

SRD : System Requirements Document

SSD : System Specifications Document

SVR : System Verification Report

SWBD : SRTM Water Body Data

SWIR : Short-Wave InfraRed

SZA : Sun Zenith Angle

TGCT : Thermal Gross Contrast Test

TIR : Thermal InfraRed

TMFT : Three Minus Four Test

TN : Technical Note

TOA : Top Of Atmosphere

TP : Technical Proposal

UCL : Université catholique de Louvain

URD : Users Requirement Document

USGS : United States Geological Survey

UV : Ultra Violet

VIIRS : Visible Infrared Imaging Radiometer Suite

VITO : Vison on Technology (Flemish Institute for Technological Research NV)

VEU : Video Electronic Unit

VGT : SPOT Vegetation

VNIR : Visible Near InfraRed

VZA : View Zenith Angle

WB : Water Bodies

WGS84 : World Geodetic System 84

© UCL-Geomatics 2016
This document is the property of the LAND_COVER_CCI partnership, no part of it shall be reproduced or transmitted without the express prior written authorization of UCL-Geomatics (Belgium).

REFERENCE DOCUMENTS

Applicable documents

ID	TITLE	ISSUE	DATE
[Ph1_SoWv1.4, 2009]	ESA Climate Change Initiative Phase I - Scientific User Consultation and Detailed Specification Statement of Work	1.4	09.11.2009
[Ph2_SoWv1.2, 2013]	Statement of Work for ESA Climate Change Initiative Phase II - CCI-PRGM-EOPS-SW-12-0012	1.2	07.06.2013
[Ph1_PGv1.0, 2013]	ESA Climate Change Initiative – Projects guidelines (EOP-DTEX-EOPS-SW-10-0002)	1.0	05.11.2010
[Ph1_TPv1.0, 2011]	ESA Climate Change Initiative Phase I - Land Cover ECV Technical proposal	1.0	05.03.2011
[Ph2_TPv1.0, 2014]	ESA Climate Change Initiative Phase II - Land Cover ECV Technical baseline for the project (update of the technical proposal with clarification and negotiation items)	1.0	13.03.2014
[Ph1_URDv2.2, 2011]	CCI-LC URD Phase I. Land Cover Climate Change Initiative - User Requirements Document	2.2	23.02.2011
[Ph2_URDv1.0, 2014]	CCI-LC URD Phase II. Land Cover Climate Change Initiative - User Requirements Document	1.0	13.07.2015

Reference documents

ID	TITLE	ISSUE	DATE
[Ackerman et al., 2006]	Ackerman, S., Strabala, K., Menzel, P., Frey, R., Moeller, C., Gumley, L., Baum, B., Wetzel Seemann, S. and Zhang, H., 2006, “Discriminating clear sky from cloud with MODIS algorithm theoretical basis document (MOD35)”.	-	2006
[Aoki et al., 2007]	Aoki, T., Hori, M., Motoyoshi, H., et al., 2007, “ADEOS-II/GLI snow/ice products — Part II: Validation results using GLI and MODIS data”. Remote Sensing Environ., 111, 274-290	-	2007
[Arino et al., 2008]	Arino O., P. Bicheron, F. Achard, J. Latham, R. Witt and J.-L. Weber. 2008, “GlobCover the most detailed portrait of Earth”, ESA Bulletin, 136, pp 25-31, November 2008.	-	2008

© UCL-Geomatics 2016
This document is the property of the LAND_COVER_CCI partnership, no part of it shall be reproduced or transmitted without the express prior written authorization of UCL-Geomatics (Belgium).

ID	TITLE	ISSUE	DATE
[Berthelot et al., 1997]	Berthelot, B., Adam, S., Kergoat, L., Cabot, F., Dedieu, G. and Maisongrande, P., 1997, "A global dataset of surface reflectances and vegetation indices derived from AVHRR/GVI time series for 1989 1990: The LAnd SUrface Reflectances (LASUR) data". In Proc. Commun. 7th Int. Symp. Physical Measurements and Signatures in Remote Sens. Courchevel, France, Apr. 7 –11, 1997.	-	1997
[Birks et al., 2007]	Birks et al., 2007, "Improvements to the AATSR IPF relating to Land Surface Temperature Retrieval and Cloud Clearing over Land", Rutherford Appleton Laboratory	-	2007
[Bourg and Etanchaud, 2007]	Bourg, L., and F. Etanchaud, 2007, The AMORGOS MERIS CFI (Accurate MERIS Ortho-Rectified Geo-location Operational Software) Software User Manual & Interface Control Document, PO-ID-ACR-GS-0003	3.0A	15/02/2007
[Bourg et al., 2011]	Bourg et al., 2011 The AMORGOS MERIS CFI (Accurate MERIS Ortho-Rectified Geo-location Operational Software) RR Processing – Validation report (PO-RP-ACR-GS-0014; L. Bourg; ACRI-ST)	1.0	15/07/2011
[Bourg et al., 2011b]	Bourg et al., 2011 MERIS 3rd data reprocessing Software and ADF updates, A879.NT.008.ACRI-ST , ACRI-ST	1.0	27/06/2011
[Bouvet and Ramoino, 2010]	Bouvet M., Ramoino F., 2010, Equalization of MERIS L1b products from the 2nd reprocessing, ESA TN TEC-EEP/2009.521/MB (available on demand at mbouvet@esa.int).	-	2010
[Brenguier et al., 2000]	Brenguier, J.-L., Pawlowska, H., Schüller, L., Preusker, R., Fischer, J. and Fouquart, Y., 2000, "Radiative properties of boundary layer clouds: droplet effective radius versus droplet concentration". J. Atmos. Sci., 57, 803-821	-	2000
[Bréon et al., 2002]	Bréon, F.M., Maignan, F., Leroy M. and Grant, I., 2002, "Analysis of hot spot directional signatures measured from space", Journal of Geophysical Research, 107, D16, 4282, 1-1 -1-15	-	2002
[Brockmann et al., 2008]	Brockmann et al., 2008, "Cloud Screening Algorithms". Proceedings in MERIS - AATSR Workshop, 2008. ESRIN, Frascati, Italy	-	2008
[Brockmann et al., 2015]	Brockmann et al., 2015, "SENTINEL 3 – LAND-WATER MASK Technical Note v1.2, IDEAS+ internal document	1.2	2015
[Cervino et al., 2000]	Cervino et al., 2000, "Cloud fraction within GOME footprint using a refined cloud clearing algorithm", Adv. SpaceRes, 25, 5, pp. 993-996	-	2000
[Colapicchioni et al., 2004]	Colapicchioni et al., 2004, "Information Mining in Remote Sensing Image - The KIM, KES and KIMV projects", ESA ESRIN Publication	-	2004

© UCL-Geomatics 2016
This document is the property of the LAND_COVER_CCI partnership, no part of it shall be reproduced or transmitted without the express prior written authorization of UCL-Geomatics (Belgium).

ID	TITLE	ISSUE	DATE
[Crist and Cicone, 1984a]	Crist, E. P. and R. C. Cicone 1984, Application of the Tasseled Cap concept to simulated Thematic Mapper data, Photogrammetric Eng Remote Sens Vol. 50(3), 343-352.	-	1984
[Crist and Cicone, 1984b]	Crist, E.P. and R. C. Cicone 1984, A physically-based transformation of Thematic Mapper data -- the TM Tasseled Cap, IEEE Trans Geoscience Remote Sens Vol. GE-22, 256-263.	-	1984
[Crist and Kauth, 1986]	Crist, E.P. and R.J. Kauth. 1986. The tasseled Cap De-Mystified. Photogrammetric Engineering and Remote Sensing 52:81-86.	-	1986
[Dierckx et al., 2015]	Dierckx, W., Swinnen, E., & Kempeneers, P. , 2015, Validation of spectral continuity between PROBA-V and SPOT-VEGETATION global daily datasets. ISPRS - International Archives of the Photogrammetry, Remote Sensing and Spatial Information Sciences, XL-7/W3(May), 1155–1162.	-	2015
[Doerffer & Schiller, 2008]	Doerffer & Schiller, 2008 R. Doerffer & H. Schiller, Algorithm Theoretical Basis Document (ATBD) - MERIS Regional Coastal and Lake Case 2 Water Project Atmospheric Correction ATBD Version 1.0, 18. May 2008, GKSS Research Centre Geesthacht, Institute for Coastal Research - GKSS-KOF-MERIS-ATBD01	-	2008
[Duchemin and Maisongrande, 2002]	Duchemin B. and Maisongrande P., 2002, “Normalisation of directional effects in 10-day global syntheses derived from VEGETATION/SPOT : I. Investigation of concepts based on simulation”, Remote Sensing of Environment 81: 90-100	-	2002
[Duchemin et al., 2002]	Duchemin et al., 2002, “Normalisation of directional effects in 10-day global syntheses derived from VEGETATION/SPOT: II. Validation of an operational method on actual data sets”, Remote Sensing of Environment 81:101-113	-	2002
[Eumetsat, 2006]	Eumetsat, Final Report for the Study on Visual Scenes Analysis of AVHRR Data.	2.0	01/2006
[Fell and Fischer, 2001]	Fell F., and J. Fischer, 2001, “Numerical simulation of the light field in the atmosphereocean system using the matrix-operator method”, Journal of Quantitative Spectroscopy & Radiative Transfer, 69, 351-388	-	2001
[Fischer et al., 2000]	Fischer, J. et al., 2000, “MERIS ESL Cloud Top Pressure ATBD” – Algorithm Theoretical Basis Document PO-TN-MEL-GS-0005, ESA	2.03	2000
[Fischer et al., 2000b]	Fischer, J. et al., 2000, “MERIS ESL Cloud Albedo and Cloud Optical Thickness ATBD” - Algorithm Theoretical Basis Document PO-TN-MEL-GS-0005, ESA	2.01	2000
[Fischer and Grassl, 1984]	Fischer J., and H. Grassl, 1984, “Radiative transfer in an atmosphere-ocean system: an azimuthally dependent matrix-operator approach”, Applied Optics, 23, 1032-1039	-	1984

© UCL-Geomatics 2016
This document is the property of the LAND_COVER_CCI partnership, no part of it shall be reproduced or transmitted without the express prior written authorization of UCL-Geomatics (Belgium).

ID	TITLE	ISSUE	DATE
[Garant and Weinman, 1986]	Garant L., and Weinman J. A., 1986, “A structural stochastic model for the analysis and synthesis of cloud images”. J. Clim. Appl. Meteorol. 25, 1052-1068	-	1986
[Geiger et al., 2003]	Geiger et al., 2003, Land Surface Albedo from Meteosat Second Generation (MSG) Observations, Geoscience and Remote Sensing Symposium, IGARSS '03. Proceedings. 2003 IEEE International., volume 4, pp.: 2617 – 2619	-	2003
[GlobAlbedo_ATBDv4.12, 2013]	GlobAlbedo ATBDv4.12, 2013 GlobAlbedo Consortium, GlobAlbedo Algorithm Theoretical Basis Document Version 4.12	v4.12	07.07.2013
[GlobAlbedo_ATBD/BBDRv3.0, 2011]	GlobAlbedo Project: GlobAlbedo_BBDR_ATBD	3.0	2011
[GlobAlbedo_ATBD/BBDRv1.0, 2010]	GlobAlbedo Project: GlobAlbedo_BBDR_ATBD	1.0	2010
[GlobAlbedo_ATBD/CLv1.0, 2013]	GlobAlbedo project - Preusker, R., Hühnerbein, A., Fischer, J., 2006, “MERIS Global Land Surface Albedo Maps”, ATBD Cloud Detection.	v1.0	2006
[GlobCover_TSDv4.0, 2008]	GlobCover 2005 project: Technical Specification Document, End-User meeting 3	4.0	27/11/2008
[GlobCover_DJFv3.8, 2008]	GlobCover 2005 project, Design Justification File, I3.8	3.8	11/12/2008
[Goodman et al., 1988]	Goodman et al., 1988, “Cloud Detection and Analysis A Review of Recent Progress”, Atmospheric Research, 21, 203-228	-	1988
[Gomez-Chova et al., 2009]	Gomez-Chova et al., 2009, “Cloud screening with combined MERIS and AATSR images”, Geoscience and Remote Sensing Symposium, IEEE International., IGARSS 2009, 4, pp.: IV-761 - IV-764	-	2009
[Gomez-Chova et al., 2007]	Gomez-Chova et al., 2007, “Cloud-Screening Algorithm for ENVISAT MERIS Multispectral Images”, IEEE Transactions on Geoscience and remote sensing, 45, 12	-	2007
[Hagolle et al., 2004]	Hagolle et al. 2004, “Quality assessment and improvement of temporally composited products of remotely sensed imagery by combination of VEGETATION 1 and 2”, Rem. Sen. Env., 94, 172-186	-	2004
[Hauser et al., 2005]	Hauser, A., Oesch, D., Foppa, N., and Wunderle, S., 2005, NOAA AVHRR derived aerosol optical depth over land, J. Geophys. Res., 110, D08204, doi:10.1029/2004JD005439, 2005	-	2005

© UCL-Geomatics 2016
This document is the property of the LAND_COVER_CCI partnership, no part of it shall be reproduced or transmitted without the express prior written authorization of UCL-Geomatics (Belgium).

ID	TITLE	ISSUE	DATE
[Heidinger, 2004]	Heidinger, Andrew,2004, CLAVR-x Cloud Mask - Algorithm Theoretical Basis Document v0.1, NOAA/NESDIS/Office of Research and Applications Washington, D.C,	v0.1	2004
[Hori et al., 2007]	Hori, M., Aoki, T., Stamnes, K., Li, W., 2007, ADEOS-II/GLI snow/ice products — Part III: Retrieved results, Remote Sensing of Environment, 111, 291-336	-	2007
[Hu et al., 1999]	Hu, B., Lucht, W., and Strahler, A. H., 1999, "The interrrelationship of atmospheric correction of reflectances and surface BRDF retrieval: a sensitivity study". IEEE Transactions on Geoscience and Remote Sensing, 37:724–738	-	1999
[Hünerbein et. al., 2010]	Hünerbein et. al., 2010 Hünerbein, A., Fischer, J. and Lorenz, P., A comparison of solar radiative flux above clouds from MODIS with BALTIMOS regional climate model simulations, Theoretical and Applied Climatology, February 2010,pp 1-7, DOI 10.1007/s00704-010-0253-3	-	2010
[Iqbal., 1983]	Iqbal., M., 1983: An Introduction To Solar Radiation. Academic Press.	-	1983
[Jacquemoud et al., 2009]	Jacquemoud, S., Verhoef, W., Baret, F., Bacour, C., Zarco-Tejada, P.J., Asner, G.P., François, C. and Ustin, S.L., 2009, "PROSPECT + SAIL models: a review of use for vegetation characterization", Remote Sensing of Environment, 113, S56-S66.	-	2009
[Kaufman, 1989]	Kaufman, Y. J., 1989, "The atmospheric effect on remote sensing and its correction". In Asrar, G., editor, Theory and Applications of optical Remote Sensing, pages 336–428. Wiley and Sons, New York.	-	1989
[Kauth and Thomas, 1976]	Kauth, R. J. and G. S. Thomas, 1976 The Tasseled Cap -- a graphic description of the spectral-temporal development of agricultural crops as seen by Landsat, Proc Symp Machine Processing of Remotely Sensed Data, Purdue University, West Lafayette, Indiana 21 June -- 1 July 1976, 4B41-4B51.	-	1976
[Kidell, 1998]	Kidwell Katherine B., 1998, NOAA POLAR ORBITER DATA USER'S GUIDE (TIROS-N, NOAA-6, NOAA-7, NOAA-8, NOAA-9, NOAA-10, NOAA-11, NOAA-12, NOAA-13 AND NOAA-14) - NOVEMBER 1998 REVISION,	-	1998
[Kokhanovsky et al., 2008]	Kokhanovsky et al., 2008, "The determination of the cloud fraction in the fraction in the sciamachy pixels using MERIS". Proceedings in the MERIS - AATSR Workshop, 2008. ESRIN, Frascati, Italy	-	2008
[Lavanant et al., 2005]	Lavanant et al., 2005, "A global Cloud detection scheme for high spectral resolution instrument", ITSC14 Conference presentation	-	2005

© UCL-Geomatics 2016
This document is the property of the LAND_COVER_CCI partnership, no part of it shall be reproduced or transmitted without the express prior written authorization of UCL-Geomatics (Belgium).

ID	TITLE	ISSUE	DATE
[Leckner, 1978]	Leckner B., The spectral distribution of solar radiation at the earth's surface - elements of a model. Sol Energy 20(2), 143-150 (1978)	-	1978
[Liou, 1992]	Liou, K.N., 1992, “Radiation and Cloud Processes in the Atmosphere”. Oxford University Press, Oxford, 487pp.	-	1992
[Lissens et al., 2000]	Lissens, G., Kempeneers, P., Fierens, F. and Van Rensbergen, J., 2000, “Development of cloud, snow, and shadow masking algorithms for VEGETATION Imagery”, IEEE International Geoscience and Remote Sensing Symposium, Honolulu, Hawaii, USA	-	2000
[Liu et al, 1996]	Liu, C.H., Chen, A.J. and Liu, G.R.:A Robust Algorithm for Correcting the Topographic Effect of Satellite Image over Mountainous Terrain, ISPRS Archives – Volume XXXI Part B7, 1996, XVIIIth ISPRS Congress Technical Commission VII: Resource and Environmental Monitoring July 9-19, 1996, Vienna, Austria, pp 105-111	-	1996
[Luo et al., 2008]	Luo et al., 2008, “Developing clear-sky cloud and cloud shadow mask for producing clear-sky composites”, Remote Sensing of Environment	-	2008
[Maignan et al., 2004]	Maignan, F., Bréon, F.M. and Lacaze, R., 2004, “Bidirectional reflectance of Earth targets: evaluation of analytical models using a large set of spaceborne measurements with emphasis on the Hot Spot”, Remote Sensing of Environment, Volume 90, Issue 2, 30, 210-220	-	2004
[Mekler and Kaufman, 1982]	Mekler, Y. and Kaufman, Y. J., 1982, “Contrast reduction by atmosphere and retrieval of nonuniform surface reflectance”. Applied Optics, 21:310–316	-	1982
[McNally et al., 2003]	McNally et al., 2003, “A cloud detection algorithm for high-spectral-resolution infrared sounders”, Q. J. R. Meteorol. Soc., 129, 3411–3423	-	2003
[Merchant et al., 2006]	Merchant et al., 2006, “Sea surface temperature for climate from the ATSRS, ESA publication, 2006.	-	2006
[Merchant et al., 2005]	Merchant et al., 2005, “PROBAbilistic physically based cloud screening of satellite infrared imagery for operational sea surface temperature retrieval”, Q. J. R. Meteorol. Soc., 131, pp. 2735–2755	-	2005

© UCL-Geomatics 2016
This document is the property of the LAND_COVER_CCI partnership, no part of it shall be reproduced or transmitted without the express prior written authorization of UCL-Geomatics (Belgium).

ID	TITLE	ISSUE	DATE
[Muller and Fischer, 2007]	Muller, J.-P. and Fischer, J., 2007, "The EU-CLOUDMAP project: Cirrus and contrail cloud-top maps from satellites for weather forecasting climate change analysis". Int. J. Remote Sensing, 28, 1915– 1919.	-	2007
[Paperin and Brockmann, 2007]	Paperin, M. and Brockmann, C., 2007, "Atmospheric Properties from Optical/Infrared, Cloud Structures". In the ENVISAT Symposium Montreux (CH), 23-27 April 2007, Conference Proceedings 3P5.8	-	2007
[Pawlowska et al., 2000]	Pawlowska, H., Brenguier, J.-L., Fouquart, Y., Armbruster, W., Bakan, S., Descloitres, J., Fischer, J., Fouilloux, A., Gayet, J.-F., Ghosh, S., Jonas, P., Parol, F., Pelon, J., Schüller, L., 2000, "Microphysics/ radiation interaction in a stratocumulus cloud: The EUCREX mission 206 case study". Atmos. Res., 55, 85-102	-	2000
[Ph1_ATBDv1.0, 2012]	CCI-LC ATBD Phase I. Land Cover Climate Change Initiative - Algorithm Theoretical Basis Document	1.0	28/09/2012
[Ph1_ATBDv2.3, 2013]	CCI-LC ATBD Phase I. Land Cover Climate Change Initiative - Algorithm Theoretical Basis Document	2.3	28/11/2013
[Ph1_DARDv1.9, 2012]	CCI-LC DARD Phase I. Land Cover Climate Change Initiative - Data Access Requirements Document	1.9	06/06/2012
[Ph2_DARDv1.0, 2014]	CCI-LC DARD Phase II. Land Cover Climate Change Initiative - Data Access Requirements Document	1.0	14/08/2014
[Ph1_DPMv2.2, 2013]	CCI-LC DPM Phase I. Land Cover Climate Change Initiative Detailed Processing Model	2.2	24/05/2013
[Ph1_IODDv1.0, 2013]	CCI-LC IODD Phase I. Land Cover Climate Change Initiative Input and Output Data Description	2.2	21/05/2013
[Ph1_PSDv1.11, 2013]	CCI-LC PSD Phase I. Land Cover Climate Change Initiative - Product Specification Document	1.11	03/07/2014
[Ph2_PSDv1.0, 2014]	CCI-LC PSD Phase II. Land Cover Climate Change Initiative - Product Specification Document	1.0	01/08/2014
[Ph1_PVASRv2.0, 2012]	CCI-LC PVASR Phase I. Land Cover Climate Change Initiative Product Validation Algorithm Selection Report	2.0	12/12/2012
[Ph1_PVIRv1.0, 2013]	CCI-LC PVASR Phase I. Land Cover Climate Change Initiative Product Validation and Intercomparison Report	1.0	23/11/2013
[Ph1_PUG2v2.0, 2013]	CCI-LC PUG LC products Phase I. Land Cover Climate Change Initiative – Product User Guide Version 2	2.0	19/05/2013
[Ph1_PUG/WBv1.0, 2013]	CCI-LC PUG WB product Phase I. Land Cover Climate Change Initiative – SAR Water Bodies User Guide version 1	1.0	22/05/2013

© UCL-Geomatics 2016
This document is the property of the LAND_COVER_CCI partnership, no part of it shall be reproduced or transmitted without the express prior written authorization of UCL-Geomatics (Belgium).

ID	TITLE	ISSUE	DATE
[Ph1_PVPv1.3, 2011]	CCI-LC PVP Phase I. Land Cover Climate Change Initiative - Product Validation Plan	1.3	04/07/2011
[Ph1_RD/WBv1.0, 2013]	CCI-LC project - Production of a reference dataset for the validation of the Water bodies product (D3 of CCN4)	1.0	07/08/2013
[Ph1_SRDv1.1, 2012]	CCI-LC SRD Phase I. Land Cover Climate Change Initiative - System Requirements Document	1.1	18.01.2012
[Ph1_SSDv1.0, 2012]	CCI-LC SSD Phase I. Land Cover Climate Change Initiative - System Specifications Document	1.0	11.12.2012
[Ph1_SVRv1.1,2012]	CCI-LC SVR Phase I. Land Cover Climate Change Initiative –System Verification Report	1.1	11/12/2012
[Ph1_TN/GEOv1.1, 2011]	CCI-LC TN Phase I. Land Cover Climate Change Initiative – Technical Note on Geolocation	1.1	06/2011
[Phulpin et al., 1983]	Phulpin T., Derrien M., and Brard A., 1983, “A two dimensional histogram procedure to analyse cloud cover from NOAA satellite high resolution imagery”. J. Clim. Appl. Meteorol. 22, 1332-1345	-	1983
[Rahman and Dedieu, 1994]	Rahman H., Dedieu G., 1994, “SMAC : a simplified method for the atmospheric correction of satellite measurements in the solar spectrum”, Int. J. Remote Sensing, 15, 1, 123-143.	-	1994
[Rathke et al., 2002]	Rathke et al., 2002, “Evaluation of four approximate methods for calculating infrared radiances in cloudy atmospheres”, Journal of Quantitative Spectroscopy & Radiative Transfer ,75, 297– 321	-	2002
[Rathke et al., 2002b]	Rathke, C., Fischer, J., Neshyba, S. and Shupe, M., 2002, “Improving IR cloud phase determination with 20 microns spectral observations”, Geophys. Res. Lett., 29 (8), 50-1–50-4,	-	2002
[Richter and Schläpfer, 2012]	Richter R. and Schläpfer D., 2014, Atmospheric / Topographic Correction for Satellite Imagery - ATCOR-2/3 User Guide, Version 8.2 BETA, February 2012, pp. 2003	-	2012
[Richter, 1996]	Richter R. Atmospheric correction of satellite data with haze removal including a haze/clear transition region // Comp. and Geosci. 1996. V. 22, N 6. P. 675–681	-	1996
[Richter, 1992]	Richter, R..1992, Model SENSAT- 4 – Sensor-Atmosphere-Target – DLR-IB 552-01/92, 1992	-	1992
[Rossow and Schiffer, 1999]	Rossow, W.B., and Schiffer, R.A., 1999, “Advances in Understanding Clouds from ISCCP”. Bull. Amer. Meteor. Soc., 80, 2261-2288	-	1999

© UCL-Geomatics 2016
This document is the property of the LAND_COVER_CCI partnership, no part of it shall be reproduced or transmitted without the express prior written authorization of UCL-Geomatics (Belgium).

ID	TITLE	ISSUE	DATE
[Roujean et al., 1992]	Roujean, J.-L., Leroy, M. and Deschamps, P. Y., 1992, "A bidirectional reflectance model of the Earth's surface for the correction of remote sensing data," J. Geophys. Res. 97, 20455–20468	-	1992
[Rummelhart and McClelland, 1986]	Rummelhart D. and J. McClelland, 1986, "Parallel Distributed Processing", MIT Press, Cambridge, Massachusetts	-	1986
[Santer et al., 2007]	Santer,R., Ramon D., Vidot J., Dilligeard E., A., 2007, "Surface Reflectance Model for Aerosol Remote Sensing over Land". International Journal of Remote Sensing, International Journal of Remote Sensing, 28, 3 & 4, pp.: 737 – 760	-	2007
[Santer, 1997]	Santer, R., 1997, MERIS ATBD Pixel identification- Algorithm Theoretical Basis Document PO-TN-MEL-GS-0005, ESA	-	1997
[Saunders and Kriebel, 1988]	Saunders R.W., and Kriebel K.T., 1988, "An improved method for detecting clear sky and cloudy radiances from AVHRR data".Int. J. Rem. Sens. 9: 123-150	-	1988
[Schiller et al., 2008]	Schiller et al., 2008, "A method for detection and classification of clouds over water", Proceedings in MERIS - AATSR Workshop, 2008. ESRIN, Frascati, Italy	-	2008
[Shi et al., 2007]	Shi et al., 2007, "Detection of daytime arctic clouds using MISR and MODIS", Remote Sensing of Environment 107, 172–184	-	2007
[Simmons et al.. 2006]	ECMWF reanalysis products from 1989 onwards. ECMWF Newsletter 110: 26–35.	-	2006
[Snyder and Wan, 1998]	Snyder, W.C. and Wan, Z., 1998, "BRDF Models to Predict Spectral Reflectance and Emissivity in the Thermal Infrared", IEEE Transactions on Geosciences and Remote Sensing, 36, 1, 214-225	-	1998
[SPOT-VGT_DataProc, 2011]	Data processing of SPOT-VGT	/	25/07/2011
[Stamnes et al., 2007]	Stamnes, K., Tsay, S. C., Wiscombe, W., and Jayaweera K., 2007, "Numerically stable algorithm for discrete-ordinate method radiative transfer in multiple scattering and emitting layered media", Appl. Optics, 27, 2502-2510	-	2007

© UCL-Geomatics 2016
This document is the property of the LAND_COVER_CCI partnership, no part of it shall be reproduced or transmitted without the express prior written authorization of UCL-Geomatics (Belgium).

ID	TITLE	ISSUE	DATE
[Sterckx et al., 2014]	Sindy Sterckx, Iskander Benhadj, Geert Duhoux, Stefan Livens, Wouter Dierckx, Erwin Goor, Stefan Adriaensen, Walter Heyns, Kris Van Hoof, Gert Strackx, Kris Nackaerts, Ils Reusen, Tanja Van Achteren, Jan Dries, Tom Van Roey, Karim Mellab, Riccardo Duca & Joe Zender ,2014, "The PROBA-V mission: image processing and calibration". International Journal of Remote Sensing, 35:7, 2565-2588, DOI: 10.1080/01431161.2014.883094	-	2014
[Steyn-Ross et al., 1992]	Steyn-Ross, D.A., Moira L. Steyn-Ross and S. Clift, 1992, "Radiance calibrations for advanced very high resolution radiometer infrared channels". J. Geophys. Res. (Oceans), 97, No. C4, pp. 5551–5568	-	1992
[Strahler et al., 1999]	Strahler, A.H., Muller, J.P., Lucht, W., Schaaf, C.B., Tsang, T., Gao, F., Li, X., Lewis P. and Barnsley, M.J., 1999, MODIS BRDF/Albedo Product: Algorithm Theoretical Basis Document Version 5.0 - MODIS Product ID: MOD43	-	1999
[Susskind et al., 1998]	Susskind et al., 1998, "Determination of ATM and surface parameters from simulated Air/AMS/HSB sounding data retrieval and clouds clearing methodology", Adv. Space Re, 21, 3. 36%384	-	1998
[SYN_DPMv2.3_2010]	SYN Detailed Processing Model	2.3	09/2010
[Tanré et al., 1992]	Tanré, D., Holben, B. N., and Kaufman, Y. J., 1992, "Atmospheric correction algorithmfor NOAA-AVHRR products: theory and application". IEEE Transactions onGeoscience and Remote Sensing, 30, 231–250.	-	1992
[Vancutsem et al., 2004]	Vancutsem C., Peckel, J-F., Boagert, P., Defourny, P., 2004, "Assessment of the mean compositing strategy for SPOT VEGETATION time serie", Int. J. of Rem. Sen	-	2004
[Vermote et al., 2009]	Vermote, E., Justice, C. and Bréon, F.M., 2009, "Toward Towards a generalized approach for correction of the BRDF effect in MODIS directional reflectances", IEEE Transactions in Geoscience and Remote Sensing, 47,3, 898-908.	-	2009
[Vermote et al., 1997]	Vermote, E. F., El-Saleous, N., Justice, C. O., Kaufman, Y. J., Privette, J. L., Remer, L., Roger, J. C., and Tanré, D., 1997, "Atmospheric correction of visible to middle infrared EOS-MODIS data over land surface: Background, operational algorithm and validation". Journal of Geophysical Research, 102:17131–17141	-	1997
[Vermote et al., 1997b]	Vermote, E. F., Tanré, D., Deuzé, J. L., Herman, M., and Morcrette, J. J., 1997, "Second Simulation of the Satellite Signal in the Solar Spectrum, 6S: An overview". IEEE Transactions on Geoscience and Remote Sensing, 35:675–686.	-	1997

© UCL-Geomatics 2016
This document is the property of the LAND_COVER_CCI partnership, no part of it shall be reproduced or transmitted without the express prior written authorization of UCL-Geomatics (Belgium).

ID	TITLE	ISSUE	DATE
[Viovy et al., 1992]	Viovy N., Arino, O., Belward, A., 1992, "The Best Index Slope Extraction (BISE): a method for reducing noise in NDVI time series", Int. J. of Rem. Sen., 13, 8, 1585-1590	-	1992
[Walton et al., 1998]	C. C. Walton, J. T. Sullivan, C. R. N. Rao, M. P. Weinreb, Corrections for detector nonlinearities and calibration inconsistencies of the infrared channels of the advanced very high resolution radiometer, Journal of Geophysical Research, 1998, 103, C2, 3323	-	1998
[Wylie, 1998]	Wylie, D., 1998, "Cirrus and Weather: A satellite perspective". OSA Meeting, pp.66-68, Baltimore, U.S.A., 6-8, Oct. 1998	-	1998

© UCL-Geomatics 2016
This document is the property of the LAND_COVER_CCI partnership, no part of it shall be reproduced or transmitted without the express prior written authorization of UCL-Geomatics (Belgium).

TABLE OF CONTENTS

SYMBOLS AND ACRONYMS 4
REFERENCE DOCUMENTS 9
TABLE OF CONTENTS 20
LIST OF FIGURES 23
LIST OF TABLES 26
LIST OF ALGORITHM 28
1 INTRODUCTION 30
1.1 Scope 30
1.2 Structure of the document 30
2 PRE-PROCESSING IN THE YEARS 1 AND 2 OF PHASE II 31
2.1 General overview 31
2.2 Products planned in the CCI-LC Phase2 32
3 QUALITY CONTROL OF THE INPUT PRODUCTS 35
3.1 Methods 35
3.1.1 MERIS FR and RR 35
3.1.2 AVHRR 36
3.1.3 PROBA-V 36
3.2 Examples of erroneous products 36
3.2.1 MERIS FR and RR 36
3.2.2 AVHRR 41
3.3 Results 43
3.3.1 MERIS FR and RR 43
3.3.2 AVHRR 44
3.3.3 PROBA-V 44
4 LAND COVER PRE-PROCESSING CHAIN 45
4.1 Geometric correction 45
4.1.1 MERIS FR and RR - AMORGOS - 4.0 46
4.1.2 Pseudo-code representation 48
4.2 Radiometric Calibration 49
4.2.1 MERIS FR and RR calibration and smile correction 49
4.2.2 PROBA-V and SPOT VGT P 52
4.2.3 AVHRR 52
4.2.4 Pseudo-code representation 56
4.3 Additional pre-processing step for the PROBA-V S1 TOA data 57

© UCL-Geomatics 2016
This document is the property of the LAND_COVER_CCI partnership, no part of it shall be reproduced or transmitted without the express prior written authorization of UCL-Geomatics (Belgium).

4.4 Land water delineation and cloud screening - pixel identification 58
4.4.1 Pixel identification 58
4.4.2 Background 58
4.4.3 Methods 61
4.4.4 Theoretical description 62
4.4.5 Practical consideration 63
4.4.5.1 Overall principles 63
4.4.5.2 Probabilistic arithmetic 64
4.4.5.3 Features 65
4.4.5.4 Processing logic 71
4.4.5.5 Thresholds 73
4.4.5.6 Water/land mask: SWBD mask 74
4.4.6 Adaptation of IdePix 75
4.4.6.1 MERIS FR and RR 75
4.4.6.2 AVHRR 76
4.4.6.3 PROBA-V and SPOT VGT 84
4.4.7 IdePix post-processing for PROBA-V 86
4.4.8 Error budget estimates 87
4.4.9 Assumptions and limitations 87
4.4.10 Improvements 87
4.4.11 Cloud shadow and cloud edge detection 88
4.4.12 Pseudo-code representation 90
4.4.12.1 Land-water delineation 90
4.4.12.2 Pixel classification feature – MERISFR and RR, SPOT VGT/ PROBA-V and AVHRR 90

4.5 Atmospheric correction - aerosol and spectral directional reflectance retrieval 96
4.5.1 MERIS FR and RR, SPOT VGT P and PROBA-V S1 TOA 100
4.5.2 AVHRR 103
4.5.3 SPOT-VGT S1 110
4.5.4 Improvements - atmospheric correction 110
4.5.5 Pseudo-code representation 113

4.6 L3-Processing 115
4.6.1 Plate-Carrée projection 115
4.6.2 Resampling 117
4.6.2.1 Nearest neighbour 117
4.6.2.2 Bi-linear interpolation 117
4.6.2.3 Cubic convolution 118
4.6.2.4 Visual comparison of the resampling methods 119
4.6.3 Temporal sample aggregation 120
4.6.4 Clear land filtering 122
4.6.4.1 Clear land feature of IdePix 122
4.6.4.2 Temporal filtering 124
4.6.5 BRDF - Correction - averaging of the surface directional reflectances 127
4.6.5.1 GlobCover experience 127
4.6.5.1.1 Method 1: BISE algorithm 127
4.6.5.1.2 Method 2: Vancutsem algorithm 128
4.6.5.1.3 Method 3: Hagolle algorithm 130

© UCL-Geomatics 2016
This document is the property of the LAND_COVER_CCI partnership, no part of it shall be reproduced or transmitted without the express prior written authorization of UCL-Geomatics (Belgium).

4.6.5.1.4 GlobCover analyses and decisions for the BRDF correction 132
4.6.5.2 Method 4: improved BRDF inversion developed by Vermote et al. 2009 [Vermote et al., 2009] 133
4.6.6 Generation of mosaics 139
4.6.7 Pseudo-code representation 140
5 VALIDATION OF ALGORITHMS 143

© UCL-Geomatics 2016
This document is the property of the LAND_COVER_CCI partnership, no part of it shall be reproduced or transmitted without the express prior written authorization of UCL-Geomatics (Belgium).

LIST OF FIGURES

Figure 2-1 Schematic representation of the CCI-LC pre-processing chain including input (pre-processing chain based on the GlobAlbedo chain) 31

Figure 2-2: Planning of datasets to be produced in the CCI-LC Phase 2 33

Figure 3-1: Example for horizontal stripes (MER_FRS_1PPEPA20031202_133502_000002252022_00110_09182_7447.N1) 36

Figure 3-2: Example for vertical fine stripes (MER_FRS_1PPEPA20110806_080919_000005123105_00179_49331_2233.N1) 37

Figure 3-3: Example for wrong colours (MER_FRS_1PPEPA20030213_094307_000000982013_00437_05000_2432.N1) 37

Figure 3-4: Example for vertical fine stripes (MER_FSG_1PNUPA20070802_170532_000000592060_00241_28351_1238.N1) 38

Figure 3-5: Example for repetitive lines (MER_FRS_1PPEPA20050127_021857_000001122034_00132_15216_1703.N1) 38

Figure 3-6: Example for vertical stripes (subset of MER_RR__1PRACR20060416_143153_000026312046_00483_21579_0000.N1) 38

Figure 3-7: Example for horizontal stripes (subset pf MER_FSG_1PNUPA20070507_173155_000003802057_00499_27106_5656.N1) 39

Figure 3-8: Example for wrong colour (MER_FRS_1PPEPA20040323_132407_000003992025_00210_10785_1095.N1) 39

Figure 3-9: Example for wrong geocoding (MER_FRS_1PPEPA20060404_024640_000002562046_00304_21400_4636.N1) 40

Figure 3-10: Example for multiple errors (MER_FRS_1PPEPA20050201_163056_000002162034_00212_15296_1861.N1) 40

Figure 3-11: Example for vertical stripes (subset of ao11090992153547_143638.l1b) 41

Figure 3-12: Example for horizontal stripes (ao11041693014332_024356.l1b) 41

Figure 3-13: Example for wrong colour (subset of ao11122892172654_233321.l1b) 41

Figure 3-14: Example for wrong geocoding (subset of ao11111592120108_074109.l1b) 42

Figure 3-15: Example for shifted geocoding between the bands (subset of ao11082692145559_114209.l1b) 42

Figure 3-16: Example for repetitive parts (subset of ao11040792073254_043411.l1b) 43

Figure 4-1: AMORGOS directory structure (from the GlobCover 2005 project – [GlobCover_DJFv3.8, 2008]) 47

Figure 4-2: Flowchart of the MERIS and AATSR synergy pre-processing module 63

Figure 4-3: Unified Pixel Classification Scheme 64

© UCL-Geomatics 2016
This document is the property of the LAND_COVER_CCI partnership, no part of it shall be reproduced or transmitted without the express prior written authorization of UCL-Geomatics (Belgium).

Figure 4-4: Origin land/water mask and SRTM SWBD map 74

Figure 4-5: AVHRR processing mask; white = processing area & black equals non processing area 76

Figure 4-6: Cloud, cloud edges and cloud shadow 88

Figure 4-7: Breadboard cloud shadow algorithm a) blue channel with cloud shadow potential area border (yellow) b) k-means cluster analysis result c) blue channel with cloud shadow d) SWIR1 channel with cloud shadow 89

Figure 4-8: Scheme of process, graphic adopted from [GlobAlbedo_ATBDv4.12, 2013] 99

Figure 4-9: Logical flow of the aerosol retrieval and the atmospheric correction scheme. Figure from [SYN_DPMv2.3_2010] 100

Figure 4-10: Flowchart of the proposed neural network based correction algorithm for the retrieval of the surface directional reflectance (from [GlobCover_DJFv3.8, 2008]) 101

Figure 4-11: Estimation of the relative error in reflectance retrieval caused by the assumption of a Lambertian surface [Lucht, and Strahler, 1999] after resampling to the GlobAlbedo AOD550 grid and the spectral response (from [GlobAlbedo_ATBD/BBDRv1.0, 2010]) 103

Figure 4-12: Subset of IKONOS image of Dresden (Germany), 18. August 2002. ©Space Imaging Europe 2002. Left: original scene, right: after haze removal. Colour coding: RGB= 4,2,1 (NIR/Green/Blue bands) (figure taken from Richter and Schläpfer, 2012 [Richter and Schläpfer, 2012]) 112

Figure 4-13: Overall logical flow of the CCI-LC L3 processing as final step of the pre-processing part (from [Ph1_DPMv2.2, 2013]) 116

Figure 4-14: Nearest Neighbour 117

Figure 4-15: Bilinear Interpolation 118

Figure 4-16: Cubic Convolution 118

Figure 4-17: Visual comparison 119

Figure 4-18: Logical flow of the pixel classification after aggregation. NX (with STATUS_X from Table 4-29) represents the number of single observations of a pixel Pi with status X, the green boxes show the final (taken from [Ph1_DPMv2.2, 2013]). 121

Figure 4-19: Exemplified prior probability density for cloud, town and land derived from MERIS FR L2- SDR pre-processing products 123

Figure 4-20: Efficiency of temporal filtering depends on the quality of the classification by IdePix and seasonal variability of the surface 126

Figure 4-21: Scheme for the BISE method. The triangles represent points of a standard profile. The profile is divided in two parts from the point where NDVI is maximal. In each part (part 1 and part 2), successive iterations on the NDVI points start from the highest point of the profile (green arrows). The time period of the sliding window is draw in vertical dashed points (figure taken from [GlobCover_DJFv3.8, 2008]) 128

Figure 4-22: Quality control of all reflectance values and mean estimation for each band (figure taken from [GlobCover_DJFv3.8, 2008]) 129

Figure 4-23: Subcycle of the viewing zenith angle (figure taken from [GlobCover_DJFv3.8, 2008]) 129

© UCL-Geomatics 2016
This document is the property of the LAND_COVER_CCI partnership, no part of it shall be reproduced or transmitted without the express prior written authorization of UCL-Geomatics (Belgium).

Figure 4-24: Scheme of the angular effects normalization procedure (figure taken from [GlobCover_DJFv3.8, 2008]) 130

Figure 4-25: BRDF model fit for VEGETATION data with (a) no a priori information and (b) a priori information. Unfilled diamonds are discarded pixels, only filled diamonds are used for the BDRF estimate (from [GlobCover_DJFv3.8, 2008]) 131

Figure 4-26 : Standard deviation of the errors calculated as a function of the minimum number of observations used in the BRDF model inversion (from [GlobCover_DJFv3.8, 2008]) 132

Figure 4-27: Example of modelled BRDF using PROSPECT/SAIL model (parameter: Cab = 30.0 (chlorophyll content [µg cm-2]); Car = 10.0 (carotenoid content [µg cm-2]); Cbrown = 0.0 (brown pigment content [arbitrary units]; Cw = 0.015 (equivalent water thickness EWT [cm]); Cm = 0.009 (leaf mass per area LMA [g.cm-2]); N = 1.5 (structure coefficient); LAI = 4 (leaf area index); angl = 50.0 (average leaf angle [degree]); psoil = 1(soil coefficient); skyl = 70 (% diffuse/direct radiation); hspot = 0.05 (hot spot - leaf size relative to canopy height)); ihot = 1.0 (hot spot flag); tts = 30.0 (solar zenith angle [degree])). daa: difference azimuth angle [degree]; oza: observer zenith angle [degree] 136

Figure 4-28: Sub cycle of the difference azimuth angle 137

Figure 4-29: Sub cycle of the viewing zenith angle 138

Figure 4-30: Articulation between the fundamental composites delivered by the pre-processing module and the seasonal composites used in the classification algorithms 140

© UCL-Geomatics 2016
This document is the property of the LAND_COVER_CCI partnership, no part of it shall be reproduced or transmitted without the express prior written authorization of UCL-Geomatics (Belgium).

LIST OF TABLES

Table 2-1: Satellite data that are planned to be used to generate the CCI-LC SR time series in the 1st and 2nd years of the Phase II 34

Table 3-1 Results of the QA of MERIS FR L1b 43

Table 3-2: Results of the QA of MERIS RR L1b 43

Table 3-3 Results of the QA of AVHRR L1b 44

Table 4-1 TOA spectral correction functions between PROBA-V and SPOT VGT [Dierckx et al., 2015] 52

Table 4-2: Values of W and F [Kidwell, 1998] 53

Table 4-3: NOAA-11 Central Wave Numbers for AVHRR IR Channels [Kidwell, 1998] 54

Table 4-4: Non-linearity errors for NOAA-11 Channel 4 and Channel 5 54

Table 4-5: Radiance correction coefficients for NOAA-14 AVHRR Channels 3, 4, and 5 55

Table 4-6: NOAA-14 Central Wave Numbers for AVHRR IR Channels [Kidwell, 1998] 56

Table 4-7: Radiance correction coefficients for NOAA-11 AVHRR Channels 3, 4, and 5 56

Table 4-8: Definition of values for classification features. 64

Table 4-9: Feature - Pixel identification 65

Table 4-10: Feature Definition for MERIS 66

Table 4-11: Feature Definition for SPOT-VGT and PROBA-V 68

Table 4-12: Feature Definition for AVHRR 70

Table 4-13: Processing logic 71

Table 4-14: Thresholds 73

Table 4-15: $RGCT_{threshold}$ 77

Table 4-16: $FMFT_{threshold}$ 78

Table 4-17: $FMFT_{adap_threshold}$ 79

Table 4-18: $TMFT_{threshold}$ 80

Table 4-19: Constants for the calculation of the Channel 3b albedo and emissivity 81

Table 4-20: Adapted processing logic for AVHRR and the classification attribute isCloud 82

Table 4-21: Adapted processing logic for AVHRR and the classification attribute isClearSnow 84

Table 4-22: Adapted processing logic for PROBA-V and the classification attributes 87

Table 4-23: Optical depth for the different stratospheric aerosols 105

Table 4-24: Selection of stratospheric aerosol type regarding the AOD 105

© UCL-Geomatics 2016
This document is the property of the LAND_COVER_CCI partnership, no part of it shall be reproduced or transmitted without the express prior written authorization of UCL-Geomatics (Belgium).

Table 4-25: Specification of the parameter and their values using for the uncertainty estimation 109

Table 4-26: Advantages and disadvantages of the nearest neighbour 117

Table 4-27: Advantages and disadvantages of the bilinear interpolation 117

Table 4-28: Advantages and disadvantages of the cubic convolution 118

Table 4-29: Final status flag 120

Table 4-30: Variables used in Level 3 mosaicing for MERIS, SPOT VGT P and AVHRR 139

© UCL-Geomatics 2016
This document is the property of the LAND_COVER_CCI partnership, no part of it shall be reproduced or transmitted without the express prior written authorization of UCL-Geomatics (Belgium).

LIST OF ALGORITHM

Algorithm 4-1: Geometric correction – MERIS - AMORGOS (see Bourg and Etanchaud, 2007) 48

Algorithm 4-2: Coherent Noise Equalisation 56

Algorithm 4-3: Smile correction 57

Algorithm 4-4: Land-water delineation 90

Algorithm 4-5: Set classification attribute 'isLand' 90

Algorithm 4-6: Set classification attribute 'isWater' 90

Algorithm 4-7: Set classification attribute 'isBright' 91

Algorithm 4-8: Set classification attribute 'isWhite' 91

Algorithm 4-9: Set classification attribute 'isBrightWhite' 91

Algorithm 4-10: Set classification attribute 'isCold' 91

Algorithm 4-11: Set classification attribute 'isVegRisk' 92

Algorithm 4-12: Set classification attribute 'isGlintRisk' 92

Algorithm 4-13: Set classification attribute 'isHigh' 92

Algorithm 4-14: Set classification attribute 'isClearSnow' 92

Algorithm 4-15: Set classification attribute 'isCloud' 93

Algorithm 4-16: Set classification attribute 'isClearLand' 93

Algorithm 4-17: Set classification attribute 'isClearWater' 93

Algorithm 4-18: 'Cloud value feature' implementation 94

Algorithm 4-19: Set classification attribute 'isDesert' 94

Algorithm 4-20: 'Additional cloud detection feature' implementation for AVHRR 94

Algorithm 4-21: 'Additional cloud/ snow-ice detection feature' implementation for SPOT VGT/ PROBA-V 95

Algorithm 4-22: Set classification attribute 'isCloudEdge' 95

Algorithm 4-23: Cloud height determination 95

Algorithm 4-24: Cloud shadow determination 95

Algorithm 4-25: 'Additional cloud detection feature' implementation for SPOT VGT/ PROBA-V 96

Algorithm 4-26: Aerosol retrieval 113

Algorithm 4-27: Interpolation of aerosol parameters (API) 113

Algorithm 4-28: Atmospheric correction 113

Algorithm 4-29: Error metric calculation 114

© UCL-Geomatics 2016
This document is the property of the LAND_COVER_CCI partnership, no part of it shall be reproduced or transmitted without the express prior written authorization of UCL-Geomatics (Belgium).

Algorithm 4-30: SDR retrieval *114*

Algorithm 4-31: SDR error retrieval *115*

Algorithm 4-32: Direct geo-location (DGL) *140*

Algorithm 4-33: Inverse geo-location (IGL) *140*

Algorithm 4-34: Plate Carrée projection *141*

Algorithm 4-35: Clear land filtering *141*

Algorithm 4-36: Temporal filtering (e.g. Level 3 sample aggregation for MERIS band 8) *141*

Algorithm 4-37: Level 3 Sample Aggregation *142*

Algorithm 4-38: Retrieval of aggregated pixel classification *142*

Algorithm 4-39: L3 generation of mosaics *142*

© UCL-Geomatics 2016
This document is the property of the LAND_COVER_CCI partnership, no part of it shall be reproduced or transmitted without the express prior written authorization of UCL-Geomatics (Belgium).

1 INTRODUCTION

1.1 Scope

This document is part of the Algorithm Theoretical Basis Document (ATBD) of the Phase II Land Cover (LC) project belonging to the European Space Agency (ESA) Climate Change Initiative (CCI). It is dedicated to the pre-processing chain.

This ATBD is written through successive increments. An initial version (v1) is dealing with the CCI-LC Phase II in general while focuses on the activities developed during the first year of the project. This second version focuses on the activities of year 2 and 3 and a last version (v3) will be released at the end of the 3rd year. The ATBD-v3 will be the final version of the document.

1.2 Structure of the document

This document gives a detailed description of the pre-processing chain. After this introduction, the document is organized in 3 main sections:

- Section 2 gives an overview of the pre-processing in CCI-LC Phase II and lists all the products that will be generated during the CCI-LC Phase 2.
- Section 3 describes the CCI-LC pre-processing chain modules in detail.
- Section 4 reminds the validation plan of algorithms.

© UCL-Geomatics 2016
This document is the property of the LAND_COVER_CCI partnership, no part of it shall be reproduced or transmitted without the express prior written authorization of UCL-Geomatics (Belgium).

2 PRE-PROCESSING IN THE YEARS 1 AND 2 OF PHASE II

2.1 General overview

The completed automated pre-processing chain performs the following operations (Figure 2-1): radiometric, geometric correction, pixel identification, atmospheric correction with aerosol retrieval as well as compositing and mosaicking (possibly including sensor merging). Improved algorithms will be developed and validated for each of these pre-processing steps.

They are exhaustively detailed in section 3.

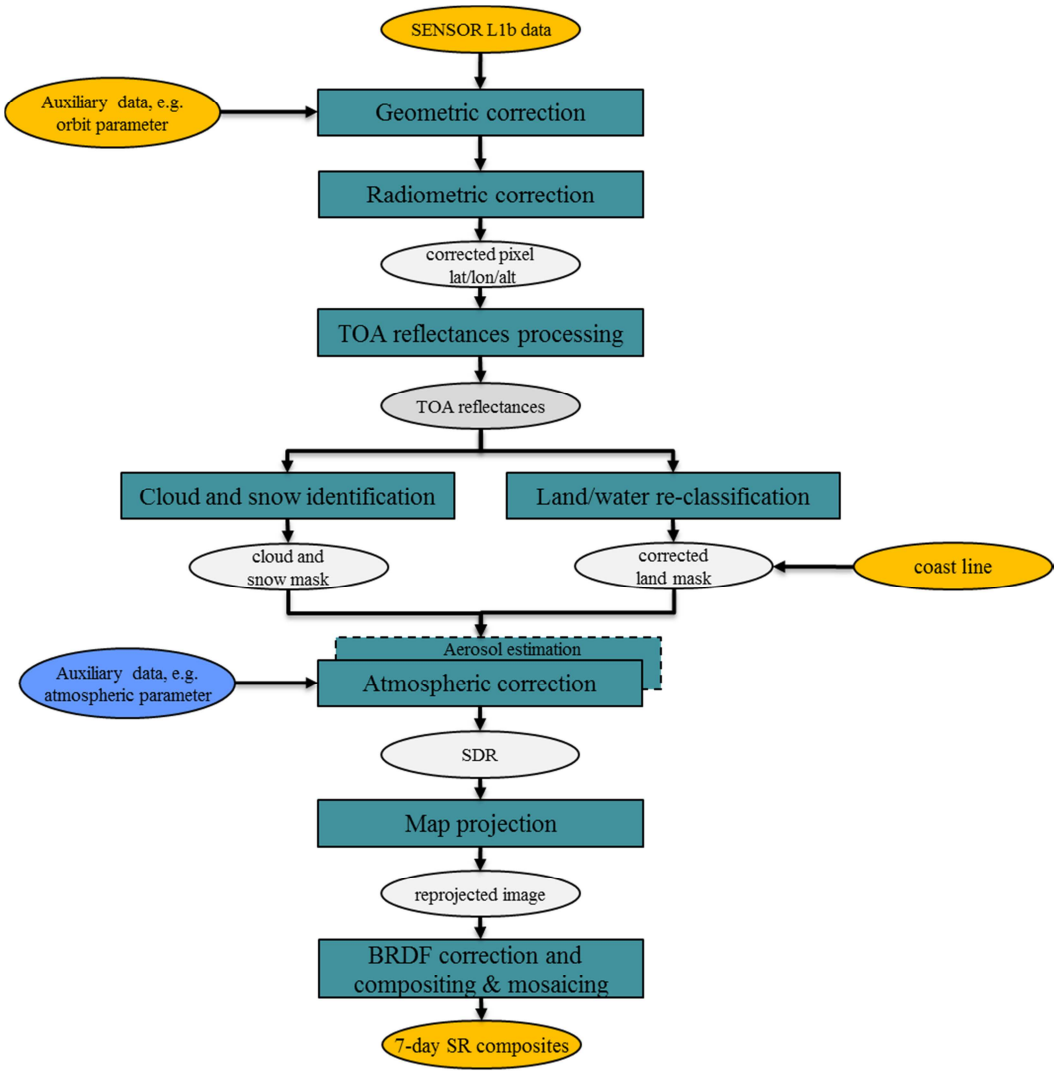


Figure 2-1 Schematic representation of the CCI-LC pre-processing chain including input (pre-processing chain based on the GlobAlbedo chain)

© UCL-Geomatics 2016
This document is the property of the LAND_COVER_CCI partnership, no part of it shall be reproduced or transmitted without the express prior written authorization of UCL-Geomatics (Belgium).

In case of PROBA-V, the input products in the pre-processing chain are the PROBA-V Level 3 Top Of Atmosphere daily synthesis product at 333m spatial resolution (S1 TOA). Therefore the pre-processing includes pixel identification, atmospheric correction with aerosol retrieval as well as compositing and mosaicking only.

2.2 Products planned in the CCI-LC Phase2

The outputs of the CCI-LC Phase 2 project concern global SR time series, global LC maps, global LS seasonality products and a global water bodies' product, all of them being delivered along with metadata. The outputs also include software systems, products documentation and validation reports. The PSD focuses on the datasets.

At the end of the 3-year long Phase 2, the key global datasets for the end-users will be:

1) Global SR time series and associated metadata over different epochs and from different sensors:
    a. Time series of AVHRR 7-day composites[1] from 1992 through 1999;
    b. Time series of ENVISAT MERIS Full Resolution 7-day composites from 2003 through 2012;
    c. Time series of ENVISAT MERIS Reduced Resolution 7-day composites from 2003 through 2012;
    d. Time series of PROBA-V 7-day composites from 2014 through 2015 (and beyond);
    e. Time series of SENTINEL-3 OLCI and SLSTR 7-day composites from 2015 (and beyond).
2) Global LC maps for the 1990s, 2000, 2005, 2010 and 2015 epochs based on the above AVHRR, SPOT-VGT, MERIS FR and RR, PROBA-V, MODIS composites and associated metadata;
3) An updated global LC map for 2015 including the above SENTINEL-3 OLCI and SLSTR composites and associated metadata[2];
4) A global LS seasonality product and associated metadata for the NDVI;
5) Global map of permanent open water bodies for the 2010 epoch based on ENVISAT ASAR time series.

In addition, prototypes products are foreseen, which will demonstrate the pre-processing and classification algorithms developed for the SENTINEL-1 and -2 missions and to expand historical time series. They include:

1) SENTINEL-2 and Landsat 8 time series of regional SR composites from 2014 (and beyond) and associated metadata;

[1] A 7-day compositing period is foreseen to be consistent with the other sensors, but this has to be confirmed according to the data coverage

[2] According to the availability of SENTINEL-3 data in terms of quantity and timing with respect to the overall project planning

© UCL-Geomatics 2016
This document is the property of the LAND_COVER_CCI partnership, no part of it shall be reproduced or transmitted without the express prior written authorization of UCL-Geomatics (Belgium).

2) Regional LC maps based on the above SENTINEL-2 and Landsat 8 composites and associated metadata;
3) Change maps dedicated to critical LC classes and/or regions according to users' priorities based on the above SENTINEL-2 and Landsat 8 composites and associated metadata;
4) Prototype water body and urban products based on SENTINEL-1 SAR data, tuned geographically to the regional LC maps obtained with SENTINEL-2 data;
5) A consistent coarse spatial resolution LC map for continental or sub-continental regions for the 1980s based on the AVHRR Global Inventory Monitoring and Modelling System (GIMMS) dataset;
6) An EvapoTranspiration (ET) Feasibility study will be performed during the first year of this second phase. Encouraging results may lead to the production of an ET seasonality product;
7) As backup the time series of SPOT-VGT 7-day composites from 1998 through 2012 in case of delayed delivery of the reprocessed SPOT VGT S1 products.

Those products will be generated throughout the project, following the planning illustrated in Figure 2-2.

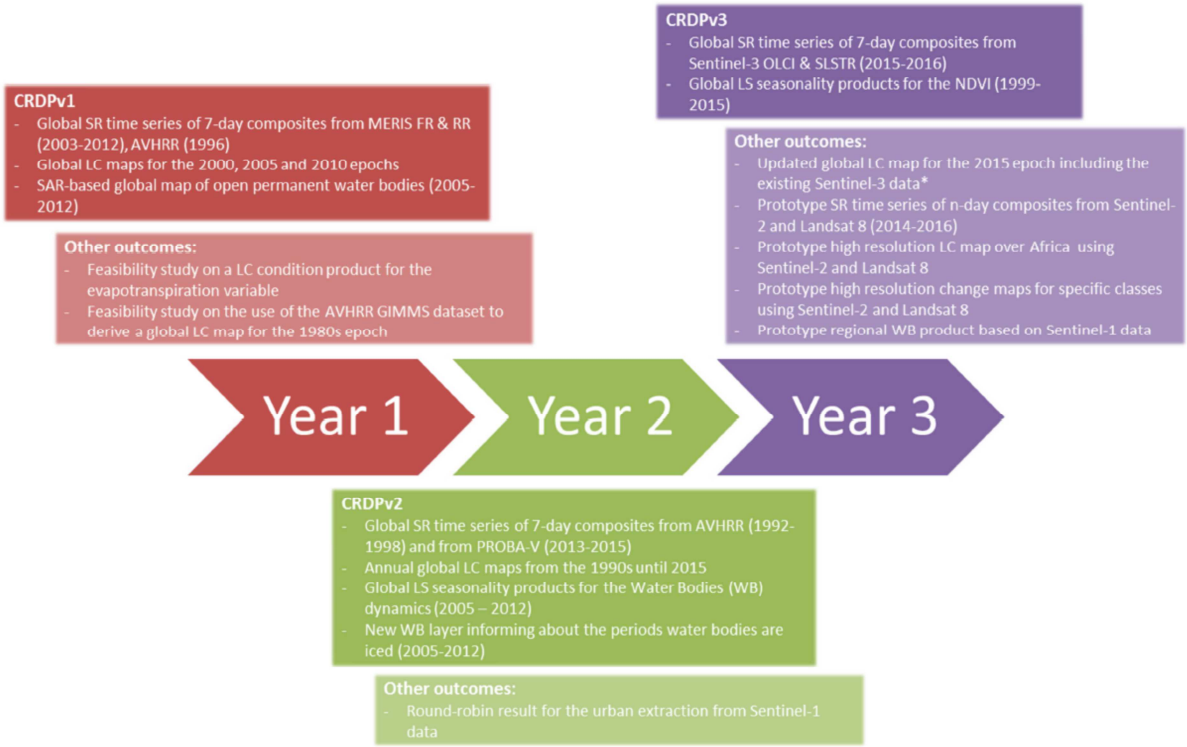


Figure 2-2: Planning of datasets to be produced in the CCI-LC Phase 2

* The reason why this update is not included in the CRDPv3 is that it will be delivered at the end of the year 3, thus not available for climate assessment

© UCL-Geomatics 2016
This document is the property of the LAND_COVER_CCI partnership, no part of it shall be reproduced or transmitted without the express prior written authorization of UCL-Geomatics (Belgium).

This version of the document focuses on the products that will be generated during the first and the second year of the project, i.e. not the SENTINEL-3 time series and not the high resolution prototype products.

Table 2-1 details the satellite dataset that are planned to be used in order to generate the global SR composite time series in the first and second year of the Phase II. The time series are made of temporal synthesis obtained over a specific compositing period. The compositing period most suitable for the classification chain – and so the temporal resolution of the SR products delivered by the project – has been decided in Phase 1 to be 7 days. The exact schema for the 7-day periods is to start at January 1 and go on 7-day by 7-day periods until the end of the year. In this way, it should be noted that the last period of December comprises 8 days. As for leap years, the 7-day period including February 29 comprises 8 days.

Table 2-1: Satellite data that are planned to be used to generate the CCI-LC SR time series in the 1st and 2nd years of the Phase II

GLOBAL SR COMPOSITE TIME SERIES	REFERENCE PERIOD	SATELLITE DATA SOURCE	TECHNICAL SPECIFICATIONS OF THE SATELLITE DATA SOURCE
AVHRR global SR composite time series[3]	1992-1999	AVHRR 2	• 1km • 5 spectral bands in visible and infrared • Global coverage
PROBA-V global SR composite time series	2014-2015(and beyond)	PROBA-V S1 TOA	• 300 m resolution • spectral bands in visible and infrared • Global coverage
MERIS global SR composite time series	2003-2012	ENVISAT MERIS FR & RR	• 300-m or 1000- m resolution full swath • 15 spectral bands in visible and near infrared (NIR) • Global coverage
SPOT-VGT global SR composite time series[4]	1998-2012	SPOT-VGT P	• 1-km resolution • spectral bands in visible and infrared • Global coverage

[3] It was planned to apply the complete pre-processing chain to AVHRR data and to deliver 7-day SR composites in Phase II year1. As a result of the delay in data delivery, it was decided to adapt the delivery plan as follows: deliver 7-day SR composites in Phase II year1. As a result of the delay in data delivery, it was decided to adapt the delivery plan as follows:

- Year1: delivery of 7-day TOA cloud free composites
- Year2: delivery of 7-day SR composites

[4] As backup - the time series of SPOT-VGT 7-day composites from 1998 through 2012 in case of delayed delivery of the reprocessed SPOT VGT S1 products.

© UCL-Geomatics 2016
This document is the property of the LAND_COVER_CCI partnership, no part of it shall be reproduced or transmitted without the express prior written authorization of UCL-Geomatics (Belgium).

3 QUALITY CONTROL OF THE INPUT PRODUCTS

3.1 Methods

In the course of the Land Cover project belonging to the European Space Agency (ESA) Climate Change Initiative (CCI) the quality assurance of the input data as well as of the output products is a crucial working step.

The quality control process of the input products comprises:

- automatic quality control;
- visual inspection of the input products which have been identified by the automatic quality control as erroneous products.

Furthermore, the quality control of the output products includes the visual inspection of the 7- day SR composites and the inspection of time series.

3.1.1 MERIS FR and RR

For the quality assessment of MERIS FR and RR L1b products the following quality criteria have been defined:

- Format error – errors regarding the metadata, file format etc.
- Blank product - no lines with data
- Short product - products less than 7 seconds
- Duplicate product - products which have the same starting time (exact duplicate) and duration or which are temporarily and spatially included
- Missing data - few blank lines within the product
- Shifted geolocation - wrong geolocation, mainly caused by missing lines
- Horizontal and vertical stripes and wrong colours - one camera clearly different than the others, these errors often occur in combination with missing data and geolocation errors.
- Repetitive lines - repetition of lines in several locations of the product

All products which have not passed the quality control have been removed and cannot be used for the calculation of the 7-day surface reflectance products. Additionally the MERIS FR and RR products acquired during a special event (Calibration, Campaign or orbit manoeuvre) have been also removed from the data set.

© UCL-Geomatics 2016
This document is the property of the LAND_COVER_CCI partnership, no part of it shall be reproduced or transmitted without the express prior written authorization of UCL-Geomatics (Belgium).

3.1.2 AVHRR

For the quality assessment of AVHRR L1b products the following quality criteria have been defined:

- Blank product - no lines with data
- Shifted geolocation - wrong geolocation or repetitive parts
- Horizontal and vertical stripes and wrong colours – one or more bands clearly different than the others

The criteria tests are based on the analysis of the band counts, row sums and columns sums of the apparent reflectance image and of the NDVI as well as of the static land /water mask. In contrast to MERIS FR and RR, only products which have not passed the quality control regarding the blank product and geolocation criteria have been removed and cannot be used for the calculation of the 7-day surface reflectance products. The other products, which have shown stripes and wrong colors, have been flagged and the erroneous parts have been masked out by the quality control process.

3.1.3 PROBA-V

At this stage of the project, no QA of the PROBA-V S1 TOA has been planned. In case of using the internal PROBA-V L1b products a QA is foreseen.

3.2 Examples of erroneous products

3.2.1 MERIS FR and RR

The following images (Figure 3-2 - Figure 3-10) illustrate the errors observed in the MERIS FR and RR L1b data.

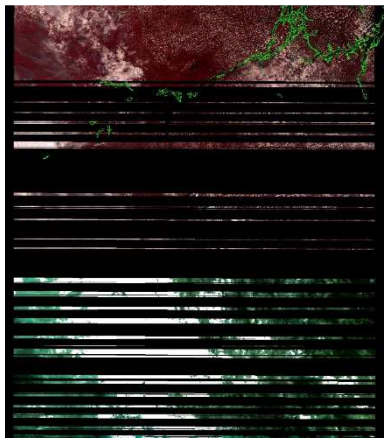


Figure 3-1: Example for horizontal stripes (MER_FRS_1PPEPA20031202_133502_000002252022_00110_09182_7447.N1)

© UCL-Geomatics 2016
This document is the property of the LAND_COVER_CCI partnership, no part of it shall be reproduced or transmitted without the express prior written authorization of UCL-Geomatics (Belgium).

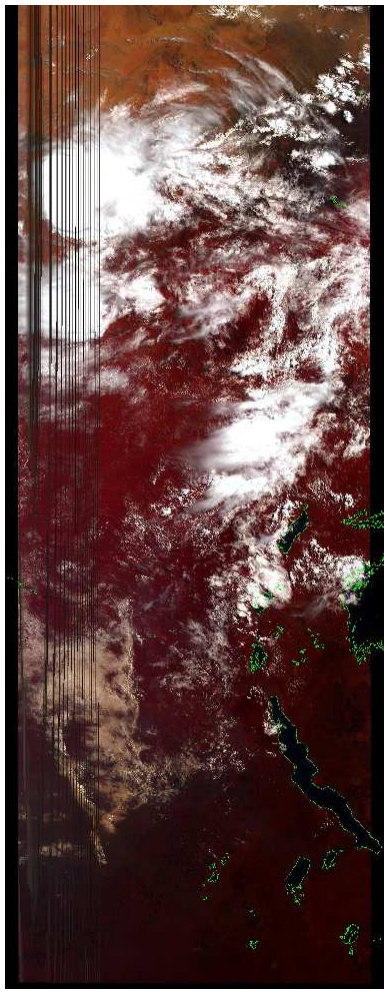


Figure 3-2: Example for vertical fine stripes
(MER_FRS_1PPEPA20110806_080919_000005123105_00179_49331_2233.N1)

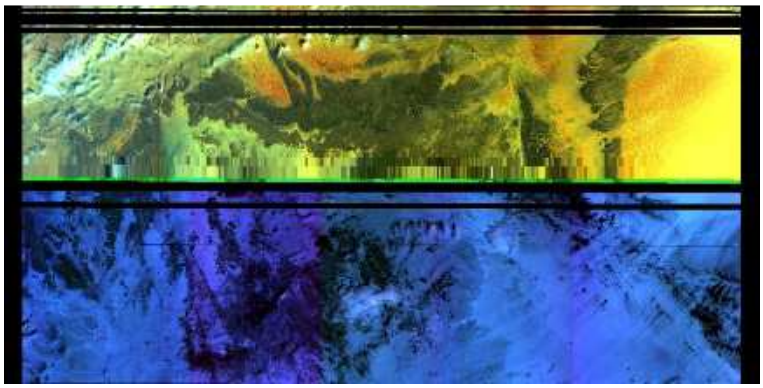


Figure 3-3: Example for wrong colours
(MER_FRS_1PPEPA20030213_094307_000000982013_00437_05000_2432.N1)

© UCL-Geomatics 2016
This document is the property of the LAND_COVER_CCI partnership, no part of it shall be reproduced or transmitted without the express prior written authorization of UCL-Geomatics (Belgium).



Figure 3-4: Example for vertical fine stripes (MER_FSG_1PNUPA20070802_170532_000000592060_00241_28351_1238.N1)

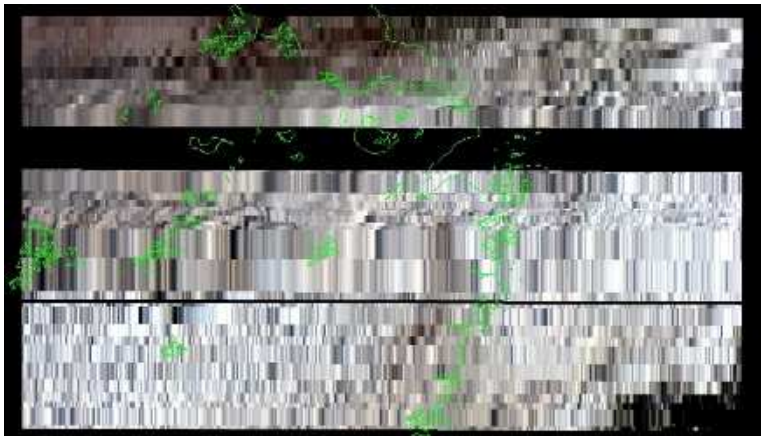


Figure 3-5: Example for repetitive lines (MER_FRS_1PPEPA20050127_021857_000001122034_00132_15216_1703.N1)

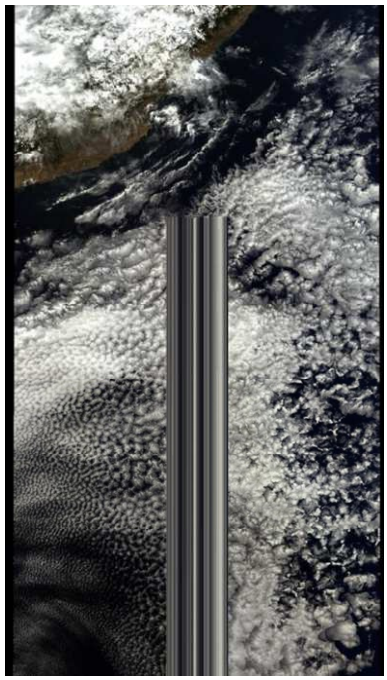


Figure 3-6: Example for vertical stripes (subset of MER_RR__1PRACR20060416_143153_000026312046_00483_21579_0000.N1)

© UCL-Geomatics 2016
This document is the property of the LAND_COVER_CCI partnership, no part of it shall be reproduced or transmitted without the express prior written authorization of UCL-Geomatics (Belgium).

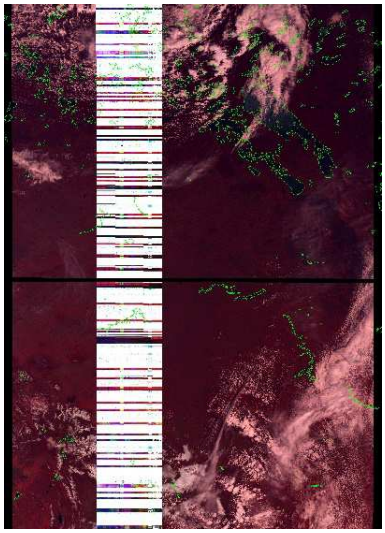


Figure 3-7: Example for horizontal stripes (subset pf MER_FSG_1PNUPA20070507_173155_000003802057_00499_27106_5656.N1)

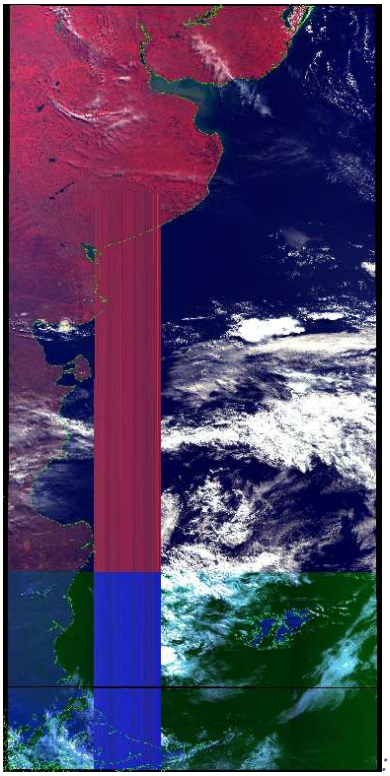


Figure 3-8: Example for wrong colour (MER_FRS_1PPEPA20040323_132407_000003992025_00210_10785_1095.N1)

© UCL-Geomatics 2016
This document is the property of the LAND_COVER_CCI partnership, no part of it shall be reproduced or transmitted without the express prior written authorization of UCL-Geomatics (Belgium).

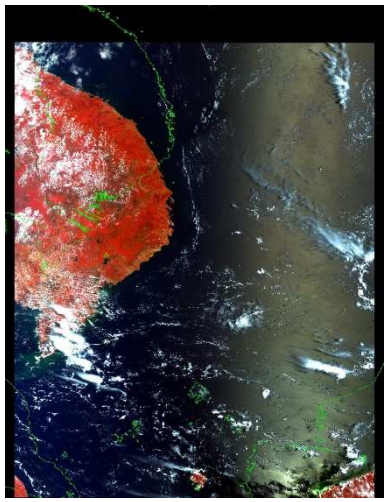


Figure 3-9: Example for wrong geocoding (MER_FRS_1PPEPA20060404_024640_000002562046_00304_21400_4636.N1)

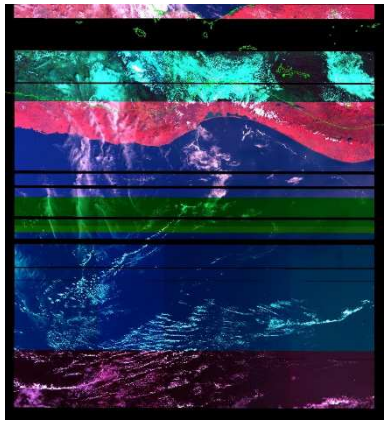


Figure 3-10: Example for multiple errors (MER_FRS_1PPEPA20050201_163056_000002162034_00212_15296_1861.N1)

© UCL-Geomatics 2016
This document is the property of the LAND_COVER_CCI partnership, no part of it shall be reproduced or transmitted without the express prior written authorization of UCL-Geomatics (Belgium).

3.2.2 AVHRR

The following images (Figure 3-11 - Figure 3-16) illustrate the errors observed in the AVHRR data.

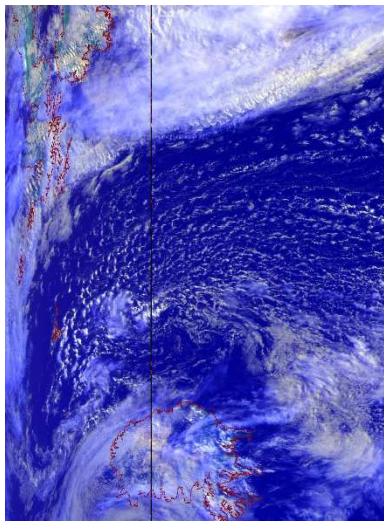


Figure 3-11: Example for vertical stripes (subset of ao11090992153547_143638.l1b)

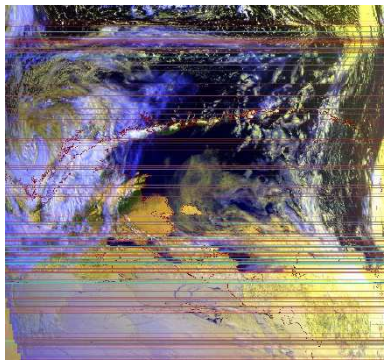


Figure 3-12: Example for horizontal stripes (ao11041693014332_024356.l1b)

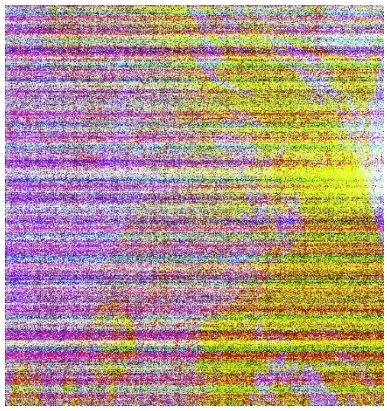


Figure 3-13: Example for wrong colour (subset of ao11122892172654_233321.l1b)

© UCL-Geomatics 2016
This document is the property of the LAND_COVER_CCI partnership, no part of it shall be reproduced or transmitted without the express prior written authorization of UCL-Geomatics (Belgium).

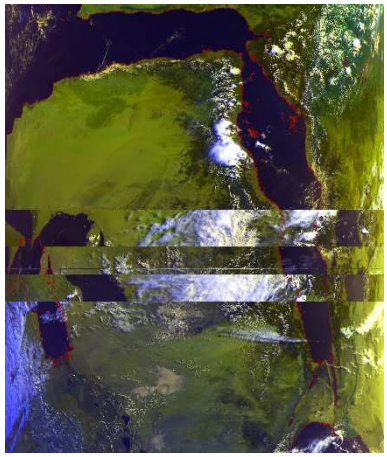


Figure 3-14: Example for wrong geocoding (subset of ao11111592120108_074109.l1b)

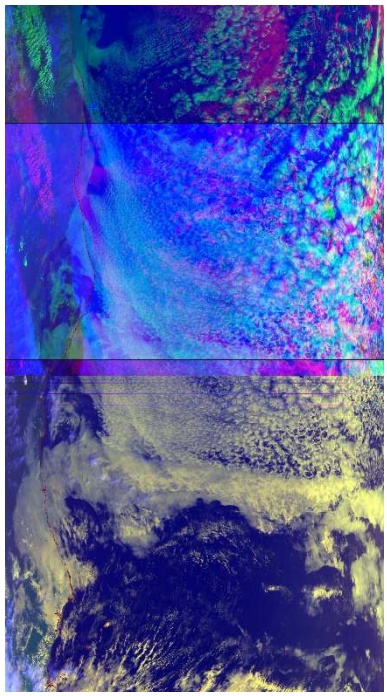


Figure 3-15: Example for shifted geocoding between the bands (subset of ao11082692145559_114209.l1b)

© UCL-Geomatics 2016
This document is the property of the LAND_COVER_CCI partnership, no part of it shall be reproduced or transmitted without the express prior written authorization of UCL-Geomatics (Belgium).

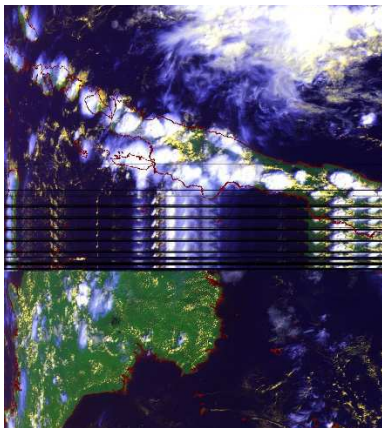


Figure 3-16: Example for repetitive parts (subset of ao11040792073254_043411.l1b)

3.3 Results

3.3.1 MERIS FR and RR

The QA of the MERIS FR v2013 data set has been finished and the erroneous products have been removed from the data set which is used for the processing of the 7-day composites. The following tables summarize the results of the QA for MERIS FR v2013 of phase II and the results of the QA for MERIS RR of phase I.

Table 3-1 Results of the QA of MERIS FR L1b

MAIN CATEGORY	SUBCATEGORY	PRODUCTS		RELATIVE
Potentially good		135010		97.84%
Corrupt		1456		1.06%
	Short		719	
	Duplicate		462	
	Blank		275	
Segregated		1522		1.10%
Sum:		137988		100%

Table 3-2: Results of the QA of MERIS RR L1b

PRODUCTS	POTENTIALLY GOOD PRODUCTS	POTENTIALLY BAD PRODUCTS
48940	48540 (99.18%)	337 + 63 (0.82%)

© UCL-Geomatics 2016
This document is the property of the LAND_COVER_CCI partnership, no part of it shall be reproduced or transmitted without the express prior written authorization of UCL-Geomatics (Belgium).

3.3.2 AVHRR

The QA of the AVHRR L1b data set has been finished and the erroneous products have been removed from the data set which is used for the processing of the 7-day composites. The following tables summarize the results of the QA for AVHRR L1b data set.

Table 3-3 Results of the QA of AVHRR L1b

MAIN CATEGORY	SUBCATEGORY	PRODUCTS		RELATIVE
Potentially good		30253		95.75%
Corrupt		1344		4.25%
	Short/ Duplicate		906	
	Stripes		201	
	Geo-Coding		200	
	Colour		37	
Sum:		31597		100%

3.3.3 PROBA-V

At this stage of the project, no QA of the PROBA-V S1 TOA has been planned. In case of using the internal PROBA-V L1b products a QA is foreseen.

© UCL-Geomatics 2016
This document is the property of the LAND_COVER_CCI partnership, no part of it shall be reproduced or transmitted without the express prior written authorization of UCL-Geomatics (Belgium).

4 LAND COVER PRE-PROCESSING CHAIN

As already mentioned, the completed automated pre-processing chain generates global various temporal resolution composites of surface reflectances of MERIS, AVHRR SPOT-VGT and PROBA-V by a series of pre-processing steps (Figure 2-1). Improved and new algorithms developed for each of these steps are presented in the sections below.

4.1 Geometric correction

MERIS

With AMORGOS (Accurate MERIS Ortho Rectified Geo-location Operational Software), ESA has made available a tool which improves MERIS FR geolocation better than 70 RMS. AMORGOS has been developed by ACRI-ST. The analysis of geolocation accuracy brought a misalignment of MERIS FR and RR forward, which is separately described in a technical note [Ph1_TN/GEOv1.1, 2011]. In brief, in all Probability, it is a combined effect of on-board resampling of CCD coordinates and on-ground geometric L0 → L1 processing. The updated version AMORGOS 4.0 is addressing this geolocation issue and therefore improves the matching between MERIS FR and RR data. This version has to be integrated in the pre-processing chain. AMORGOS 4.0 is not applicable to any other sensors by definition.

The investigation of the geolocation accuracy of the MERIS FSG and RRG revealed that the geometric accuracy of all products fulfils the CCI-LC requirements [Ph1_PVASRv2.0, 2012].

SPOT VGT P + PROBA-V

The investigation of the geolocation accuracy of the SPOT VGT P products revealed that the geometric accuracy of all products fulfils the CCI-LC requirements [Ph1_PVASRv2.0, 2012].

In case of PROBA-V, the absolute geometric accuracy has been determined as 300 m in the VIS and 400 m VIS/SWIR as well as the relative geometric accuracy is 150 m in the VIS and 225 m VIS/SWIR. Therefore the geometric accuracy of PROBA-V fulfils the CCI-LC requirements [Sterckx et al., 2014].

AVHRR

In case of the AVHRR HRPT L1b products, the relative geolocation accuracy of near nadir pixel in a flat area has been determined as +/- one pixel. In mountainous areas or for off-nadir pixel larger deviation can be observed. Therefore around 700 border pixels of both sides along the swath of all AVHRR HRPT L1b products have been omitted. Despite this restriction the geometric accuracy of the AVHRR HRPT L1b products doesn't fulfil the initial CCI-LC requirements, but it fulfils the requirement regarding the classification.

© UCL-Geomatics 2016
This document is the property of the LAND_COVER_CCI partnership, no part of it shall be reproduced or transmitted without the express prior written authorization of UCL-Geomatics (Belgium).

All other sensors

In order to achieve consistent geolocation accuracy across all used instrument data, a new module will have to be developed if the geometric accuracy of other products does not fulfil the CCI-LC requirements with respect to the geolocation.

4.1.1 MERIS FR and RR - AMORGOS - 4.0

AMORGOS includes a precise orbit determination, instrument pointing and performs an ortho-rectification. The AMORGOS Software User Manual and Interface Control Document as well as the Software Transfer Document (Issue 2.0) were made available by ESA to the GlobCover team [Arino et al., 2008] on 23.12.2005. This document is included in the GlobCover Design Justification File [GlobCover_DJFv3.8, 2008] as Amorgos_ICD-SUM_2.0.doc and Amorgos_STD_i1r0.doc.

AMORGOS is run once for every MERIS_FRS_1P file and generates the corresponding MER_FSO_1P file. Re-build of the instrument projection is done using MER_FRS_1P internal data, the so-called MERIS detector index data set, and some additional MERIS Level 1b auxiliary data, the FR frame offset, extracted from appropriate MER_INS_AX file. For each MERIS pixel restored in instrument projection, an ortho-rectification algorithm computes the first intersection between the pixel's line of sight and the Earth surface, represented by interpolation of the Digital Elevation Model (DEM) cells elevations on top of the reference ellipsoid. Line of sight is determined using its pointing vector expressed relative to the satellite, the satellite location and attitude, which are in turn determined from Orbit and Attitude files using the appropriate CFI routines. Location of the intersection is expressed as longitude, geodetic latitude and geodetic altitude.

AMORGOS is producing a so called FSG (Full Swath Geo-corrected) product. This is structurally identical with the FRS product but with 3 additional bands for the precise and corrected latitude, longitude and altitude.

AMORGOS is executable software, which takes a MERIS FRS product as input and generates an FSG product as output. AMORGOS performs an improved navigation and pointing calculation and orthocorrects the data using an external digital elevation model. The FSG product in principle is an FRS product with three additional bands: corrected latitude and longitude, and the altitude. An important issue is the limitation of frame numbers for the FSG product. Due to output product time limits, the number of lines of an FSG product cannot exceed the value of 10305. Because the input FRS product may consist of up to 12865 lines, the processing of such a product has to be performed in two steps. AMORGOS provides input switches in the configuration file to handle this constraint.

Since AMORGOS is a binary distribution for Linux, it runs only under this operating system. It expects a certain directory structure, as depicted in the following Figure 4-1, which is taken from the AMORGOS Software Transfer Document. The figure does not contain the DEM directory, where the tiles of the digital elevation model reside.

© UCL-Geomatics 2016
This document is the property of the LAND_COVER_CCI partnership, no part of it shall be reproduced or transmitted without the express prior written authorization of UCL-Geomatics (Belgium).

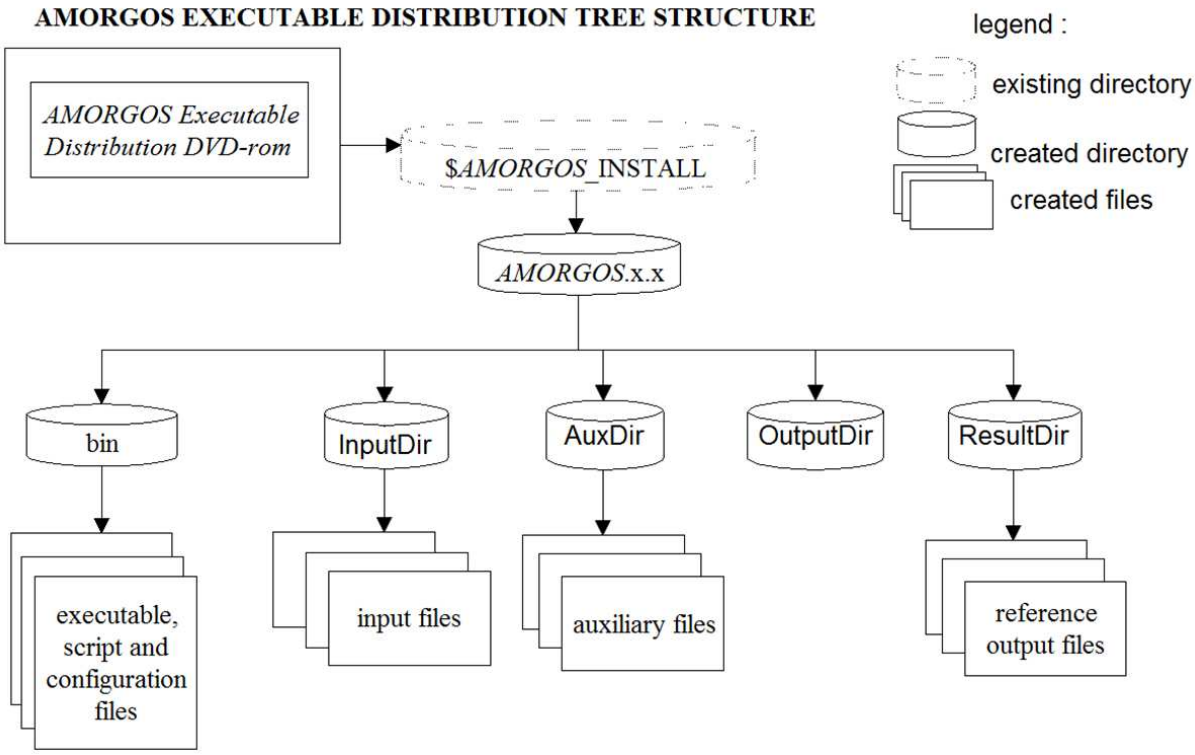


Figure 4-1: AMORGOS directory structure (from the GlobCover 2005 project – [GlobCover_DJFv3.8, 2008])

The improvements of AMORGOS V4.0 with respect to previous version (V3.0p1) are:

- the processing of MERIS RR L1b products (MER_RR__1P) into geo-referenced RR L1B (MER_RRG_1P);
- the handling of the both reprocessing 2 and reprocessing 3 data (the difference affecting the format of an L1b processor auxiliary data file also used by AMORGOS, not the MERIS L1b products).

Consequently, the testing philosophy addresses the two changes listed above by verifying that: MERIS RR georeferenced products generated by AMORGOS V4.0 give results equivalent to:

- MERIS FR georeferenced products with same coverage generated by AMORGOS V4.0, the FR mode being already validated;
- MERIS RR georeferenced products are generated by MEGS, the MERIS Ground Segment test platform, in which the geo-reference option has been implemented and validated for both RR and FR.
- MERIS FR georeferenced products generated by AMORGOS V4.0 give results equivalent to products with same coverage generated by AMORGOS V3 (or MEGS, the latter having been validated against AMORGOS V3);
- AMORGOS V4.0 results are equivalent when obtained from MERIS 2nd re-processing data and MERIS 3rd reprocessing data with identical coverage, and that for both RR and FR.

© UCL-Geomatics 2016
This document is the property of the LAND_COVER_CCI partnership, no part of it shall be reproduced or transmitted without the express prior written authorization of UCL-Geomatics (Belgium).

Test scenes have been selected so as to offer various types of terrain, in particular including mountainous areas with a high variability of elevation. In all cases, validation is assessed through comparisons of (a) pixel altitudes with respect to the reference and (b) pixel geolocation through computation of ground distance with respect to the reference geolocation [Bourg et al., 2011].

Short summary of validation results:

- AMORGOS V4.0 RR versus FR - test is fully satisfactory;
- AMORGOS V4.0 RR versus MEGS RR - test is fully satisfactory;
- AMORGOS V4.0 FR versus MEGS FR- test is fully satisfactory;
- AMORGOS V4.0 from re-processing 3 versus AMORGOS V4 from re-processing 2 - test is fully satisfactory for both resolutions.

4.1.2 Pseudo-code representation

This subsection provides an overview of the geometric correction from the software development point of view. A more detailed description of the logical flow and individual processing steps can be found in the CCI Land Cover DPM [Ph1_DPMv2.2, 2013]. Furthermore the input and output products being used within the LC-CCI processing modules are described in the CCI Land Cover IODD [Ph1_IODDv1.0, 2013] in more detail.

GEOMETRIC CORRECTION – MERIS

```
algorithm AMORGOS is
    input: MERIS reduced or full resolution Level 1B product: either a Full Swath
              or a standard half-swath Scene product MER_XXX_1P
           ENVISAT Orbit files: DOR_VOR_AX and/or, DOR_POR_AX and/or, AUX_FRO_AX
           Restituted Attitude file: AUX_FRA_AX
           the Julian Date, date
           configfile (Linux only)
    output: MER_FSO_1P, MER_FSG_1P or MER_FRG_1P or MER_RRG_1P
            Status and error log files
            optional: TIFF format output radiance files.X , X stands
               for the spectral band index, in [1,15], TIFF format flags
              file, TIFF format geolocation data files
A detailed description of the single algorithms used within AMORGOS is
beyond the scope of this document, more comprehensive information on this
tool can be found in [Bourg and Etanchaud, 2007].
```

Algorithm 4-1: Geometric correction – MERIS - AMORGOS (see Bourg and Etanchaud, 2007)

© UCL-Geomatics 2016
This document is the property of the LAND_COVER_CCI partnership, no part of it shall be reproduced or transmitted without the express prior written authorization of UCL-Geomatics (Belgium).

4.2 Radiometric Calibration

4.2.1 MERIS FR and RR calibration and smile correction

MERIS calibration

Spectral and radiometric calibrations are key processes for all quantitative algorithms which exploit the spectral shape and magnitude. The spectral calibration of MERIS is performed by using measurements of a coloured diffuser and by a spectral matching technique using the measurements of the $O_{2\text{-}A}$ absorption band. The spectral calibration has been proved to be within 0.1nm accuracy. This is considered to be adequate for the generation of CCI-LC products. The radiometric accuracy is more critical. MERIS has two diffusers on-board, the first one being used regularly to monitor the radiometric response and the second one being exposed to sun light only 3 to 4 times per year in order to monitor the ageing of the first diffuser. With this technique it was possible to derive a new degradation model of the instrument, which is applied for the third reprocessing of Reduced Resolution products and for the reprocessing of Full Resolution products. This reprocessing quality is required for CCI-LC.

The radiometric calibration as described below is a non-linear process including several steps. The radiometric gains are the second last step before the L1b are written. However, the last step is the straylight correction which is a non-linear process and not revertible from L1b product. The improved Calibration is therefore only an approximation.

The valid MERIS samples are digital counts resulting from the detection and acquisition by MERIS of a bi-dimensional field of spectral radiance in front of the instrument. The objective of the radiometric processing, together with the stray light correction, is to estimate that spectral radiance. An inverse model of the MERIS processing is used for that purpose, using parameters stored in the Characterisation and Radiometric Calibration data bases and the MERIS samples themselves. The MERIS acquisition model may be described as:

$$X_{b,k,m,f} = NonLim_{b,m}\left[g\left(T_f^{VEU}\right)\left[A_{b,k,m}\left(L_{b,k,m,f} + G_{b,k,m}\left(L_{*,*,*,f}\right)\right) + Sm_{b,k,m,f}\left(L_{b,k,m,*}\right)\right] + g_c\left(T_f^{CCD}\right)C^0_{b,k,m}\right] + \varepsilon$$

eq. 4-1

where

- m is the camera (or module); b is the spectral band; k is the pixel column; f is a frame (processing unit of number of image lines)
- $X_{b,k,m,f}$ is the MERIS raw sample
- $NonLim_{b,m}$ is a non-linear function, representing the non-linear transformations which take place in the CCD, amplifier and A/D converter; NonLin depends on band and gain settings
- T_f^{VEU} is the temperature of the MERIS amplifiers (VEUs) at the time of frame f
- T_f^{CCD} is the temperature of the MERIS detectors (CCDs) at the time of frame f
- g and g_c are (dimensionless) temperature correction functions

© UCL-Geomatics 2016
This document is the property of the LAND_COVER_CCI partnership, no part of it shall be reproduced or transmitted without the express prior written authorization of UCL-Geomatics (Belgium).

- $AL_{b,k,m}$ the "absolute radiometric gain" in counts/radiance unit; AL depends on band & gain settings
- $L_{b,k,m,f}$ the spectral radiance distribution in front of MERIS
- $Sm_{b,k,m,f}$ the smear signal., due to continuous sensing of light by MERIS
- $C^{0}_{b,k,m}$ the calibrated dark signal (possibly including an on-board compensation), dependent on band and gain settings
- $G_{b,k,m}$ a linear operator (weighted sum) representing the stray light contribution to the signal. For a given sample, some stray light is expected from all the other samples in the module, spread into the sample by specular (ghost image) or scattering processes
- ε is a random process representative of the noise and measurement errors

This model is inverted during processing: The inverse of the absolute instrument gain $AL_{b,k,m}$ is applied to the valid samples of all bands after dark and smear signal subtraction, with a compensation for the estimated temperature which is expressed as a function of time:

$$R_{b,k,m,f} = \left(AL_{b,k,m}\right)^{-1}\left\{\left(X'_{b,k,m,f} - S_{b,k,m,f}\right)\cdot\left[g_0 + g_1\left(t_f - t_{ref}\right) + g_2\left(t_f - t_{ref}\right)^2\right] - C_{b,k,m,f}\right\}$$

eq. 4-2

where $R_{b,k,m,f}$ are the spectral radiances before the straylight correction. The CoastColour Improved calibration is assuming the final straylight corrected radiances as equal to this $R_{b,k,m,f}$.

Coherent noise equalisation

The MERIS equalization module performs a radiometric equalisation of the MERIS L1b products. It reduces detector-to-detector and camera-to-camera systematic radiometric differences and results into a diminution of the vertical stripping observed on MERIS L1b products. The MERIS swath is imaged by a CCD. The radiance at each pixel of a MERIS L1b products results from the measurements of 5 cameras spread across the swath, each one imaging a part of the swath with 740 so-called detectors in FR (corresponding to 185 mean detectors in RR). This results into 3700 detectors imaging the swath of MERIS FRS product (925 in RR). The response of each one of these detectors is calibrated during the routine operation of the instrument. Residual uncertainties in the calibration process result into detector-to-detector and camera-to-camera systematic radiometric differences. The equalisation corrects for these radiometric differences via a set of detector dependant coefficients correcting for the residual uncertainties in the calibration process. These coefficients are retrieved via a methodology described by Bouvet and Ramino, [Bouvet and Ramoino, 2010], based on observations of the Antarctica plateau spread out throughout the MERIS mission lifetime.

The coefficients are different for MERIS Reduced and Full Resolution products. While the compilation of a full mission data set in reduced resolution, and subsequently the calculation of the noise equalisation coefficients, this process is not yet completed for full resolution data. Consequently the coherent noise equalisation is not included in the CoastColour Preliminary Processing [Bouvet and Ramoino, 2010].

© UCL-Geomatics 2016
This document is the property of the LAND_COVER_CCI partnership, no part of it shall be reproduced or transmitted without the express prior written authorization of UCL-Geomatics (Belgium).

Smile correction

MERIS is measuring the reflected sun light using CCD technique. A CCD is measuring in one of its dimensions one image line, and in the other dimension the spectrally dispersed radiance for each pixel along the image line. I.e., the spectral measurements of each pixel along an image line is made by it's own set of sensors of the CCD. This causes small variations of the spectral wavelength of each pixel along the image. This is called the "smile effect".

The MERIS instrument is composed of 5 cameras, each equipped with it is own CCD sensor. The variation of the wavelength per pixel is in order of 1nm from one camera to another, while they are in the order of 0.1nm within one camera.

Even though this variation is small compared to the spectral bandwidth of a band, which is typical 10nm, and can hardly be seen in an image, it can cause disturbances in processing algorithms which require very precise measurements, for example the retrieval of chlorophyll in the ocean. These disturbances can result in visual artefact ("camera borders") or reduced accuracy of the Level 2 products. Therefore, the MERIS Level 2 processor corrects the smile effect. The Level 1b product is not smile corrected, because this product shall provide the user exactly what the instrument is measuring, and that is in fact the radiance at the given wavelength of each pixel.

The smile correction consists actually of two parts: a radiance correction and a reflectance correction. The reflectance correction consists of an estimation of the reflectance spectral slope from the measurements in two neighbouring bands, and the interpolation of the reflectance along this slope from the actual pixel wavelength to the nominal wavelength of the considered band. It is defined in an external configuration data file, which bands will be corrected, and which bands are used for the slope estimation. The smile corrected reflectance $\rho_{sm-corr}$ is calculated according to:

$$\rho_{slope} = \frac{\rho_{brr}(b_2) - \rho_{brr}(b_0)}{\lambda_{pix}(b_2,\ detector(j)) - \lambda_{pix}(b_0, detector(j))}$$

$$\rho_{sm-corr}(b_1) = \rho_{brr}(b_1) + \rho_{slope} \cdot (\lambda_{nom}(b_1) - \lambda_{pix}(b_1, detector(j)))$$

eq. 4-3

where

- ρ_{brr} is the Bottom-of-Rayleigh reflectance
- λ_{pix} is the wavelength per pixel
- λ_{nom} is the nominal wavelengths
- $detector(j)$ is the the detector index at the pixel location of the spectra
- b_1 is the band index of reflectance to be corrected
- b_2 is the upper band index for interpolating the slope
- b_0 is the lower band index for interpolating the slope
- ρ_{slope} is the slope of reflectance

© UCL-Geomatics 2016
This document is the property of the LAND_COVER_CCI partnership, no part of it shall be reproduced or transmitted without the express prior written authorization of UCL-Geomatics (Belgium).

4.2.2 PROBA-V and SPOT VGT P

Quantitative algorithms, which exploit the spectral shape and magnitude, require the spectral and radiometric calibrations as key activities. The quality of the spectral and the radiometric calibration of the SPOT VGT P as well as PROBA-V sensors are carefully monitored by the satellite data provider. Furthermore the calibration information released by VITO has been taken into account. The consistency of TOA reflectance values of SPOT VGT P and MERIS RR has been assessed over the CEOS LandNet sites and other stable areas. A more detailed description can be found in the CCI-LC PVASR [Ph1_PVASRv2.0, 2012].

In case of PROBA-V, the spectral correction function will be applied to calculate the equivalent SPOT VGT P measurements. As a result, the processing chain will be the same as for Spot-VGT P [Dierckx et al., 2015].

Spectral correction function [Dierckx et al., 2015]:

The top-of-atmosphere reflectance values of PROBA-V can be transformed to the top-of-atmosphere reflectance values of SPOT VGT P using the spectral correction function as follows:

$$\rho_{SPOT-VGT\ band\ i} = slope_i \cdot \rho_{PROBA-V\ band\ i} + offset_i$$

eq. 4-4

where Band i = Blue, Red, NIR, SWIR.

Table 4-1 TOA spectral correction functions between PROBA-V and SPOT VGT [Dierckx et al., 2015]

	OFFSET	SLOPE	AGREEMENT COEFFICIENT	RMSE
BLUE	0.0034	0.9971	0.999	0.0032
RED	0.0029	0.9983	0.999	0.0030
NIR	0.0024	1.0005	0.999	0.0031
SWIR	0.0062	1.0214	0.986	0.0100

4.2.3 AVHRR

The quality of the spectral and the radiometric calibration of AVHRR sensor are monitored carefully by the satellite data provider. Therefore, we will take into account available documentation and findings (e.g. improved correction corrections) published in peer reviewed publications as well as follow calibration information released by NOAA. It is planned to assess consistency of TOA reflectance values of AVHRR and SPOT VGT P over the CEOS LandNet sites and other stable areas. With these actions, we will try to be up-to-date with most recent calibration, and we will be able to detect major anomalies.

© UCL-Geomatics 2016
This document is the property of the LAND_COVER_CCI partnership, no part of it shall be reproduced or transmitted without the express prior written authorization of UCL-Geomatics (Belgium).

Visible channel calibration of AVHHR [Kidwell, 1998]:

The percent albedo A_i measured by the sensor channel i is calculated as a linear function of the input data value C [counts] as follows:

$$A_i = S_i C + I_i \; and \; A_i^{norm} = A_i \cdot d^2_{sun/earth} / \cos(\theta_{sun})$$

$$d^2_{sun/earth} \approx \frac{1}{1 + 0.033 \, cos\left[\frac{2\pi d}{365}\right]}$$

eq. 4-5

where S_i and I_i are respectively, the scaled slope and intercept values, d the sun/earth distance in AU. The slopes and intercepts for AVHRR Channels 1 and 2 are included in the used IGBP USGS L1b products. To retrieve the spectral radiance R [W/(m^2-µm-sr)] from percent albedo A, the following equation have to be applied:

$$R_i = A_i \left[\frac{F_i}{100 \, \pi \, W_i}\right]$$

eq. 4-6

where F [W/m^2] is integrated solar spectral irradiance, weighted by the spectral response function of the channel and W is the equivalent width of the spectral response function µ.

Table 4-2: Values of W and F [Kidwell, 1998]

SATELLITE	W_1	F_1	W_2	F_2
NOAA-11	0.113	184.10	0.229	241.10
NOAA-14	0.136	221.42	0.245	252.29

Thermal channel calibration of AVHHR [Kidwell, 1998]:

The radiance E_i [mW/(m^2-sr-cm^{-1})] measured by the sensor channel i is calculated as a linear function of the input data value C [counts] as follows:

$$E_i = S_i C + I_i$$

eq. 4-7

where S_i and I_i are respectively, the scaled slope and intercept values. The slopes and intercepts for AVHRR Channels 3, 4 and 5 are included in the used IGBP USGS L1b products. To retrieve the brightness temperature from radiance E, the following equation has to be applied:

$$T(E_i) = \frac{c_2 \, \nu}{ln\left[1 + \frac{c_1 \nu^3}{E_i}\right]}$$

eq. 4-8

where T [K] is temperature for radiance value E, ν is the central wave number of the channel (cm^{-1}), and C_1 and C_2 are constants (C_1 = 1.1910659 x 10-5 mW/(m^2 sr cm^{-4}) and C_2 = 1.438833 cm K). The

© UCL-Geomatics 2016
This document is the property of the LAND_COVER_CCI partnership, no part of it shall be reproduced or transmitted without the express prior written authorization of UCL-Geomatics (Belgium).

central wave numbers (cm-1) for Channels 3, 4, and 5 as a function of temperature can be found in Table 4-3.

Table 4-3: NOAA-11 Central Wave Numbers for AVHRR IR Channels [Kidwell, 1998]

TEMPERATURE RANGE (K)	CHANNEL 3 (CM-1)	CHANNEL 4 (CM-1)	CHANNEL 5 (CM-1)
180-225	2663.50	926.81	841.40
225-275	2668.15	927.36	841.81
275-320	2671.40	927.83	842.20
270-310	2670.96	927.75	842.14
Note: The 270-310 K range is applicable for sea surface temperatures.			

To account for non-linearities in case of NOAA-11, the correction terms are provided in Table 4-4 and have to be added to the scene brightness temperatures computed from the linear calibration.

Table 4-4: Non-linearity errors for NOAA-11 Channel 4 and Channel 5

TARGET TEMPERATURE [K]	INTERNAL TARGET TEMPERATURE [°C]					
	NOAA-11 CHANNEL 4			NOAA-11 CHANNEL 5		
	10	**15**	**20**	**10**	**15**	**20**
320	4.29	3.71	3.25	1.43	1.26	1.12
315	3.50	2.98	2.55	1.23	1.03	0.89
310	2.85	2.33	1.91	1.05	0.84	0.70
305	2.23	1.73	1.32	0.85	0.64	0.47
295	1.05	0.68	0.22	0.43	0.28	0.09
285	0.24	-0.21	-0.67	0.07	-0.07	-0.23
275	-0.45	-0.79	-1.15	-0.19	-0.34	-0.47
265	-1.06	-1.37	-1.66	-0.37	-0.51	-0.60
255	-1.41	-1.72	-2.03	-0.60	-0.77	-0.78
245	-1.70	-1.96	-2.22	-0.72	-0.90	-0.92
235	-1.87	-2.10	-2.28	-0.84	-1.02	-1.00
225	-1.90	-2.14	-2.36	-0.94	-1.06	-1.16
215	-1.82	-2.02	-2.20	1.43	1.26	1.12
205	-1.54	-1.76	-1.98	1.23	1.03	0.89

To account for non-linearities in case of NOAA-14, an alternate method of handling the-non-linearity has been proposed, which can be applied to radiances instead of brightness temperatures. This method can be also applied to the AVHRR data of NOAA-11 [Walton et al., 1998] [Steyn-Ross et al., 1992].

© UCL-Geomatics 2016
This document is the property of the LAND_COVER_CCI partnership, no part of it shall be reproduced or transmitted without the express prior written authorization of UCL-Geomatics (Belgium).

As was the case with previous instruments, gain and slope calibration coefficients for each channel are imbedded in the Level 1b data stream which allows the user to perform a linear calibration. However, these coefficients are derived using a non-zero radiance of space, R_{sp} which is a constant for each channel and which makes the radiance corrections independent of the internal calibration target temperature. The slope and intercept coefficients are derived with the following equation:

$$G = \frac{R_T - R_{sp}}{C_T - C_{sp}} \; and \; I = R_{sp} - G \cdot C_{sp}$$

eq. 4-9

where G is the slope, I is the intercept, R_T is the radiance of the target, C_T is the counts of the target, and C_{sp} is counts of space. These coefficients provide a linear radiance, R_{lin}: where C is the counts of the channel:

$$R_{lin=} G \cdot C + I$$

eq. 4-10

The following equation provides a corrected radiance, RAD, for AVHRR channels 3, 4 and 5 which is a function only of the linear radiance:

$$RAD = A \cdot R_{lin} + B \cdot R_{lin}^2 + D$$

eq. 4-11

The regression coefficients (A, B and D) to apply this equation for NOAA-11 AVHRR Channels 3, 4 and 5 are contained in Table 4-7 as well as for NOAA-14 AVHRR Channels 3, 4 and 5 are contained in Table 4-5. This corrected radiance can be converted to the brightness temperature [W/(m^2-µm-sr)] temperatures using the following equation:

$$T(E_i) = \frac{c_2 \, \nu}{ln\left[1 + \frac{c_1 \nu^3}{E_i}\right]}$$

eq. 4-12

where T [K] is temperature for radiance value E, ν is the central wave number of the channel (cm^{-1}), and C_1 and C_2 are constants (C_1 = 1.1910659 x 10-5 mW/(m^2 sr cm^{-4}) and C_2 = 1.438833 cm K). The central wave numbers (cm-1) for Channels 3, 4, and 5 as a function of temperature can be found in Table 4-3 or Table 4-6.

Table 4-5: Radiance correction coefficients for NOAA-14 AVHRR Channels 3, 4, and 5

RADIANCE CORRECTION COEFFICIENTS	CHANNEL 3	CHANNEL 4	CHANNEL 5
A	1.00359	0.92378	0.96194
B	0.0	0.0003822	0.0001742
D	-0.0031	3.72	2.00
Radiance of Space, Rsp	0.0069	-4.05	-2.29

© UCL-Geomatics 2016
This document is the property of the LAND_COVER_CCI partnership, no part of it shall be reproduced or transmitted without the express prior written authorization of UCL-Geomatics (Belgium).

Table 4-6: NOAA-14 Central Wave Numbers for AVHRR IR Channels [Kidwell, 1998]

Temperature Range (K)	Ch. 3 (cm-1)	Ch. 4 (cm-1)	Ch. 5 (cm-1)
190-230	2638.652	928.2603	834.4496
230-270	2642.807	928.8284	834.8066
270-310	2645.899	929.3323	835.1647
290-330	2647.169	929.5878	835.374
Note: The 270-310 K range is applicable for sea surface temperatures.			

Table 4-7: Radiance correction coefficients for NOAA-11 AVHRR Channels 3, 4, and 5

Radiance Correction Coefficients	Channel 3	Channel 4	Channel 5
A	1.0	0.8412000	0.9460000
B	0.0	0.0008739	0.0002504
D	0.0	7.2100000	2.9200000
Radiance of Space, Rsp	-	-8.0500000	--3.5100000

4.2.4 Pseudo-code representation

This subsection provides an overview of the radiometric calibration from the software development point of view. A more detailed description of the logical flow and individual processing steps can be found in the CCI Land Cover DPM [Ph1_DPMv2.2, 2013]. Furthermore the input and output products being used within the LC-CCI processing modules are described in the CCI Land Cover IODD [Ph1_IODDv1.0, 2013] in more detail.

Coherent noise equalisation - MERIS

```
algorithm coherent_noise_equalisation is
    input: the equalisation coefficients, array coeff[]
              (from auxdata file: [Bouvet and Ramoino, 2010])
           the reflectance to be equalised, rho
           the Julian Date, date
    output: the equalised reflectance, rho_Eq
    return rho_Eq
```

Algorithm 4-2: Coherent Noise Equalisation

Smile correction - MERIS

```
algorithm smile_correction is
    input:  the spectrum of Bottom-of-Rayleigh reflectances, array rhoBrr[]
```

© UCL-Geomatics 2016
This document is the property of the LAND_COVER_CCI partnership, no part of it shall be reproduced or transmitted without the express prior written authorization of UCL-Geomatics (Belgium).

```
            the band index, b
            the upper band indices for slope computation, array upperIndex[]
                        (from auxdata file: [Ph1_IODDv1.0, 2013], section 5.5)
            the lower band indices for slope computation, array lowerIndex[]
                        (from auxdata file: [Ph1_IODDv1.0, 2013], section 5.5)
            the detector index, d
            a land/water indicator, isLand
            the pixel wavelengths, array pixWvl[]
                        (from auxdata file: [Ph1_IODDv1.0, 2013], section 5.5)
            the nominal wavelengths, array nomWvl[]
                        (from auxdata file: [Ph1_IODDv1.0, 2013], section 5.5)
    output: corrected reflectance for given band index, rhoSmCorr_b
    return rhoSmCorr_b
```

Algorithm 4-3: Smile correction

4.3 Additional pre-processing step for the PROBA-V S1 TOA data

The PROBA-V S1 TOA data are synthesise products, which do not include the observation time on a pixel-basis. Therefore the observation time (UTC) has to be calculated based on the azimuth angle and the longitude as follows:

$$\mathrm{TIME} = \frac{WOZ - \frac{lon}{15} - \frac{E_T}{60}}{24}$$

$$\mathrm{HOUR} = INTEGER[24 \cdot TIME]$$

$$\mathrm{MINUTE} = INTEGER[60 \cdot (24 \cdot TIME - HOUR)]$$

$$\mathrm{SECOND} = INTEGER\left[3600 \cdot \left(24 \cdot TIME - HOUR - \frac{Minute}{60}\right)\right]$$

$$\Gamma = \frac{2\pi \cdot (d-1)}{365}$$

$$\delta = 0.006918 - 0.399912\cos\Gamma + 0.070257\sin\Gamma - 0.006758\cos 2\Gamma + 0.000907\sin 2\Gamma - 0.002697\cos 3\Gamma + 0.00148\sin 3\Gamma$$

$$E_T = 229.18312 \cdot (0.000075 + 0.001868\cos\Gamma - 0.032077\sin\Gamma - 0.014615\cos 2\Gamma - 0.04089\sin 2\Gamma)$$

$$\mathrm{WOZ} = \frac{12 \cdot SAA}{\pi} + 12$$

eq. 4-13

© UCL-Geomatics 2016
This document is the property of the LAND_COVER_CCI partnership, no part of it shall be reproduced or transmitted without the express prior written authorization of UCL-Geomatics (Belgium).

where d is the day number (DOY), such that d = 1 on the 1st January, lon is the longitude [degree], Γ is the Day angle, δ is the declination, E_T is the equation of time, WOZ is the "true local time" and SAA is the sun azimuth angle [rad] (it has the origin at due south, measures angles clockwise, so that due east is negative and west positive).

4.4 Land water delineation and cloud screening - pixel identification

The Multi Sensor Pixel Identification approach (which is also applied in the GlobAlbedo project) classifies each pixel to be processed according to a series of pixel categories, which include cloud, clear-land, clear-water and clear-snow. Cloudy pixels are not processed in CCI-LC project, while land, water and snow pixels must be distinguished because of the particular processing steps associated to each surface type. In particular, water pixels must be separated from land surfaces even in the case of continental water bodies, as these are flagged in the final pre-processed product. Snow and snow-free surfaces will also be considered separately in the final pre-processed product.

The Pixel Identification approach has been will be applied to MERIS FR and RR, AVHRR SPOT VGT P as well as PROBA-V data.

4.4.1 Pixel identification

The term "Pixel identification" refers to a classification of a measurement made by a space borne radiometer, for the purpose of identifying properties of the measurement which are influencing further algorithmic processing steps. Most importantly is the classification of a measurement as being made over cloud, a clear sky land surface or a clear sky ocean surface. The term "pixel" is often used for such a measurement in order to express it being part of a spatially oriented collection of many measurements, which all are geo- located and which form, as a whole, an image of the earth below the satellite.

While the information if a pixel is made over water or land can be taken from a static map, provided the geo-location of the pixel is better than the size of the pixel, as a good first guess, the cloud coverage is spatially and temporally highly variable and needs to be derived from the measurement itself. After knowing whether a pixel is cloudy or clear, in the clear sky case the land-water information can be refined using the measurement. This is particularly necessary in the coastal zone where the actual land-water boundary is changing due to tides, when the pixel size is small enough to resolve this difference. Also maps are not always correct so that a radiometric refinement is advisable.

4.4.2 Background

A large portion of the earth surface is covered by clouds [Paperin and Brockmann, 2007]. Consequently, most earth observation images in the visible spectral domain include a significant amount of cloudy pixels. Such measurements are treated in two opposite ways: either cloud properties are retrieved , e.g. for weather forecast or climate studies ([Wylie, 1998], [Rossow and Schiffer, 1999], [Liou, 1992]), or the focus of the interest is the earth surface – being it land or water – which is then masked by the cloud [Luo et al., 2008]. In the latter case, the presence of the cloud needs to be identified, and the change of the surface reflectance due to the cloud has to be estimated.

© UCL-Geomatics 2016
This document is the property of the LAND_COVER_CCI partnership, no part of it shall be reproduced or transmitted without the express prior written authorization of UCL-Geomatics (Belgium).

An image pixel can be cloud free, totally cloudy, or partly cloudy. In the cloud free case there are no water droplets or ice crystals in the atmosphere which change the surface reflectance. In the totally cloudy case the optical thickness is so high that the portion of surface reflectance at the signal measured by the satellite is negligible. The partly cloudy case comprises all intermediate situations where the measured reflectance is a mixture of a significant portion of the surface reflectance, but modified due to the presence of a cloud. This can be either due to an optically thin cloud, or the cloud is covering only a fraction of a pixel in the field of view of the sensor [GlobAlbedo_ATBD/CLv1.0, 2013].

Cloud free and totally cloudy pixels can be identified rather easily, and most of the tests used in earth observation processing systems for cloud identification today, assign either of these two stages, and hence also partly cloudy cases have to be assigned to either of these two classes [Eumetsat, 2006]. For spatial high resolution instruments such a binary cloud flag is not appropriate if several different higher level processing algorithms are applied, each of which having a different robustness to partial cloudy pixel [Brockmann et al., 2008]. Some novel algorithms therefore deliver a graduated scale, as an indicator of the extent to which a signal is influenced by the presence of clouds ([Schiller et al., 2008], [Gomez-Chova et al., 2007], [Merchant et al., 2006]). Such an indicator can be related to cloud properties, e.g. apparent cloud optical thickness, the atmospheric transmission ([Schiller et al., 2008], or cloud features ([Schiller et al., 2008].

Clouds have certain characteristics which can be used for their identification and characterisation [Luo et al., 2008]: brightness, whiteness, cold temperature and high altitude. However, none of these characteristics is always given if a pixel is cloudy; this is the main problem of cloud identification.

Thin clouds are difficult to differentiate from bright land surfaces and clouds in the mountains can be lower than the mountain ridges around. Then other methods not based on the features given below must be used. In particular, the clouds can be also detected using the spatial and temporal variability of the reflected radiation. In addition, clouds screen the tropospheric gases. This leads to the increase in the reflection inside corresponding gaseous absorption bands (e.g. H_2O, CO_2, O_2) which is routinely used for the cloud top height monitoring [Fischer et al., 2000].

One way to detect clouds would be to work directly with optical measurements. Further, derived cloud physical properties can be used to characterise clouds and assess their impact on the retrieved signal. This includes, amongst others, cloud fraction, cloud top temperature, cloud top pressure, cloud type, cloud phase, cloud optical depths and cloud effective particle size. Such properties can be studied using the radiative transfer modelling. Extensive work in this respect over the past years can be found in the literature ([Fischer et al., 2000], [Fischer et al., 2000b], [Muller and Fischer, 2007], [Rathke et al., 2002], [Brenguier et al., 2000] and [Pawlowska et al., 2000]). They have developed the MERIS algorithms for cloud top pressure, cloud optical thickness, cloud albedo and cloud type retrieval and have translated this knowledge into a probability based cloud detection algorithm [[GlobAlbedo_ATBD/CLv1.0, 2013].

Cloud detection became important with the systematic processing of the NOAA AVHRR instrument in the 1980s. Statistical histogram analysis methods were developed [Phulpin et al., 1983]. Most common used were threshold algorithms (e.g. in [Saunders and Kriebel, 1988]). Large scale textures were identified using pattern recognition techniques [Garant and Weinman, 1986]. These methods worked quite well over the ocean but exposed problems in Polar Regions (separation of clouds from

© UCL-Geomatics 2016
This document is the property of the LAND_COVER_CCI partnership, no part of it shall be reproduced or transmitted without the express prior written authorization of UCL-Geomatics (Belgium).

ice and snow) and in the tropics (low level, warm clouds). A good overview of the cloud screening techniques at the late 80s is given in [Goodman et al., 1988]. Improved methods are later proposed for the AVHRR and for ATSR.

The cloud screening algorithms for the ATSR 1 and 2 in the 1990s were mainly based on previous work for AVHRR and use spectral threshold tests [Birks et al., 2007]. The thermal band at 12µm is used as main tool to identify the cold cloud surface by a threshold, supported by other thresholds on band differences and on the histogram of the radiance distribution in the image. The unique feature of two views under different angles of the same pixel and the spatial coherence of the radiance are also exploited. The cloud screening of the AATSR is basically the same with refined and additional tests due to additional bands. Recently, tests on vegetation and snow indices have been introduced [Birks et al., 2007]. However, application oriented projects are not satisfied with the standard cloud screening and are proposing alternative methods, for example for the GlobCarbon processing.

The MERIS Level 2 cloud screening is a combination of 8 different tests [Santer et al., 2007]. Three of those are classical threshold tests on spectral radiances or differences, and five are connected with the pressure estimates derived from the differential oxygen A-band absorption measurements. However, due to the current insufficient quality of the standard pressure products derived from the measurements, these tests are not used.

The potential of the O_{2A} feature has been addressed recently in ESA funded projects, namely "Exploitation of the oxygen absorption band" and "MERIS AATSR Synergy". The result of these activities has led to an upgrade of the operational MERIS pixel classification in the third reprocessing. Major improvement is due to including dedicated pressure algorithms for detection of the height of the scattering surface over land and ocean.

The strong water vapour absorption at 1.38µm can be used to detect the presence of high clouds, including thin cirrus under daytime viewing conditions. With sufficient atmospheric water vapour in the beam path, almost no upwelling reflected radiance from the earth's surface reaches the satellite which is in particular handy for snow covered surfaces. However, precipitable water is often less than 1 cm over polar and in high elevation regions. The 1.38 µm reflectance threshold is set to 0.03 for MODIS [Ackerman et al., 2006].

A big problem is the distinction between clouds and snow/ice, in particular for instruments which do not have spectral bands in the NIR and SWIR. An extensive study including the cloud screening over snow and ice has been undertaken ([Aoki et al., 2007], [Hori et al., 2007], [Stamnes et al., 2007]). Snow and ice are less reflective in the NIR spectral region, and the so called normalized differentiation ice index (NDII) and the corresponding snow index (NDSI) is a good tool to differentiate clouds from snow and ice. These indices are defined as follows:

$$NDII = \frac{R(0.545\mu m) - R(1.050\mu m)}{R(0.545\mu m) + R(1.050\mu m)}; NDSI = \frac{R(0.545\mu m) - R(1.640\mu m)}{R(0.545\mu m) + R(1.640\mu m)}$$

eq. 4-14

The reflectance for ice decreases with the wavelength must faster as compared to snow. Therefore, large values of NDII signify the bare ice case.

© UCL-Geomatics 2016
This document is the property of the LAND_COVER_CCI partnership, no part of it shall be reproduced or transmitted without the express prior written authorization of UCL-Geomatics (Belgium).

Also measurements of trace gas vertical columns (e.g., SCIAMACHY on-board ENVISAT) are disturbed by cloud presence because corresponding instruments have large fields of view to enhance the sensitivity to small gaseous concentrations. Cloud clearing algorithms are described for GOME in [Cervino et al., 2000], and [Kokhanovsky et al., 2008] reports on using MERIS to support the cloud screening for SCIAMACHY.

4.4.3 Methods

Cloud detection methods can be categorized in the following classes [Brockmann et al., 2008]:

Spectral threshold methods

Spectral characteristics, such as temperature, brightness, whiteness or height of the scatterer are tested against a threshold value. The threshold can be parameterized by viewing geometry, location or time. Most cloud screening algorithms given in the reference list include such tests.

A special subsection of these tests concern spectral high resolution methods. Feature selection or PCA pre-processing is sometimes applied to reduce the dimensionality of the dataset ([Lavanant et al., 2005], [McNally et al., 2003], [Rathke et al., 2002b] and [Susskind et al., 1998]).

Feature extraction and classification

The spectral data space, if transformed into a feature space, can be statically or dynamically (i.e. scene dependent) separated into cloud or clear classes. This group of algorithms also includes spatial structure based algorithms. Examples are given [Gomez-Chova et al., 2007].

Learning algorithms

The Bayesian probability approach and general data mining techniques are employed. Cloud probability or cloudiness index values are generated after training the algorithm with simulated or measured data. Examples are given in ([Merchant et al., 2005], [Gomez-Chova et al., 2007]) for AATSR and in [Schiller et al., 2008] for MERIS. A generic approach of a learning algorithm has been developed [Colapicchioni et al., 2004].

Multi-temporal analysis

Pixels are not always cloud covered and a time series of data is used to separate cloudy from clear cases. For example, such kind of method is applied in the Cyclopes processing [Shi et al., 2007].

Multi-sensor approach

In cases, where multiple sensors are on the same platform and perform simultaneous measurements, the synergetic algorithms can be used to better identify clouds. This was considered, for example, in the case of MERIS and SCIAMACHY [Kokhanovsky et al., 2008] and MISR and MODIS [Shi et al., 2007].

As it follows from the discussion given above, the screening procedures are of great importance for successful retrievals of snow properties from space.

© UCL-Geomatics 2016
This document is the property of the LAND_COVER_CCI partnership, no part of it shall be reproduced or transmitted without the express prior written authorization of UCL-Geomatics (Belgium).

4.4.4 Theoretical description

The current operational detection of clouds in SPOT-VGT data relies on spectral threshold tests using the reflectance in the blue and SWIR bands [Lissens et al., 2000]. Different threshold combinations are used to identify cloudy and clear pixels. A pixel which does not pass either test is declared uncertain. A snow mask is calculated using spectral threshold tests on the red and MIR channels combined with 3 spectral slope tests which exploit the lower scattering of snow in MIR and SWIR bands compared with clouds. A cloud shadow is finally added based on an estimation of a potential cloud shadow and a test on the NDVI of concerned pixels.

Current MERIS cloud screening uses spectral thresholds on shortwave bands, complemented by spectral slope tests in order to recover bright land surface and snow [Santer, 1997]. In the current reprocessing of MERIS these cloud and snow tests are significantly changed and improved [Bourg et al., 2011b] by adding tests on the height of the scattering surface (based on the oxygen absorption measurements in MERIS band 11), and new tests for snow and ice detection using the MERIS Differential Snow Index (MDSI), based on the ratio of bands 13 (865nm) and 14 (885nm).

Both MERIS and AATSR cloud screening are not optimal because of missing spectral information in each of the single instrument (SWIR and TIR bands in MERIS, O_2 and water vapour bands in AATRS). In the framework of the MERIS – AATSR synergy project an algorithm has been developed that combines the data from both instruments [Gomez-Chova et al., 2009]. A thorough analysis has been undertaken on the information content w.r.t to cloud detection in both instruments, and a set of 19 features has been identified as optimal with respect to the number of features (which should be kept low) and information content. These features include the spectral reflectances of the two instruments, and a number of band combinations. The cloud screening algorithm is a combination of feature extraction and supervised classification and spectral unmixing. The training vectors for the supervised classification have been obtained from a database of radiative transfer calculations. The results of the algorithm are a binary cloud mask resulting from the feature tests and a cloud abundance values (between 0 and 1) from the unmixing. These two values can be used by subsequent algorithms to decide if a pixel can be processed, or a final logic is applied to conclude on the pixel status.

A critical step for the synergistic use of MERIS and AATSR is the collocation of the products. Due to the high spatial and temporal dynamic of clouds, misalignment of the two data sets would impact the cloud retrieval. Figure 4-2 shows the steps included in the pre-processing of the data of the two instruments.

Neither of the single instrument algorithms discussed in the previous section is considered of sufficient quality for the purpose of the GlobAlbedo project. The MERIS and AATSR cloud screening algorithms have been criticised on the MERIS-AATSR user workshops, and also the SPOT-VGT algorithm does not screen out sufficiently the doubtful cloudy pixels. The reason is that the global Level 2 algorithms cannot be too severe in order to permit analysis of single Level 2 products. On the contrary, for a Level 3 product such as the albedo, a clear sky conservative (i.e. severe cloud screening) approach is required. Even a small number of undetected clouds can significantly impact the final albedo product. This has been demonstrated in the MERIS GlobAlbedo and the GlobCover projects [Arino et al., 2008].

© UCL-Geomatics 2016
This document is the property of the LAND_COVER_CCI partnership, no part of it shall be reproduced or transmitted without the express prior written authorization of UCL-Geomatics (Belgium).

The synergistic method presented in [Gomez-Chova et al., 2009] is a significant improvement. It exploits optimally all features available in both instruments and combines these in a non-linear, self-trained mathematical way. The comparison shown in the MERIS-AATSR-Synergy Project demonstrates the improvements compared to the standard MERIS and AATSR algorithms.

However, for the CCI-LC a synergistic use of MERIS and AATSR is not foreseen because of (1) the limitation of AATSR to the centre of the MERIS swath, thus not providing data for half of the MERIS swath and (2) the overall design of the processing architecture which does not foresee multi-sensor processing at this stage. The first point will change with SENTINEL 3, and the latter point could of course be resolved if AATSR would be included.

The CCI-LC pixel classification is a unique method, adapting the principles and mathematical implementation of several of the above approaches and features provided by the MERIS and SPOT-VGT, each treated separately.

In a first step the features will be combined in a logical order of a sequence of threshold tests, but working on and resulting in probability values between [0 … 1]. The combination will be done by arithmetic operations, addition and multiplication. This extends the Boolean logic into a probabilistic space. If tests result in the extreme 0 and 1, the probabilistic calculations are identical with the Boolean expressions.

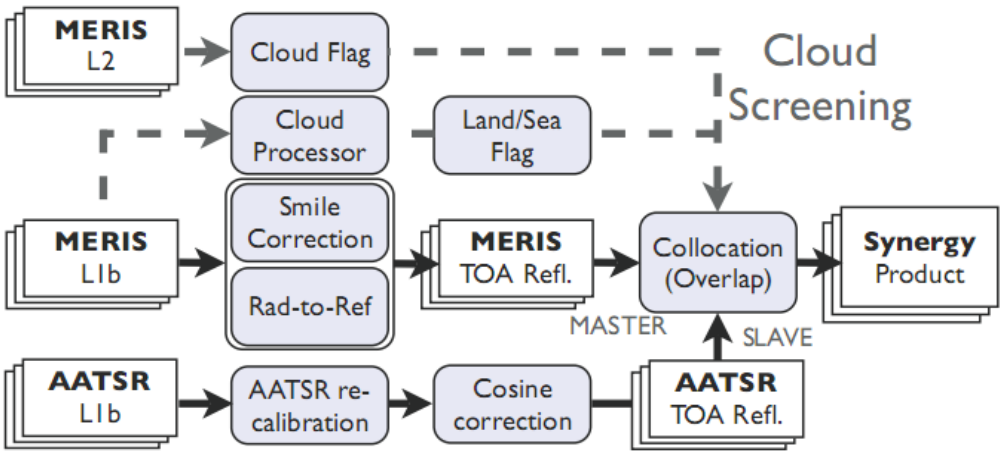


Figure 4-2: Flowchart of the MERIS and AATSR synergy pre-processing module

4.4.5 Practical consideration

4.4.5.1 *Overall principles*

The CCI-LC pixel identification is a unique classification for the MERIS FR, RR, SPOT-VGT, AVHRR and PROBA-V data considered (Figure 4-3). The uniqueness consists of a certain set of features, which are calculated for each instrument and probabilistic combination of these features in order to calculate a set of pixel classification attributes. The implementation how the features are

© UCL-Geomatics 2016
This document is the property of the LAND_COVER_CCI partnership, no part of it shall be reproduced or transmitted without the express prior written authorization of UCL-Geomatics (Belgium).

calculated is instrument specific. This approach has the advantage to be easily extendable to other instruments, and it is also applied in the GlobAlbedo project, where additionally AATSR is used.

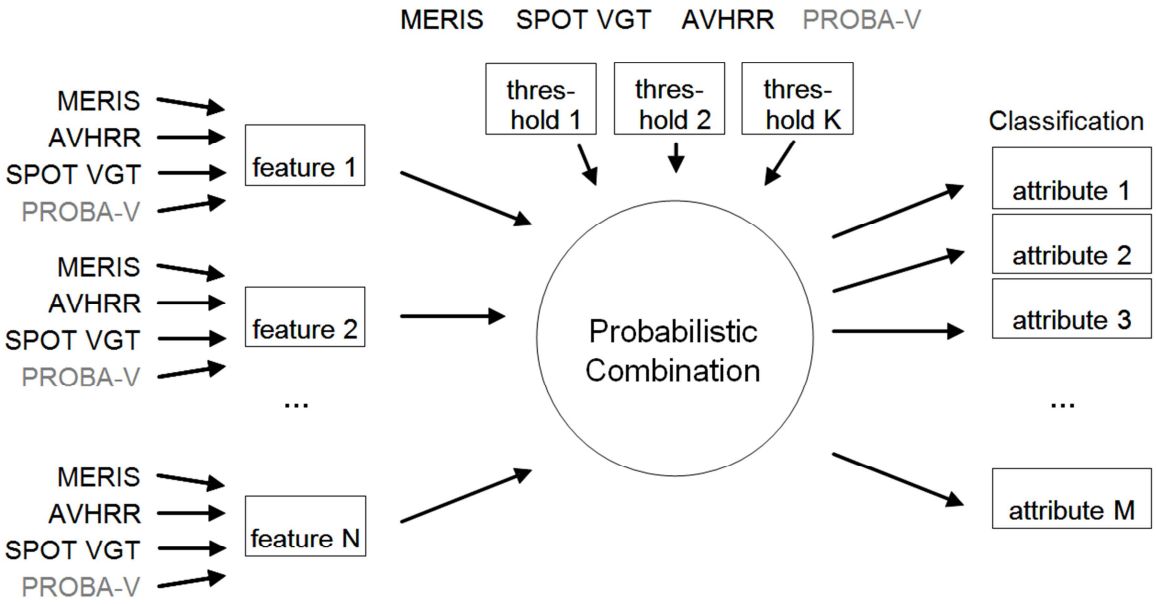


Figure 4-3: Unified Pixel Classification Scheme

4.4.5.2 *Probabilistic arithmetic*

A feature is a probabilistic quantity with a value between 0 and 1, with the following meaning:

Table 4-8: Definition of values for classification features.

VALUE	MEANING
0	the feature is definitively not true
0.5	status of the feature not known
1	feature is definitively true

Features are combined by simple arithmetic averaging. Let's assume, as an example, two features, f1 and f2, which do have no dependency from each other, and both being an indication that a third feature, f3, is true. Then, f3 is the average of f1 and f2: f3 = (f1 + f2)/2

As a first example let's assume the case where we are 100% sure that both f1 and f2 are true, i.e. f1=f2=1.0 then also f3=1.0. Another example is when we are 100% about f1, but less sure about f2, let's say f2= 0.8. Then the resulting probability of f3 is f3=0.9. When don't know anything about f1, i.e. f1=0.5 but are sure that f2 is false, i.e. f2=0, then f3=0.25, i.e. quite likely that it is false. If f1=0 and f2=1, i.e. a contradiction, then f3=0.5, i.e. we can't say if it is true or false.

The introduction of the probability scale [0 … 1] has further the advantage that it enable decoupling of feature values from the instruments. It doesn't matter how a physical quantity is derived because it will be mapped to the interval [0 … 1]. For example, the brightness feature will be calculated from

© UCL-Geomatics 2016
This document is the property of the LAND_COVER_CCI partnership, no part of it shall be reproduced or transmitted without the express prior written authorization of UCL-Geomatics (Belgium).

top of atmosphere radiances in the case of MERIS, whereas it will be calculated from reflectances in the case of SPOT-VGT and PROBA-V. These are different physical quantities, but they are both scaled to [0 … 1].

The scaling from a physical quantity, such as radiance or temperature, to a probability value may include a non-linear mapping. This can express the (un-)certainty that we have in value ranges in the physical data space. For example, very low temperatures have a very high probability to be a cloud, whereas above a certain temperature value the probability decreases exponentially.

Not every feature can be calculated for every instrument. In such cases the feature value is constant equal to 0.5. This convention allows formulating the logical combination of features even if a feature is not available for a certain instrument, and hence the logical combination can be formulated instrument independently.

4.4.5.3 *Features*

The following features are used in the probabilistic combination, and how they are calculated for each instrument.

Table 4-9: Feature - Pixel identification

FEATURE	EXPLANATION
Pressure	Indicating a high altitude from where the photons are scattered. Can be derived from measurements in gaseous absorption bands, e.g. O2A or water vapour
NDVI	A high vegetation index is an indication of a (semi-) transparent atmosphere
NDSI	The NDSI is a meaningful quantity only above bright surfaces. Then it can be used to separate snow/ice from clouds
White	A bright and spectrally flat signal; can be a cloud or snow/ice
Spectral Flatness	A spectrally flat signal; The colour can be anything from black over grey to white.
Temperature	Temperature of the emitting surface; clouds can be very cold[5].
Bright	Brightness of the scattering surface
Glint Risk	The glint risk can be calculated from the observation geometry and wind speed, assuming a certain wave distribution (e.g. Cox and Munk). Glint and clouds are hardly separable and hence it is useful to identify glint risk in addition with the cloud/water classification[6]

[5] Temperature information is not available from MERIS and SPOT VGT as well as PROBA-V, but it is included as a feature in the logic because the overall approach is to be sensor independent; temperature is generally a very powerful criterion for cloud detection.

[6] CCI-LC requires atmospheric correction over water bodies; this implies cloud detection over water, which is problematic under sun glint conditions.

© UCL-Geomatics 2016
This document is the property of the LAND_COVER_CCI partnership, no part of it shall be reproduced or transmitted without the express prior written authorization of UCL-Geomatics (Belgium).

FEATURE	EXPLANATION
Radiometric Land Value	A classification of the surface type as land, provided that the pixel is clear and the measurement can be used to assess the surface type.
Radiometric Water Value	A classification of the surface type as water, provided that the pixel is clear and the measurement can be used to assess the surface type.
A priori Land Value	Classification of the pixel using a static background map and the geolocation of the pixel.
A priori Water Value	Classification of the pixel using a static background map and the geolocation of the pixel.

Feature Definition for MERIS

The index used in array notation below is starting with 0.

Table 4-10: Feature Definition for MERIS

FEATURE	MERIS	COMMENT

Pressure	if (isLand()) {
	press_value = (pbaro - p1)/1000.0;
	} else if (isWater()) {
	press_value =(pbaro - pscatt)/1000.0;
	}
		p1 and pscatt are apparent pressure products, defined in dedicated ATBDs from R. Santer, developed within the ESA O2 project. pbaro is the barometric pressure.

NDVI	value = brr[b753]-brr[b620])/ (brr[b753]+brr[b620]	brr is the reflectance corrected for gaseous absorption and Rayleigh scattering
NDSI	value = brr[b865]-brr[b885]) / (brr[b865]+brr[b885]	

White	if (brightValue()>BRIGHT_FOR_WHITE_THRESH) {
	white_value=spectralFlatnessValue();
	} else {
	white_value = 0;
	}	

© UCL-Geomatics 2016
This document is the property of the LAND_COVER_CCI partnership, no part of it shall be reproduced or transmitted without the express prior written authorization of UCL-Geomatics (Belgium).

FEATURE	MERIS	COMMENT
Spectral Flatness	slope0 = spectralSlope(brr[b412], brr[b 490]) slope1 = spectralSlope(brr[b560], brr[b620]) slope2 = spectralSlope(brr[b665], brr[b753]) spectralFlatness = 1.0f - Math.abs(1000.0 * (slope0 + slope1 + slope2) / 3.0);	
Temperature	0.5	
Bright	bright_value = brr[b442] /(6.0 * brr442Thresh)	brr442Thresh is a value read from a LUT; the LUT is a theoretical maximal reflectance for a given geometry and a bright land surface. It has been calculated by R. Santer and is available from the auxiliary data of the MERIS operational processor.
Glint Risk	Shall be calculated from geometry and wind speed from tie points. Not available in current IDEPIX version	currently set to FALSE

Radiometric Land Value	if {
	refl[b753] >= refl[620] && refl[620] > refl620_Land_Thresh
	}
	radiom_land_value = 1.0
	} else {
	radiom_land_value = 0.5
	}
		in case of cloudy pixel: radiom_land_value = 0.5

Radiometric Water Value	if {
	refl[b753] < refl[620] && refl[620] < refl620_Water_Thresh
	}
	radiom_water_value = 1.0
	} else {
	value = 0.5
	}
		in case of cloudy pixel: radiom_water_value = 0.5

© UCL-Geomatics 2016
This document is the property of the LAND_COVER_CCI partnership, no part of it shall be reproduced or transmitted without the express prior written authorization of UCL-Geomatics (Belgium).

FEATURE	MERIS	COMMENT

A priori Land Value	if (l1FlagLand) {
	return 1.0f;
	} else {
	return 0.0f;
	}	

A priori Water Value	if (!l1FlagLand) {
	return 1.0f;
	} else {
	return 0.0f;
	}	

Feature Definition for SPOT VGT and PROBA-V

- refl[0] … reflectance in band 0 at 450nm
- refl[1] … reflectance in band 2 at 645nm
- refl[2] … reflectance in band 3 at 835nm
- refl[3] … reflectance in band MIR at 1.6µm

Table 4-11: Feature Definition for SPOT-VGT and PROBA-V

FEATURE	SPOT VGT & PROBA V	COMMENT
Pressure	0.5	
NDVI	ndvi_value = (refl[2] - refl[1])/ (refl[2] + refl[1]	
NDSI	ndsi_value = refl[1] - refl[3])/ (refl[1] + refl[3])	

White	if (brightValue()>BRIGHT_FOR_WHITE_THRESH) {
	return spectralFlatnessValue();
	} else {
	return 0f;
	}
		The spectral flatness gives a high value even if the spectrum is black. In order to be an indicator for white, a minimum brightness is required.

Spectral Flatness	slope0 = spectralSlope(refl[0], refl[1]) slope1 = spectralSlope(refl[1], refl[2]) spectralFlatness = 1.0f - Math.abs(2000.0 * (slope0 + slope1)/2);	

© UCL-Geomatics 2016
This document is the property of the LAND_COVER_CCI partnership, no part of it shall be reproduced or transmitted without the express prior written authorization of UCL-Geomatics (Belgium).

FEATURE	SPOT VGT & PROBA V	COMMENT
Temperature	0.5	
Bright	bright_value = (refl[0] + refl[1])/2.0f	

Glint Risk	if (isWater() && isCloud() &&
	spectralSlope(refl[0], refl[1]) > GLINT_THRESH)
	{
	glint_risk = 1.0;
	} else {
	glint_risk = 0.0;
	}	

Radiometric Land Value	if (refl[2] ≥ refl[1] &&
	refl[2] > REFL835_LAND_THRESH) {
	radiom_land_value = 1.0;
	} else if (
	refl[2] > REFL835_LAND_THRESH) {
	radiom_land_value = 0.75f;
	} else {
	radiom_land_value = 0.25;
	}
		in case of cloudy pixel: radiom_land_value = 0.5

Radiometric Water Value	if (refl[0] > refl[1] &&
	refl[1] > refl[2] &&
	refl[2]<REFL835_WATER_THRESH) {
	value=1.0;
	} else {
	value = 0.25;
	}
		in case of cloudy pixel: radiom_water_value = 0.5

A priori Land Value	if (smLand) {
	return 1.0f;
	} else {
	return 0.0f;
	}	

© UCL-Geomatics 2016
This document is the property of the LAND_COVER_CCI partnership, no part of it shall be reproduced or transmitted without the express prior written authorization of UCL-Geomatics (Belgium).

FEATURE	SPOT VGT & PROBA V	COMMENT

A priori Water Value	if (!smLand) {
	return 1.0f;
	} else {
	return 0.0f;
	}	

Feature Definition for AVHRR7

- refl[0] … reflectance in band 1 at 580 – 680 nm
- refl[1] … reflectance in band 2 at 725 – 1100 nm
- refl[2] … reflectance in band 3b at 3.55 – 3.93 µm
- BT[0] … brightness temperature in band 3b at 3.55 – 3.93 µm
- BT[1] … brightness temperature in band 4 at 10.3 – 11.3 µm
- BT[2] … brightness temperature in band 5 at 11.5 – 12.5 µm

Table 4-12: Feature Definition for AVHRR

FEATURE	AVHRR	COMMENT
Pressure	not defined yet	
NDVI	ndvi_value = (refl[1] - refl[0])/ (refl[1] + refl[0])	
NDSI	ndsi_value = refl[0] - refl[2])/ (refl[1] + refl[2])	
White	not defined	
Spectral Flatness	not defined	
Temperature	not defined	
Bright	not defined	
Glint Risk	not defined	
Radiometric Land Value	not defined	

[7] Cloud screening based on CLAVR and Idepix, not all feature and feature thresholds of IdePix have to be defined, because the result of cloud screening is sufficient.

© UCL-Geomatics 2016
This document is the property of the LAND_COVER_CCI partnership, no part of it shall be reproduced or transmitted without the express prior written authorization of UCL-Geomatics (Belgium).

FEATURE	AVHRR	COMMENT
Radiometric Water Value	not defined	

A priori Land Value	if (smLand) {
	return 1.0f;
	} else {
	return 0.0f;
	}	

A priori Water Value	if (!smLand) {
	return 1.0f;
	} else {
	return 0.0f;
	}	

4.4.5.4 *Processing logic*

The following classification attributes (binary values, also named flags) are derived from the features with given logic. This logic is no longer instrument dependent.

Table 4-13: Processing logic

CLASSIFICATION ATTRIBUTE	DEFINITION	COMMENT
isCloud	return (whiteValue() + brightValue() + pressureValue() + temperatureValue() > CLOUD_THRESH && !isClearSnow())	The final binary cloud flag. A pixel is either Cloud, ClearLand or ClearWater.or ClearSnow
isClearSnow	return (isBrightWhite() && ndsiValue() > NDSI_THRESH)	isBrightWhite is defined below

isClearLand	if (radiometricLandValue() != 0.5) {
	landValue = radiometricLandValue();
	} else if (aPrioriLandValue() > 0.5) {
	landValue = aPrioriLandValue();
	} else {
	return false;
	// this means: if we have no information about land, we return isClearLand = false
	}
	return (!isCloud() && landValue > LAND_THRESH)
		If a radiometric land value is available, i.e. it is not the uncertainty value of 0.5, than this is used in the subsequent test. Otherwise the a priori land value is used in the test.
		The test simply compares the value with a threshold. The choice of the threshold depends on the user. If he wants to be really sure he should use a value close to 1.

© UCL-Geomatics 2016
This document is the property of the LAND_COVER_CCI partnership, no part of it shall be reproduced or transmitted without the express prior written authorization of UCL-Geomatics (Belgium).

CLASSIFICATION ATTRIBUTE	DEFINITION	COMMENT

isClearWater	if (radiometricWaterValue() !=0.5) {
	waterValue = radiometricWaterValue();
	} else if (aPrioriWaterValue() > 0.5) {
	waterValue = aPrioriWaterValue();
	} else {
	return false;
	// this means: if we have no information about water, we return isClearWater = false
	}
	return (!isCloud() && waterValue > WATER_THRESH);
		same logic as for the ClearLand test

isBrightWhite	return (whiteValue() + brightValue() > BRIGHTWHITE_THRESH)	A pixel that has one of the two characteristics, bright or white, has a potential to be cloudy. The stronger both features are the higher the probability.
isLand	return (aPrioriLandValue() > LAND_THRESH)	This is the surface type of the pixel, regardless if it is snow covered or if a cloud is above during measurement.
isWater	return (aPrioriWaterValue() > WATER_THRESH)	
isBright	return (brightValue() > BRIGHT_THRESH)	These tests map the real values of the features to binary flags
isWhite	return (whiteValue() > WHITE_THRESH)	
isCold	return (temperatureValue > TEMPERATURE_THRESH)	
isVegRisk	return (ndviValue() > NDVI_THRESH)	
isGlintRisk	return (glintRiskValue > GLINT_RISK_THRESH)	
isHigh	return (pressureValue() > PRESSURE_THRESH)	

© UCL-Geomatics 2016
This document is the property of the LAND_COVER_CCI partnership, no part of it shall be reproduced or transmitted without the express prior written authorization of UCL-Geomatics (Belgium).

4.4.5.5 *Thresholds*

The following table lists the nominal values for the scalar thresholds. It should be noted that these are subject to tuning and may change for the version used for product mass production.

Table 4-14: Thresholds

THRESHOLD	VALUE		
	MERIS	SPOT VGT & PROBA V	AVHRR[8], [9]
BRIGHTWHITE_THRESH	1.5	0.65	not defined
NDSI_THRESH	0.68	0.5	not defined
PRESSURE_THRESH	0.9	0.9	not defined
CLOUD_THRESH	1.65	1.65	not defined
UNCERTAINTY_VALUE	0.5	0.5	not defined
LAND_THRESH	0.9	0.9	not defined
WATER_THRESH	0.9	0.9	not defined
BRIGHT_THRESH	0.25	0.3	not defined
WHITE_THRESH	0.9	0.5	not defined
BRIGHT_FOR_WHITE_THRESH	0.8	0.2	not defined
NDVI_THRESH	0.7	0.4	not defined
TEMPERATURE_THRESH	0.9	0.9	not defined
REFL835_LAND_THRESH	n.a	0.15	not defined
REFL835_WATER_THRESH	n.a	0.1	not defined
GLINT_THRESH	n.a	0.000365	not defined

[8] Cloud screening based on CLAVR and Idepix, not all feature and feature thresholds of IdePix have to be defined, because the result of cloud screening is sufficient.

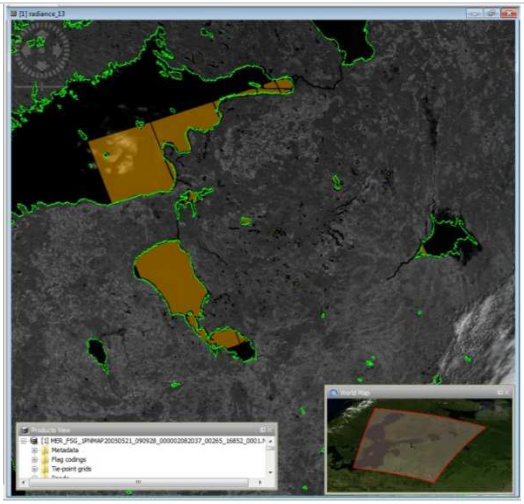
[9] The nominal values for the scalar thresholds regarding to AVHRR will be defined if the standard feature definition for AVHRR is requested.

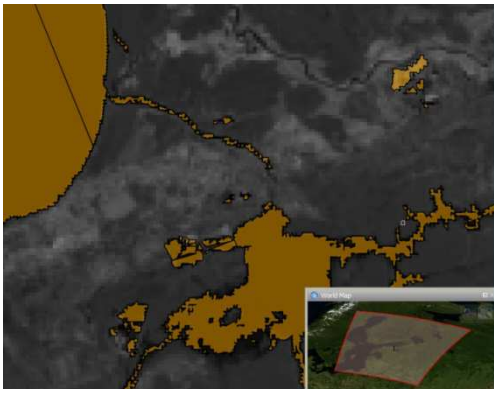
© UCL-Geomatics 2016
This document is the property of the LAND_COVER_CCI partnership, no part of it shall be reproduced or transmitted without the express prior written authorization of UCL-Geomatics (Belgium).

4.4.5.6 *Water/land mask: SWBD mask*

Both classes, the a priori Land Value and the a priori Water Value are determined by a static background map as well as the geo-location of the corresponding pixel. The SRTM SWBD map (NGA) is used in the phase I of the project from http://dds.cr.usgs.gov/srtm/version2_1/SWBD/ or http://eros.usgs.gov/#/Find_Data/Products_and_Data_Available/Shuttle_Radar_Topography_Mission_Water_Body_Dataset. Figure 4-4 shows the origin land/water mask (green) and the application of the new SRTM SWBD map (brown). The improvement is clearly visible.

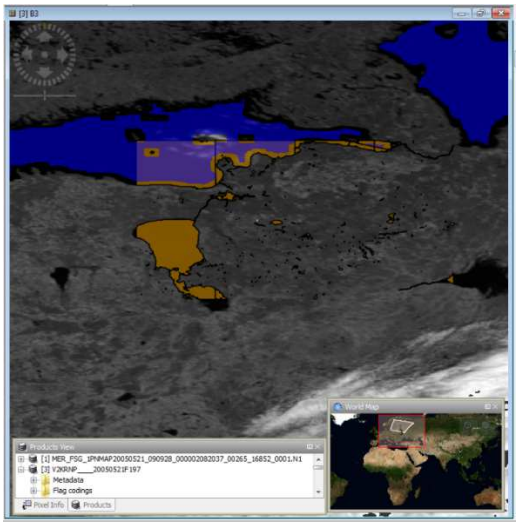
For a refinement of the classification the CCI-LC SAR water body product has been developed and the assessment of the suitability is currently ongoing.

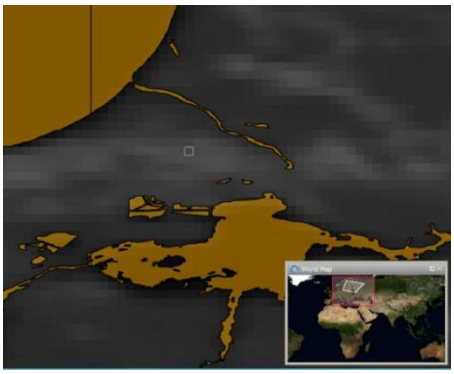




MERIS

MER_FSG_1PNMAP20050521_090928_000002082037_00265_16852_0001.N1





SPOT-VGT

V2KRNP____20050521F197.ZIP

Figure 4-4: Origin land/water mask and SRTM SWBD map

© UCL-Geomatics 2016
This document is the property of the LAND_COVER_CCI partnership, no part of it shall be reproduced or transmitted without the express prior written authorization of UCL-Geomatics (Belgium).

4.4.6 Adaptation of IdePix

The assessment of MERIS FR and RR SR products using the former IdePix shows that the data quality has not yet reached the expected level, mainly due to clouds. A better pixel classification w.r.t. the class “clear land” is required. Therefore new pixel identification features for the CCI-LC processing has been developed and applied.

4.4.6.1 *MERIS FR and RR*

Temporal Features

An improvement of pixel identification is accessible by analysing their temporal characteristic. Based on this approach a temporal filter has also been applied and is described in detail in the section 4.6.4.

Spectral Features

The following new spectral features have been considered, investigated und applied:

- blue band feature;
- cloud value feature;
- clear land feature.

The **blue band feature** based on the Blue Band Cloud Screening of the GlobCover Project and the entire description may be found in the GlobCover Design Justification File [GlobCover_DJFv3.8, 2008]. A simple blue band test has been adopted for MERIS by using the 412 nm channel. The developed cloud screening method is applied to reflectances. A first threshold for band 1 reflectances is used to detect the most brilliant dense clouds. The clear pixels are tested by a filter which performs the reflectance ratio of band11 and band10 related to the altitude of the scattering surface. An optimised threshold permits identifying thin clouds which are not detected by the first blue band test. Three states are supposed: 0=Out of Orbit, 1=Clear and 2=Cloud. The optimised cloud mask is globally coherent with the bright flag of standard MERIS products. However, a higher performance of the cloud screening over semi-transparent clouds can be observed. Large areas are not detected by the bright flag or probability algorithms. The analysis shows that the blue band algorithm is more able to detect semi-transparent clouds.

The **cloud value feature** is predicted by two neuronal network models or to put it more succinctly, they are back-propagation neuronal networks with one input and one output layer. The NNs have been trained with a back-propagation learning algorithm by using the PixBox data whereas the training dataset was splitted w.r.t. the surface properties land and water and these two datasets have been used separately for the training. Therefore we get a so called LandNN and a WaterNN for the prediction of the cloud value. The PixBox data are described in the PVASR [Ph1_PVASRv2.0, 2012]. The decision which NN will be used is only depending on the classified surface type through IdePix. Afterwards the cloud value is calculated through the NN by using the MERIS FSG respectively and RRG TOA reflectance spectrum as input. The cloud value has a range from 0 through 2. The user defined thresholds - 1.25 for the LandNN and 1.35 for the WaterNN are used for the verification of the current pixel status as clear land or clear water. If the cloud value is greater than the particular threshold then the pixel status is set to cloud. The PixBox data has been extended with SPOT VGT P and AVHRR

© UCL-Geomatics 2016
This document is the property of the LAND_COVER_CCI partnership, no part of it shall be reproduced or transmitted without the express prior written authorization of UCL-Geomatics (Belgium).

data, therefore the cloud value feature is also applicable to SPOT VGT P and adapted PROBA-V as well as AVHRR data.

The **clear land feature** of pixel identification bases on the analysis of the spectral characteristic in the HSV (Hue Saturation Value) - colour space. The clear land feature is described in detail in the section 4.6.4. This feature is only applicable to MERIS data.

4.4.6.2 *AVHRR*

Temporal Features

As mentioned in section 4.4.6.1, further improvements of pixel identification are accessible by analysing their temporal characteristic. Based on this approach a temporal filter has also been applied and is described in detail in the section 4.6.4.

Spectral Features

As mentioned in section 4.4.6.1, the PixBox data has been extended with AVHRR data, therefore the **cloud value feature** is also applicable to AVHRR data.

AVHRR processing mask

To reduce processing time and costs a global processing mask was implemented. This mask is derived from the global land/ocean mask for the fourth MERIS/ATSR reprocessing and SENTINEL-3 processing [Brockmann et al., 2015]. Landmasses were expanded by 40 km to ensure consistently processing of AVHRR over land. The mask is shown in Figure 4-5.

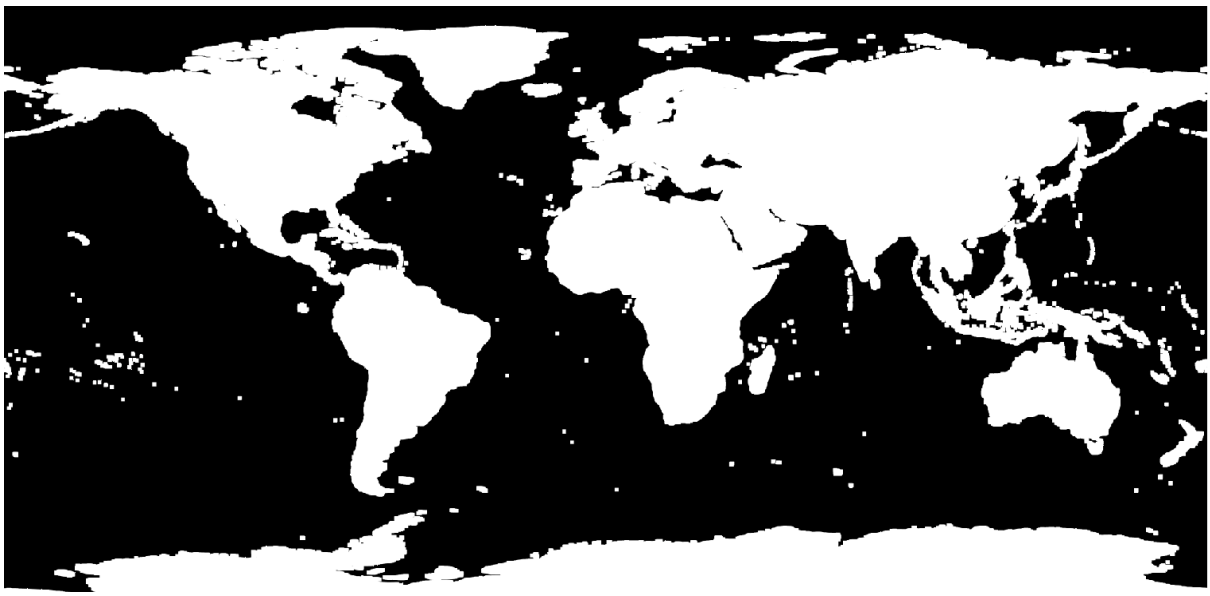


Figure 4-5: AVHRR processing mask; white = processing area & black equals non processing area

© UCL-Geomatics 2016
This document is the property of the LAND_COVER_CCI partnership, no part of it shall be reproduced or transmitted without the express prior written authorization of UCL-Geomatics (Belgium).

Additional spectral cloud and snow features

The following additional AVHRR cloud features based on the AVHRR – cloud screening approach CLAVR [Heidinger,2004] have been applied to the AVHRR data to improve the accuracy of the cloud screening:

- **RGCT - Reflectance Gross Contrast Test over land**
- **RRCT - Reflectance Ratio Contrast Test over land**
- **C3AT - Channel 3b Reflectance Test over land**
- **TGCT - Thermal Gross Contrast Test**
- **FMFT - Four Minus Five Test (11 - 12 um)**
- **$FMFT_{adap}$ - Four Minus Five Test (11 - 12 um) - adapted**
- **TMFT - Three Minus Four Test (4 - 11 um)**
- **Channel 3b Emissivity Test over land**

Desert Area Mask

$$\text{DESERT} = \begin{cases} 5° \leq \text{lat} \leq 50° & \text{and} \quad 30° \leq \text{lon} \leq 60° \\ 25° \leq \text{lat} \leq 50° & \text{and} \quad 60° \leq \text{lon} \leq 110° \\ -31° \leq \text{lat} \leq 19° & \text{and} \quad 121° \leq \text{lon} \leq 141° \\ 10° \leq \text{lat} \leq 35° & \text{and} \quad -20° \leq \text{lon} \leq 30° \\ 35° \leq \text{lat} \leq 50° & \text{and} \quad 110° \leq \text{lon} \leq 127° \end{cases}$$

eq. 4-15

with lat is the latitude in degree and lon is the longitude in degree.

In the following subsection all additional AVHRR features including required thresholds have been defined:

RGCT - Reflectance Gross Contrast Test (RGCT) over land:

$$if\ \rho_1 > RGCT_{threshold}\ than\ cloud$$

eq. 4-16

with ρ_1 is the reflectance in Band 1

Table 4-15: $RGCT_{threshold}$

NDVI	$RGCT_{THRESHOLD}$
-0.05	0.80
0.0	0.60
0.05	0.50

© UCL-Geomatics 2016
This document is the property of the LAND_COVER_CCI partnership, no part of it shall be reproduced or transmitted without the express prior written authorization of UCL-Geomatics (Belgium).

NDVI	$RGCT_{THRESHOLD}$
0.10	0.40
0.15	0.35
0.20	0.30
> 0.25	0.25

RRCT - Reflectance Ratio Contrast Test over land:

$$\rho_{21} = \frac{\rho_2}{\rho_1}\ (\rho_1 > 0)\ ; if\ \rho_{21} < RRCT_{threshold} = 1.1\ and\ no\ desert\ \ than\ cloud$$

eq. 4-17

with ρ_1 is the reflectance in Band 1 and ρ_2 is the reflectance in Band 2

C3AT - Channel 3b Reflectance Test over land:

$$if\ \rho_{3b} > RRCT_{threshold} = 0.06\ (0.09\ for\ potenial\ snow) and\ no\ desert\ than\ cloud$$

eq. 4-18

with ρ_{3b} is the reflectance in Band 3b

TGCT - Thermal Gross Contrast Test:

$$if\ BT4 < TGCT_{threshold} = 244K\ than\ cloud$$

eq. 4-19

With BT4 is the brightness temperature in Band 4

FMFT - Four Minus Five Test (11 - 12 um):

$$BT45 = BT4 - BT5; if\ BT45 > FMFT_{threshold}(BT4)\ than\ cloud$$

eq. 4-20

with BT 4 is the brightness temperature in Band 4 and with BT5 is the brightness temperature in Band 5

Table 4-16: $FMFT_{threshold}$

	THRESHOLD									
BT4	0	1	2	3	4	5	6	7	8	9
200.0	0.00	0.00	0.00	0.00	0.00	0.00	0.00	0.00	0.00	0.00
210.0	0.00	0.00	0.00	0.00	0.00	0.00	0.00	0.00	0.00	0.00
220.0	0.00	0.00	0.00	0.00	0.00	0.00	0.00	0.00	0.00	0.00

© UCL-Geomatics 2016
This document is the property of the LAND_COVER_CCI partnership, no part of it shall be reproduced or transmitted without the express prior written authorization of UCL-Geomatics (Belgium).

	Threshold									
BT4	0	1	2	3	4	5	6	7	8	9
230.0	0.00	0.00	0.00	0.00	0.00	0.00	0.00	0.00	0.00	0.00
240.0	0.00	0.00	0.00	0.00	0.00	0.00	0.00	0.00	0.00	0.00
250.0	0.00	0.00	0.00	0.00	0.00	0.00	0.00	0.00	0.00	0.00
260.0	0.00	0.01	0.03	0.05	0.08	0.11	0.14	0.18	0.23	0.28
270.0	0.34	0.41	0.48	0.57	0.66	0.76	0.87	1.00	1.13	1.27
280.0	1.42	1.59	1.76	1.94	2.14	2.34	2.55	2.77	3.00	3.24
290.0	3.48	3.73	3.99	4.26	4.52	4.80	5.08	5.35	5.64	5.92
300.0	6.20	6.48	6.76	7.03	7.30	7.80	7.80	7.80	7.80	7.80
310.0	7.80	7.80	7.80	7.80	7.80	7.80	7.80	7.80	7.80	7.80
320.0	7.80									

$FMFT_{adap}$ - Four Minus Five Test (11 - 12 um) – adapted:

$$BT45 = BT4 - BT5; if\ FMFT_{Min}(BT4) < BT45 < FMFT_{Max}(BT4)\ than\ clear$$

eq. 4-21

with BT 4 is the brightness temperature in Band 4 and with BT5 is the brightness temperature in Band 5

Table 4-17: $FMFT_{adap_threshold}$

	Satellite viewing angle							
	$Threshold_{Min}$				$Threshold_{Max}$			
BT4	7.5	22.5	37.5	52.5	7.5	22.5	37.5	52.5
190.0	0.595	0.725	0.685	-99.000	-0.465	-1.485	-1.025	-99.000
200.0	0.595	0.725	0.685	-99.000	-0.465	-1.485	-1.025	-99.000
210.0	0.595	0.725	0.685	-99.000	-0.465	-1.485	-1.025	-99.000
220.0	0.595	0.725	0.685	-99.000	-0.465	-1.485	-1.025	-99.000
230.0	0.775	0.745	0.775	0.715	-1.205	-1.615	-1.145	-1.345
240.0	0.745	0.745	0.755	0.795	-1.305	-1.385	-1.265	-1.275
250.0	0.855	0.815	0.765	0.775	-1.375	-1.455	-1.385	-1.485
260.0	0.875	0.875	0.905	0.885	-1.525	-1.455	-1.665	-1.525
270.0	1.185	1.155	1.275	1.135	-1.215	-1.255	-1.205	-1.295
280.0	2.835	3.255	3.295	3.175	-1.245	-1.095	-1.035	-0.975
290.0	5.475	5.395	5.245	5.325	-0.445	-0.395	-0.315	-0.465
300.0	6.195	6.035	6.055	6.105	-0.445	-0.395	-0.315	-0.465

© UCL-Geomatics 2016
This document is the property of the LAND_COVER_CCI partnership, no part of it shall be reproduced or transmitted without the express prior written authorization of UCL-Geomatics (Belgium).

	SATELLITE VIEWING ANGLE							
	$THRESHOLD_{MIN}$				$THRESHOLD_{MAX}$			
BT4	7.5	22.5	37.5	52.5	7.5	22.5	37.5	52.5
310.0	6.185	6.225	6.835	5.925	-0.445	-0.395	-0.315	-0.465
320.0	6.185	6.225	6.835	5.925	-0.445	-0.395	-0.315	-0.465

TMFT - Three Minus Four Test (4 - 11 um):

$$BT34 = BT3 - BT4; if\ \mathrm{TMFT}_{Min}(BT4) < BT34 < \mathrm{TMFT}_{Max}(BT4)\ than\ clear$$

eq. 4-22

with BT 3 is the brightness temperature in Band 3 and with BT4 is the brightness temperature in Band 4

Table 4-18: $TMFT_{threshold}$

	SATELLITE VIEWING ANGLE							
	$THRESHOLD_{MAX}$				$THRESHOLD_{MIN}$			
BT4	7.5	22.5	37.5	52.5	7.5	22.5	37.5	52.5
190.0	2.635	2.505	3.395	3.500	0.145	-0.165	-0.075	-0.075
200.0	2.635	2.505	3.395	3.500	0.145	-0.165	-0.075	-0.075
210.0	2.635	2.505	3.395	3.500	0.145	-0.165	-0.075	-0.075
220.0	2.635	2.505	3.395	3.500	0.145	-0.165	-0.075	-0.075
230.0	2.615	2.655	2.685	2.505	-0.805	-0.975	-0.795	-1.045
240.0	1.865	1.835	1.845	1.915	-1.195	-1.065	-1.125	-1.175
250.0	1.815	1.785	1.815	1.795	-1.225	-1.285	-1.285	-1.285
260.0	1.885	1.885	1.875	1.875	-2.425	-1.325	-2.105	-1.975
270.0	2.135	2.115	2.095	2.105	-1.685	-1.595	-1.535	-2.045
280.0	6.825	7.445	8.305	7.125	-4.205	-4.145	-3.645	-3.585
290.0	19.055	18.485	17.795	17.025	-2.425	-1.715	-2.275	-2.015
300.0	20.625	19.775	19.355	19.895	0.585	-0.585	0.825	0.345
310.0	18.115	15.935	20.395	16.025	0.655	1.905	0.475	1.385
320.0	18.115	15.935	20.395	16.025	0.655	1.905	0.475	1.385

Channel 3b Emissivity Test over land:

$$if\ \varepsilon_{3b} > 0.022\ than\ cloud$$

eq. 4-23

with ρ_{3b} is the reflectance in Band 3b

© UCL-Geomatics 2016
This document is the property of the LAND_COVER_CCI partnership, no part of it shall be reproduced or transmitted without the express prior written authorization of UCL-Geomatics (Belgium).

Both channel 3b tests (channel 3b emissivity test and channel 3b reflectance test over Land) requires additional calculations. Therefore the calculation of the emissivity and the reflectance in channel 3b has been included and the corresponding equations are given by:

Channel 3b albedo ρ_{3b} and emissivity ε_{3b}:

$$T_{3b_Bo} = \begin{cases} A_o + B_o BT4 + C_o(BT4 - BT5) \; if \; (BT4 - BT5) > 1 \\ BT4 \; else \end{cases}$$

$$R_{3b-em} = \begin{cases} \left[\frac{c_1 \nu^3}{e^{\frac{c_2 \nu}{\frac{T_{3b_Bo} - a1_{3b}}{a2_{3b}}}} - 1} \right] if \; BT4 > 0 \\ 0.00 \; else \end{cases}$$

$$\varepsilon_{3b} = \begin{cases} \frac{R_{3b}}{R_{3b-em}} \; if \; BT4 > 0 \\ 0.00 \; else \end{cases}$$

$$\rho_{3b} = \begin{cases} \pi \frac{R_{3b} - R_{3b-em}}{\frac{B_{0_{3b}} \cos(\theta_{sun})}{d^2_{\frac{earth}{sun}}} - \pi R_{3b-em}} \; if \; \theta_{sun} < 90 \; and \; R_{3b-em} > 0 \; and \; R_{3b} > 0 \\ 1 - \varepsilon_{3b} \; if \; \theta_{sun} > 90 \; and \; \varepsilon_{3b} > 0 \\ NaN \; else \end{cases}$$

$$with \; B_{0_3b} = \; 1000.0 \cdot \frac{solar_{3b}}{ew_{3b}} and \; d^2_{\frac{earth}{sun}} \approx \frac{1}{1 + 0.033 \; cos\left[\frac{2\pi d}{365}\right]}$$

eq. 4-24

Table 4-19: Constants for the calculation of the Channel 3b albedo and emissivity

	NOAA 11	NOAA14
solar_3b	4.448	4.448
ew_3b	278.85792	284.69366
A0	6.34384	4.00162
B0	2.68468	0.98107
C0	-1.70931	1.97890
$a1_{3b}$	-1.738973	-1.885330
$a2_{3b}$	1.003354	1.003839
c_1	1.1910659 x 10-5 mW/(m^2 sr cm^{-4})	
c_2	1.438833 cm K	

© UCL-Geomatics 2016
This document is the property of the LAND_COVER_CCI partnership, no part of it shall be reproduced or transmitted without the express prior written authorization of UCL-Geomatics (Belgium).

To eliminate remaining haze and small cumulus clouds the following additional tests were applied differentiated between desert and non-desert areas using a desert mask:

- HCODT: Haze or Cumulus Over Desert Test
- HCONT: Haze or Cumulus Over Non-desert Test

HCODT – Haze or Cumulus Over Desert Test:

$$HCODT = TRUE\ if \left(\left(\rho_1 > 0.11\ AND\ \frac{BT4}{BT3} < 0.98\ AND\ BT4 < 285\right) OR \left(\frac{(\rho_1 + \rho_2 + \rho_3)}{3} > 0.23\ AND\ BT4 < 302\ AND\ \frac{BT4}{BT3} < 0.965\ AND\ 0.105 < \rho_3 < 0.27\ AND\ BT3 < 304\right)\right)$$

eq. 4-25

with ρ_1 is the reflectance in Band 1, ρ_2 is the reflectance in Band 2, ρ_{3b} is the reflectance in Band 3b, BT3 is the brightness temperature in Band 3 and BT 4 is the brightness temperature in Band 4.

HCONT – Haze or Cumulus Over Non-desert Test:

$$HCONT = TRUE\ if \left(\left(\rho_1 > 0.11\ AND\ \frac{BT4}{BT3} < 0.98\ AND\ BT4 < 291\right) OR \left(\frac{(\rho_1 + \rho_2 + \rho_3)}{3} > 0.17\ AND\ BT4 < 302\ AND\ \frac{BT4}{BT3} < 0.96\ AND\ \rho_3 > 0.105\ AND\ BT3 < 318\right)\right)$$

eq. 4-26

with ρ_1 is the reflectance in Band 1, ρ_2 is the reflectance in Band 2, ρ_{3b} is the reflectance in Band 3b, BT3 is the brightness temperature in Band 3 and BT 4 is the brightness temperature in Band 4.

The two different tests are used based on the following condition:

$$if\ DESERT\ then\ HCODT\ else\ HCONT$$

eq. 4-27

For AVHRR this leads to an adaption of the classification for isCloud (see Table 4-13):

Table 4-20: Adapted processing logic for AVHRR and the classification attribute isCloud

CLASSIFICATION ATTRIBUTE	DEFINITION
isCloud	cloud value feature || additional AVHRR cloud features || (NOT TGCT && NDSI > 0.8)

© UCL-Geomatics 2016
This document is the property of the LAND_COVER_CCI partnership, no part of it shall be reproduced or transmitted without the express prior written authorization of UCL-Geomatics (Belgium).

The following additional AVHRR snow features based on CLAVR-X [Heidinger, 2004] have been applied to the AVHRR data to improve the accuracy of the snow screening:

- **HNLST – High Northern Latitude Snow Test over land**
- **HSLST - High Southern Latitude Snow Test over land**
- **MLHEST – Mid Latitude High Elevation Snow Test over land**

HNLST – High Northern Latitude Snow Test over land:

$$HNLST = TRUE\ if\ \left(-27 < BT4 < 1.35\ AND\ \rho_1 > 0.4\ AND\ 0.8 < \frac{\rho_2}{\rho_1} < 1.15\ AND\ \rho_{3b} < 0.013\ AND\ el > 300\ AND\ (BT5 - BT3) > -14\ AND\ 0.98 > \frac{BT5}{BT3} > 0.9486\ AND\ \frac{(\rho_1 - \rho_3)}{(\rho_2 + \rho_3)} > 0.98\right)$$

OR

$$\left(\frac{(\rho_1 - \rho_3)}{(\rho_2 + \rho_3)} > 0.98\ AND\ \rho_1 > 0.15\ AND\ (BT5 - BT3) > -8\right)$$

AND

$$LAT > 62\ AND\ F.LAND = TRUE$$

eq. 4-28

with ρ_1 is the reflectance in Band 1, ρ_2 is the reflectance in Band 2, ρ_{3b} is the reflectance in Band 3b, BT3 is the brightness temperature in °C of Band 3, BT 4 is the brightness temperature in °C of Band 4, BT 5 is the brightness temperature in °C of Band 5, el is the elevation from GETASSE 30[10] in meter, LAT is the latitude in Degree and F.LAND $F.LAND$ is the priori Land Value derived from IdePix (see 4.4.5.6.).

HSLST - High Southern Latitude Snow Test over land:

$$HSLST = TRUE\ if\ (-27 < BT4 < 1.35\ AND\ \rho_1 > 0.55\ AND\ 0.85 < \frac{\rho_2}{\rho_1} < 1.15\ AND\ \rho_{3b} < 0.03\ AND\ (BT5 - BT3) > -13\ AND\ \frac{\rho_1 - \rho_3}{\rho_2 + \rho_3} > 1.05\ AND\ LAT < -62)$$

eq. 4-29

[10] http://www.brockmann-consult.de/beam/doc/help-4.7/visat/GETASSE30ElevationModel.html

© UCL-Geomatics 2016
This document is the property of the LAND_COVER_CCI partnership, no part of it shall be reproduced or transmitted without the express prior written authorization of UCL-Geomatics (Belgium).

with ρ_1 is the reflectance in Band 1, ρ_2 is the reflectance in Band 2, ρ_{3b} is the reflectance in Band 3b, BT3 is the brightness temperature in °C of Band 3, BT 5 is the brightness temperature in °C of Band 5 and LAT is the latitude in Degree.

MLHEST - Mid Latitude High Elevation Snow Test over land:

$$MLHEST = TRUE\ if\ (-15 < BT4 < 1.35\ \ AND\ \ \rho_1 > 0.4\ AND\ \ 0.80 < \frac{\rho_2}{\rho_1} < 1.15\ \ AND\ \rho_{3b} < 0.035\ \ AND\ \ (BT5 - BT3) > -14\ \ AND\ F.LAND = TRUE\ AND\ \Big((el > 1000\ AND\ (-63 \leq LAT \leq -7\ OR\ 7 \leq LAT \leq 62))\ OR\ \big(el > 3500\ AND\ (-7 < LAT < 7)\big)\Big))$$

eq. 4-30

with ρ_1 is the reflectance in Band 1, ρ_2 is the reflectance in Band 2, ρ_{3b} is the reflectance in Band 3b, BT3 is the brightness temperature in °C of Band 3, BT 5 is the brightness temperature in °C of Band 5, el is the elevation from GETASSE 30[11] in meter, LAT is the latitude in Degree and $F.LAND$ is the land flag derived from IdePix.

For AVHRR this leads to an adaption of the classification for isClearSnow (see Table 4-13):

Table 4-21: Adapted processing logic for AVHRR and the classification attribute isClearSnow

CLASSIFICATION ATTRIBUTE	DEFINITION
isClearSnow	additional AVHRR snow features

4.4.6.3 *PROBA-V and SPOT VGT*

Temporal Features

As mentioned in section 4.4.6.1, further improvements of pixel identification are accessible by analysing their temporal characteristic. Based on this approach a temporal filter has also been applied and is described in detail in the section 4.6.4.

Spectral Features

As mentioned in section 4.4.6.1, the PixBox data has been extended with SPOT VGT-P data. The adaption of the PROBA-V data to SPOT VGT data allows the calculation of **cloud value feature** based on SPOT-VGT-P PixBox data for PROBA-V data.

[11] http://www.brockmann-consult.de/beam/doc/help-4.7/visat/GETASSE30ElevationModel.html

© UCL-Geomatics 2016
This document is the property of the LAND_COVER_CCI partnership, no part of it shall be reproduced or transmitted without the express prior written authorization of UCL-Geomatics (Belgium).

Additional spectral cloud and snow features

The following additional SPOT VGT / PROBA-V features have been applied to the PROBA-V data to improve the accuracy of the cloud screening:

- **HTUA – Haze Test over Urban Areas**
- **HTNUA - Haze Test over Non-Urban Areas**

These tests are based on Tasseled Cap Transformation ([Kauth and Thomas, 1976], [Crist and Kauth, 1986], [Crist and Cicone, 1984a], [Crist and Cicone, 1984b]). The following Tasseled Cap Components have been derived:

$$TC1 = 0.332 * \rho_1 + 0.603 * \rho_2 + 0.676 * \rho_3 + 0.263 * \rho_4$$

$$TC2 = 0.283 * \rho_1 - 0.66 * \rho_2 + 0.577 * \rho_3 + 0.388 * \rho_4$$

$$TC3 = 0.9 * \rho_1 + 0.428 * \rho_2 + 0.0759 * \rho_3 - 0.041 * \rho_4$$

$$TC4 = 0.016 * \rho_1 + 0.428 * \rho_2 - 0.452 * \rho_3 + 0.882 * \rho_4$$

eq. 4-31

with ρ_1 is the reflectance in Band 1, ρ_2 is the reflectance in Band 2, ρ_3 is the reflectance in Band 3, and ρ_4 is the reflectance in Band 4.

HTUA – Haze Test over Urban Areas:

$$HTUA = TRUE\ if\ ((TC4 - TC3) < -0.07\ AND\ (TC3 - TC2) \geq -0.01\ AND\ UM = TRUE)$$

eq. 4-32

with UM being the urban area extracted from LC-CCI land cover map 2010 version 1.6.1.

HTNUA – Haze Test over Non-Urban Areas :

$$HTNUA = TRUE\ if\ ((TC4 - TC3) < -0.1\ AND\ (TC3 - TC2) \geq -0.01\ AND\ UM = TRUE)$$

eq. 4-33

with UM being the urban area extracted from LC-CCI land cover map 2010 version 1.6.1.

The following additional PROBA-V feature has been applied to the PROBA-V data to improve the accuracy of the snow screening:

- **HEST – High Elevation Snow Test**

© UCL-Geomatics 2016
This document is the property of the LAND_COVER_CCI partnership, no part of it shall be reproduced or transmitted without the express prior written authorization of UCL-Geomatics (Belgium).

HEST – High Elevation Snow Test:

$$HEST = TRUE\ if\ ((NDSI > 0.4\ AND\ \rho_3 < 0.13\ AND\ el > 600)\ OR\ NDSI > 0.7)$$

eq. 4-34

with ρ_3 is the reflectance in Band 3, and el is the elevation from GETASSE 30[12] in meter.

4.4.7 IdePix post-processing for PROBA-V

For PROBA-V a post-processing of IdePix flags has been conducted to further refine the IdePix results. The following PROBA-V S1 TOA and IdePix flags have been used for refinement (eq. 4-1):

$$smClear = SM_F_CLEAR$$
$$smCloud = SM_F_CLOUD$$
$$idepixLand = F_LAND$$
$$idepixClearLand = F_CLEAR_LAND$$
$$idepixWater = F_WATER$$
$$idepixClearWater = F_CLEAR_WATER$$
$$idepixClearSnow = F_CLEAR_SNOW$$
$$idepixCloud = F_CLOUD$$

eq. 4-35

with F_* flag defined by IdePix, and SM_F_* flag delivered with PROBA-V S1 TOA product.

The following flag refinements have been defined:

$$safeClearLand = if\ (smClear\ AND\ idepixLand\ AND\ idepixClearLand\ AND\ NOT\ idepixClearSnow)$$

$$safeClearWater = if\ (smClear\ AND\ idepixWater\ AND\ idepixClearWater\ AND\ NOT\ idepixClearSnow)$$

$$potentialCloudSnow = if(NOT\ safeClearLand\ AND\ idepixLand)$$

$$safeSnowIce = if\ (potentialCloudSnow\ AND\ idepixClearSnow)$$

$$safeCloud = if(idepixCloud\ OR\ \begin{pmatrix} potentialCloudSnow\ AND \\ (NOT\ safeSnowIce\ AND\ NOT\ safeClearWater) \end{pmatrix})$$

[12] http://www.brockmann-consult.de/beam/doc/help-4.7/visat/GETASSE30ElevationModel.html

© UCL-Geomatics 2016
This document is the property of the LAND_COVER_CCI partnership, no part of it shall be reproduced or transmitted without the express prior written authorization of UCL-Geomatics (Belgium).

$$safeClearWaterFinal = if\left(\left(\begin{matrix}NOT\ safeClearLand\\ AND\ NOT\ safeSnowIce\ AND\ NOT\ safeCloud\ AND\ NOT\ smCloud\\ idepixWater\end{matrix}\right)AND\ safeClearWater\right)OR$$

$$safeClearLandFinal = if\left(\left(\begin{matrix}NOT\ safeSnowIce\ AND\ NOT\ idepixCloud\ AND\ NOT\ smCloud\\ AND\ NOT\ safeClearWaterFinal\end{matrix}\right)AND\ idepixLand\ safeClearLand\right)OR$$

$$safeCloudFinal = if(safeCloud\ AND\ (NOT\ safeClearLand\ AND\ NOT\ safeClearWaterFinal))$$

eq. 4-36

For PROBA-V this leads to an adaption of the classification attributes and the classification (see Table 4-13) was adapted as follows:

Table 4-22: Adapted processing logic for PROBA-V and the classification attributes

CLASSIFICATION ATTRIBUTE	DEFINITION
isCloud	safeCloudFinal
isClearSnow	safeSnowIce
isClearLand	safeClearLandFinal
isClearWater	safeClearWaterFinal

4.4.8 Error budget estimates

The adaption of IdePix by including the new features has influenced the error estimation. Now the error cannot simply be calculated automatically by the probabilistic arithmetic. Therefore as a first guess we will introduce a measure of certainty that the inspected pixel is covered by a cloud. This measure of certainty for each pixel is calculated by counting the number of the true cloud features. So the measure of certainty for a pixel is very high, if all cloud feature has been classified this pixel as cloudy.

4.4.9 Assumptions and limitations

None

4.4.10 Improvements

Spatial Features

© UCL-Geomatics 2016
This document is the property of the LAND_COVER_CCI partnership, no part of it shall be reproduced or transmitted without the express prior written authorization of UCL-Geomatics (Belgium).

Further improvements of pixel identification are accessible if features which are not only calculated by using the radiometric characteristics of each single pixel but analysing their individual neighbourhood.

4.4.11 Cloud shadow and cloud edge detection

A more comprehensive representation of clouds is provided by two additional pixel properties, 'cloud edge' and 'cloud shadow'. These two properties are also kept in the pixel identification flag and can be considered as a kind of "post-processing" in the cloud detection.

To detect dark cloud shadow pixels -whose spectra are polluted by the shadow- the position of the shadow will be determined by projecting the 'cloud pixels' onto the ground using the sun position, the pixel's altitude on Earth, and the cloud height estimated from cloud top pressure.

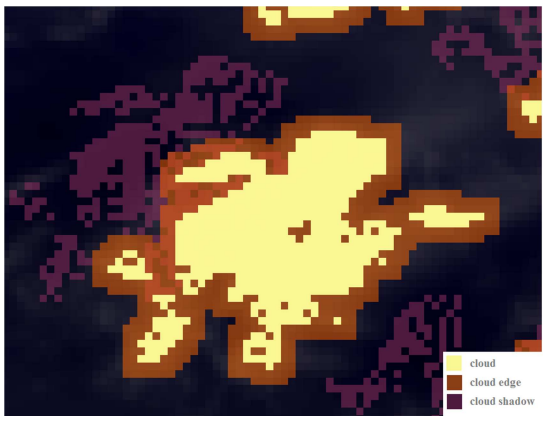


Figure 4-6: Cloud, cloud edges and cloud shadow

Cloud edge pixels are in principle regarded as neighbour pixels of a 'cloud' as identified before in the pixel classification. The width of this edge (in number of pixels) can be set by the user. In brief, the algorithm to identify cloud edge pixels works as follows:

- use a 2x2 square with reference pixel in upper left
- move this square row-by-row over the given tile
- if reference pixel was not cloud, don't do anything
- if reference pixel is cloudy:
- if 2x2 square only has cloud pixels, then set cloud buffer of two pixels in both x and y direction of reference pixel;
- if 2x2 square also has non-cloudy pixels, do the same but with cloud buffer of only 1.

Improvement for the cloud shadow detection

The improvement of Phase II algorithms of the CCI-LC project includes also the improvement of the cloud shadow detection. At this stage of the project, the new proposed algorithm is implemented and could be subjected to an assessment. The algorithm contains three main parts which are explained in the following. The results of the individual steps are presented visual for a better comprehension (see Figure 4-7).

© UCL-Geomatics 2016
This document is the property of the LAND_COVER_CCI partnership, no part of it shall be reproduced or transmitted without the express prior written authorization of UCL-Geomatics (Belgium).

Step 1: Cloud top height (CTH) and cloud base (CBH) estimation

- CTH: Use temperature (MODIS, Landsat, AVHRR) or O_2 absorption (MERIS) to estimate CTH, Otherwise set CTH=12km (SENTINEL 2)
- CBH: use constant CBH=0 of min_{window}(CTH)

Step 2: potential cloud shadow area identification

- Intersection of line-of-sight with cloud
- Identify connected potential cloud shadow areas (seed-growing algorithm)

Step 3: cloud shadow identification

- for each connected cloud shadow area perform k-means cluster analysis with k = 4 clusters
- Add local variance as additional feature into clustering for high spatial resolution sensors (shadow areas are less contrasted)
- Sort clusters into either clear and cloud shadow

In case of the shadow detection for MERIS only step 1 and step 2 have been applied. At this stage of the project, the assessment of the cloud screening for AVHRR isn't finished and therefore the new proposed cloud shadow algorithm should be subjected to a comprehensive evaluation after finishing this activity.

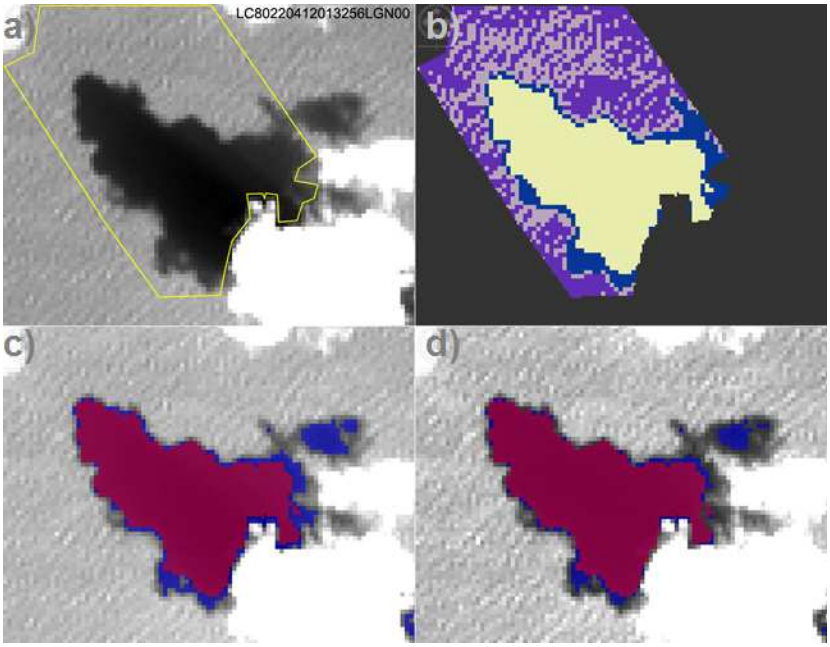


Figure 4-7: Breadboard cloud shadow algorithm a) blue channel with cloud shadow potential area border (yellow) b) k-means cluster analysis result c) blue channel with cloud shadow d) SWIR1 channel with cloud shadow

© UCL-Geomatics 2016
This document is the property of the LAND_COVER_CCI partnership, no part of it shall be reproduced or transmitted without the express prior written authorization of UCL-Geomatics (Belgium).

4.4.12 Pseudo-code representation

This subsection provides an overview of the pixel classification (IdePix) from the software development point of view. A more detailed description of the logical flow and individual processing steps can be found in the CCI Land Cover DPM [Ph1_DPMv2.2, 2013]. Furthermore the input and output products being used within the LC-CCI processing modules are described in the CCI Land Cover IODD [Ph1_IODDv1.0, 2013] in more detail.

4.4.12.1 *Land-water delineation*

```
algorithm land_water_delineation is
    input:  the L1 flag from either MERIS or SPOT_VGT/PROBA-V for given pixel,
            L1_FLAG
            the SRTM land/water flag for given pixel, SRTM
    output: the land/water flag for given pixel which will be used in
            pixel classification, LW_FLAG
    return LW_FLAG
```

Algorithm 4-4: Land-water delineation

4.4.12.2 *Pixel classification feature – MERISFR and RR, SPOT VGT/ PROBA-V and AVHRR*

```
algorithm isLand is
    input:  the a priori land value for the given instrument (MERIS or
            SPOT_VGT/PROBA-V),
               priorL
            the land classification threshold, LAND_THRESH
    output: the boolean 'isLand' attribute, isLand
    return isLand
```

Algorithm 4-5: Set classification attribute 'isLand'

```
algorithm isWater is
    input:  the a priori water value
               for the given instrument (MERIS or SPOT_VGT/PROBA-V), priorW
            the water classification threshold, WATER_THRESH
    output: the boolean 'isWater' attribute, isWater
    return isWater
```

Algorithm 4-6: Set classification attribute 'isWater'

© UCL-Geomatics 2016
This document is the property of the LAND_COVER_CCI partnership, no part of it shall be reproduced or transmitted without the express prior written authorization of UCL-Geomatics (Belgium).

```
algorithm isBright is
    input:  the brightness value for the given instrument (MERIS or SPOT_VGT/
            PROBA-V), br
            the bright threshold, BRIGHT_THRESH
    output: the boolean 'isBright' attribute, isBright
    return isBright
```

Algorithm 4-7: Set classification attribute 'isBright'

```
algorithm isWhite is
    input:  the whiteness value for the given instrument (MERIS or SPOT_VGT/
            PROBA-V), wh
            the white threshold, WHITE_THRESH
    output: the boolean 'isWhite' attribute, isWhite
    return isWhite
```

Algorithm 4-8: Set classification attribute 'isWhite'

```
algorithm isBrightWhite is
    input:  the brightness value for the given instrument (MERIS or SPOT_VGT/
            PROBA-V), br
            the whiteness value for the given instrument (MERIS or SPOT_VGT/
            PROBA-V), wh
            the brightwhite threshold, BRIGHTWHITE_THRESH
    output: the boolean 'isBrightWhite' attribute, isBrightWhite
    return isBrightWhite
```

Algorithm 4-9: Set classification attribute 'isBrightWhite'

```
algorithm isCold is
    input:  the temperature for the given instrument (MERIS or SPOT_VGT/PROBA-V), T
            the temperature threshold, TEMPERATURE_THRESH
    output: the boolean 'isCold' attribute, isCold
    return isCold
```

Algorithm 4-10: Set classification attribute 'isCold'

```
algorithm isVegRisk is
    input:  the NDVI value for the given instrument (MERIS or SPOT_VGT/PROBA-V),
            ndvi
            the NDVI threshold, NDVI_THRESH
```

© UCL-Geomatics 2016
This document is the property of the LAND_COVER_CCI partnership, no part of it shall be reproduced or transmitted without the express prior written authorization of UCL-Geomatics (Belgium).

```
    output: the boolean 'isVegRisk' attribute, isVegRisk
    return isVegRisk
```

Algorithm 4-11: Set classification attribute 'isVegRisk'

```
algorithm isGlintRisk is
    input:  the glint risk value for the given instrument (MERIS or SPOT_VGT/
            PROBA-V), gl
            the glint risk threshold, GLINT_RISK_THRESH
    output: the boolean 'isGlintRisk' attribute, isGlintRisk
    return isGlintRisk
```

Algorithm 4-12: Set classification attribute 'isGlintRisk'

```
algorithm isHigh is
    input:  the pressure value for the given instrument (MERIS or SPOT_VGT/
            PROBA-V), p
            the pressure threshold, PRESSURE_THRESH
    output: the boolean 'isHigh' attribute, isHigh
    return isHigh
```

Algorithm 4-13: Set classification attribute 'isHigh'

```
algorithm isClearSnow is
    input:  the brightness value for the given instrument (MERIS or SPOT_VGT/
            PROBA-V), br
            the NDSI value for the given instrument (MERIS or SPOT_VGT/PROBA-V),
            ndsi
            a boolean flag indicating if 'brightwhite' attribute is set,
                isBrightWhite
            the NDSI threshold, NDSI_THRESH
    output: the boolean 'isClearSnow' attribute, isClearSnow
    return isClearSnow
```

Algorithm 4-14: Set classification attribute 'isClearSnow'

```
algorithm isCloud is
    input:  the brightness value for the given instrument (MERIS or SPOT_VGT/
            PROBA-V), br
            the whiteness value for the given instrument (MERIS or SPOT_VGT/
            PROBA-V), wh
            the pressure value for the given instrument (MERIS or SPOT_VGT/
```

© UCL-Geomatics 2016
This document is the property of the LAND_COVER_CCI partnership, no part of it shall be reproduced or transmitted without the express prior written authorization of UCL-Geomatics (Belgium).

PROBA-V), *p*

the temperature value for the given instrument (MERIS or SPOT_VGT/PROBA-V), *T*

a boolean flag indicating if 'clearSnow' attribute is set, *isClearSnow*

the cloud classification threshold, *CLOUD_THRESH*

output: the boolean 'cloud' attribute, *isCloud*

return *isCloud*

Algorithm 4-15: Set classification attribute 'isCloud'

algorithm isClearLand **is**

input: the radiometric land value for the given instrument (MERIS or SPOT_VGT/PROBA-V), *radL*

the a priori land for the given instrument (MERIS or SPOT_VGT/PROBA-V), *priorL*

a boolean flag indicating if 'cloud' attribute is set, *isCloud*

the land classification threshold, *LAND_THRESH*

output: the boolean 'isClearLand' attribute, *isClearLand*

return *isClearLand*

Algorithm 4-16: Set classification attribute 'isClearLand'

algorithm isClearWater **is**

input: the radiometric water value for the given instrument (MERIS or SPOT_VGT/PROBA-V), *radW*

the a priori water value for the given instrument (MERIS or SPOT_VGT/PROBA-V), *priorW*

a boolean flag indicating if 'cloud' attribute is set, *isCloud*

the water classification threshold, *WATER_THRESH*

output: the boolean 'isClearWater' attribute, *isClearWater*

return *isClearWater*

Algorithm 4-17: Set classification attribute 'isClearWater'

algorithm cloud_value_feature **is**

input: per pixel, the MERIS or SPOT VGT/PROBA-V or AVHRR TOA/ reflectance spectrum,

ρ (bands 1-15)

the pixel result value from water neural net, nn_{water}

the pixel result value from land neural net, nn_{land}

© UCL-Geomatics 2016
This document is the property of the LAND_COVER_CCI partnership, no part of it shall be reproduced or transmitted without the express prior written authorization of UCL-Geomatics (Belgium).

```
            the pixel identification flag, F
    output: the pixel identification flag modified by 'cloud value' cloud detection
            information, F'
    return F'
```

Algorithm 4-18: 'Cloud value feature' implementation

```
algorithm isDesertArea is
    input:  per pixel, latitude and longitude value, latitude and longitude
    output: the boolean 'isDesertArea' attribute, isDesertArea
    return isDesertArea
```

Algorithm 4-19: Set classification attribute 'isDesert'

```
algorithm isCloudSnowIceFromDecisionTree()is
    input:  per pixel, AVHRR TOA reflectance spectrum and brightness temperature,
               ρ (bands 1-2) and BT (bands 3-5)
            the RGCT threshold, rgctThresh
            the RRCT threshold, rrctThresh
            the C3AT threshold, c3atThresh
            the FMFT threshold, fmtpThresh
            the FMFT_adap threshold, fmtp_AdapThresh
            the TGCT threshold, TGCT_THRESH
            the TMFT MIN threshold, tmftMinThresh
            the TMFT MAX threshold, tmftMaxThresh
            the Emissivity threshold, EMISSIVITY_THRESH
    output: the pixel identification flag modified by additional cloud detection
            information, F'
    return F'
```

Algorithm 4-20: 'Additional cloud detection feature' implementation for AVHRR

```
algorithm isRefineCloudSnowIceFlag()is
    input:  per pixel, SPOT VGT/PROBA-V TOA reflectance spectrum and urban map
               ρ (bands 1-4)
            the HTUA threshold, htuaThresh
            the HTNUA threshold, htnuaThresh
            the HEST threshold, hest_THRESH
```

© UCL-Geomatics 2016
This document is the property of the LAND_COVER_CCI partnership, no part of it shall be reproduced or transmitted without the express prior written authorization of UCL-Geomatics (Belgium).

```
    output: the pixel identification flag modified by additional cloud detection
            information, F'
    return F'
```

Algorithm 4-21: 'Additional cloud/ snow-ice detection feature' implementation for SPOT VGT/ PROBA-V

```
algorithm cloud_edge is
    input:  the rectangle representing the tile being processed, R
            the pixel identification flag, F
    output: the pixel identification flag extended by cloud edge information, F'
    return F'
```

Algorithm 4-22: Set classification attribute 'isCloudEdge'

```
algorithm cloud_height is
    input:  the cloud top pressure, ctp
            the surface standard pressure, p0
    output: the cloud height, hc
    return hc
```

Algorithm 4-23: Cloud height determination

```
algorithm cloud_shadow is
    input:  the cloud top pressure, ctp
            the cloud height, h_c
            the surface altitude, h_0
            the sun zenith angle, sza
            the sun azimuth angle, saa
            the view zenith angle, sza
            the view azimuth angle, sza
            the radius of the Earth, R_Earth
            the cloud geographical position, (lat,lon)_Cloud
    output: the cloud shadow geographical position, (lat,lon)_Shadow
    return (lat,lon)_Shadow
```

Algorithm 4-24: Cloud shadow determination

© UCL-Geomatics 2016
This document is the property of the LAND_COVER_CCI partnership, no part of it shall be reproduced or transmitted without the express prior written authorization of UCL-Geomatics (Belgium).

```
algorithm isFinalIdePixFlag()is
    input:  per pixel, IdePix feature, status map feature and additional cloud/
            snow-ice detection feature
    output: the final pixel identification flag
    return F'
```

Algorithm 4-25: 'Additional cloud detection feature' implementation for SPOT VGT/ PROBA-V

4.5 Atmospheric correction - aerosol and spectral directional reflectance retrieval

The atmospheric correction includes the correction for the absorbing and scattering effects of atmospheric gases, in particular ozone, oxygen and water vapour, of the scattering of air molecules (Rayleigh scattering) and the correction of absorption and scattering due to aerosol particles. All components except aerosols can be rather easily corrected. Ozone can be taken from other satellites, available from met services, and oxygen and water vapour can be taken from sensor measurements thanks to dedicated spectral bands or can be taken also from metrological data sets, e.g. ERA Interim data set [Simmons et al. 2006]. However, aerosols are spatially and temporally highly variable and do not have a distinct spectral absorption features, so that they cannot be measured easily from MERIS, SPOT-VGT and PROBA-V measurements. Techniques exists to derive aerosol information from measurements where the surface signal is low (LARS technique, developed by R. Santer and implemented in the MERIS ground segment), but the areas where the surface is dark enough are sparse and spatial-temporal interpolation is necessary. Also, these derived aerosols optical properties are connected with a substantial error. The aerosol correction is the largest contributor the error of the atmospheric correction. The challenge for CCI-LC is to minimize this error and to quantify it reliably. The method should ideally work across different instruments.

The aerosol correction typically consists of two parts: the calculation of these aerosol properties and secondly the actual correction of the reflectance (after Rayleigh and gas absorption correction). This can be a sequential process where the reflectance correction takes an aerosol optical depth and its spectral dependency as input, or a one-step approach where aerosol properties and reflectance corrections are one implicit step. In the current GlobCover processing the aerosol property retrieval is done offline using the aerosol retrieved from the corresponding MERIS L2 product, as well as monthly and yearly aerosol climatology derived from MERIS, and finally climatological background values. This gives a gap free product, which is important for the correction step. Although it has been demonstrated that this approach is by far advantageous compared to any other source for aerosols available at the time of development, the results were far from being perfect. It seems obvious that the quality needs to be improved to meet GCOS requirements.

A new approach for retrieval of aerosol properties for MERIS, AATSR and SPOT VGT has been developed throughout recent years by the University Swansea for the GlobAlbedo project. It is based on an inverse modelling approach, working on a larger area of 8 x 8km to estimate the aerosol properties, which is then used to correct each single pixel. This method provides significantly more aerosol retrievals than the LARS method, which is the baseline for the GlobCover aerosols. Also the

© UCL-Geomatics 2016
This document is the property of the LAND_COVER_CCI partnership, no part of it shall be reproduced or transmitted without the express prior written authorization of UCL-Geomatics (Belgium).

quality of the retrieved aerosols has been proven to be good. This method has proven its strength with AATSR data and also with MERIS and SPOT VGT as well as AATSR in synergistic mode. It has further been applied successfully to Chris/PROBA, and it works also well with MERIS data alone [GlobAlbedo_ATBDv4.12, 2013].

As mentioned in section 4.2.2, the spectral correction function has been applied on the PROBA-V measurements to calculate the equivalent SPOT VGT P measurements [Dierckx et al., 2015]. As a result, the processing chain atmospheric correction module will be the same as for Spot-VGT P data. Because the PROBA-V S1TOA products do not include auxiliary data of the actual atmospheric state which are essential for the atmospheric correction, the ERA Interim data set is used as source of the meteorological data [Simmons et al. 2006].

Due to the fact that the design of AVHRR2 sensor, the atmospheric conditions and the aerosol properties cannot be measured or calculated easily from the AVHRR measurements. Different approaches or techniques exist to derive aerosol information from measurements for instance, a multi-temporal approach is proposed by [Hauser et al., 2005]. As already described for the PROBA-V S1 TOA data, it was decided also to include the ERA Interim data set as source of the meteorological data [Simmons et al. 2006]. Furthermore the aerosol climatology provided by the Aerosol CCI is used as the auxiliary data set. The general atmospheric correction algorithm developed in Phase I had to be adapted for the AVHRR data and this adaptions are summarized in the section 4.5.2.

The aerosol retrieval developed under the GlobAlbedo project for Surface Directional Reflectance (SDR) estimation; this is fully discussed in [GlobAlbedo_ATBDv4.12, 2013] and here we give a brief summary of points relevant to aerosol estimation. The iterative retrieval of atmospheric aerosol requires a fast approximation of atmospheric radiative transfer, to relate TOA to surface reflectance for varying aerosol loading.

To retrieve estimates of aerosol properties from measured satellite radiances, we need to solve the inverse problem to separate the atmospheric and surface scattering contributions to the observed signal. This normally requires some assumptions to be made on the land surface brightness. Within the proposed framework, these assumptions are expressed as constraints defined by error of fit to a parameterized model describing the surface angular or spectral reflectance. For the single view instruments we apply constraints based on the dark object method (DOM).

The aerosol retrieval includes the calculation of the aerosol optical depth (AOD). Estimates of aerosol extinction are needed for the conversion from top-of-atmosphere measurements to surface reflectance. Aerosol optical depth and aerosol model plus an estimate of the uncertainty in AOD are derived by the Aerosol Retrieval processor from every data set to be processed. It must be noted that AOD and aerosol model are assumed to sufficiently account for the variability in the atmospheric conditions to calculate these terms, while water vapour and ozone column contents are needed in addition to aerosol parameters in order to retrieve the most accurate Lambertian equivalent reflectance. All other atmospheric constituents are just set to climatology values in the algorithm. This selection is justified by the relatively higher impact of aerosol extinction in the spectral channels of MERIS and SPOT-VGT instruments, particularly in the visible.

The problem of surface reflectance and aerosol retrieval can essentially be formulated as one of multivariate optimisation subject to multiple constraints:

© UCL-Geomatics 2016
This document is the property of the LAND_COVER_CCI partnership, no part of it shall be reproduced or transmitted without the express prior written authorization of UCL-Geomatics (Belgium).

- Given a set of satellite TOA reflectance and an initial guess of atmospheric profile, the corresponding set of surface reflectance is estimated
- Application of the observed set to the estimated set of reflectance results in an error metric, where a lower value of the metric corresponds to a set of surface reflectance (and hence atmospheric profile) that is more realistic

These two steps are repeated with refined atmospheric profiles until convergence at an optimal solution. Given a certain aerosol model, the logical flow of the pixel-wise retrieval of aerosol properties is illustrated in Figure 4-9. It consists of the following steps:

- Atmospheric correction of averaged TOA radiance using an estimate of aerosol optical thickness. The resulting estimate of surface reflectance for each input channel is calculated by means of lookup tables. Besides the aerosol optical depth the atmospheric correction depends on the aerosol model, viewing and illumination geometry, surface pressure, and ozone content
- Error metric calculation
- Optimisation of the estimated aerosol optical thickness by means of minimisation of the error metric as implicit function of aerosol optical thickness.
- The implicit dependency of aerosol optical thickness is given by the surface reflectance estimated in Step 1

The algorithm components are therefore (i) design of an efficient and accurate scheme for deriving surface reflectance for known atmospheric profile, and (ii) formulation of constraints on the land surface reflectance suitable spectral sampling of the instruments used (SPOT-VGT, PROBA-V and MERIS). The method is applied to estimate aerosol at a more coarse spatial resolution (8x8 km) than the underlying surface reflectance, and a subsequent interpolation step is used to obtain per-pixel values.

© UCL-Geomatics 2016
This document is the property of the LAND_COVER_CCI partnership, no part of it shall be reproduced or transmitted without the express prior written authorization of UCL-Geomatics (Belgium).

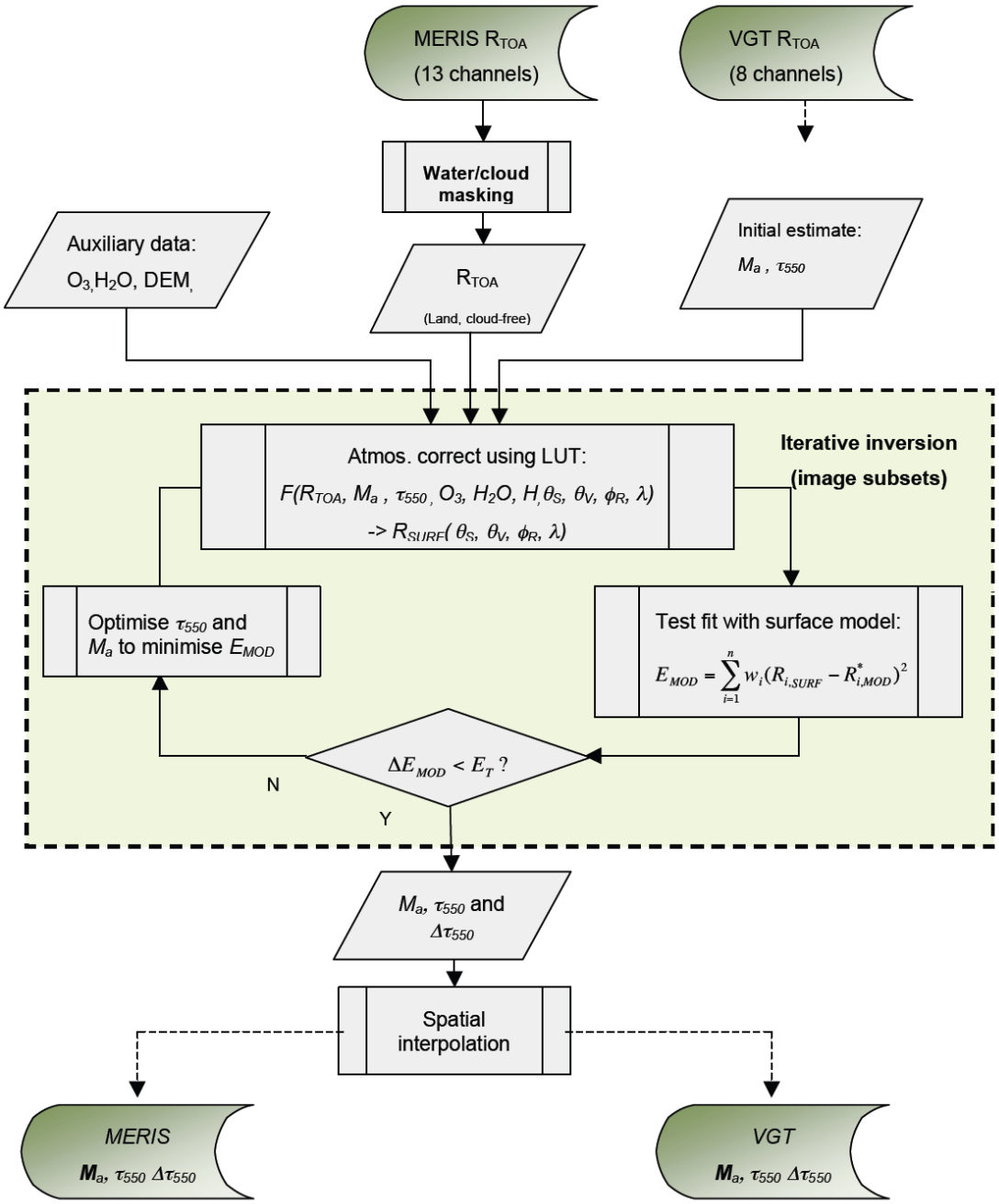


Figure 4-8: Scheme of process, graphic adopted from [GlobAlbedo_ATBDv4.12, 2013]

© UCL-Geomatics 2016
This document is the property of the LAND_COVER_CCI partnership, no part of it shall be reproduced or transmitted without the express prior written authorization of UCL-Geomatics (Belgium).

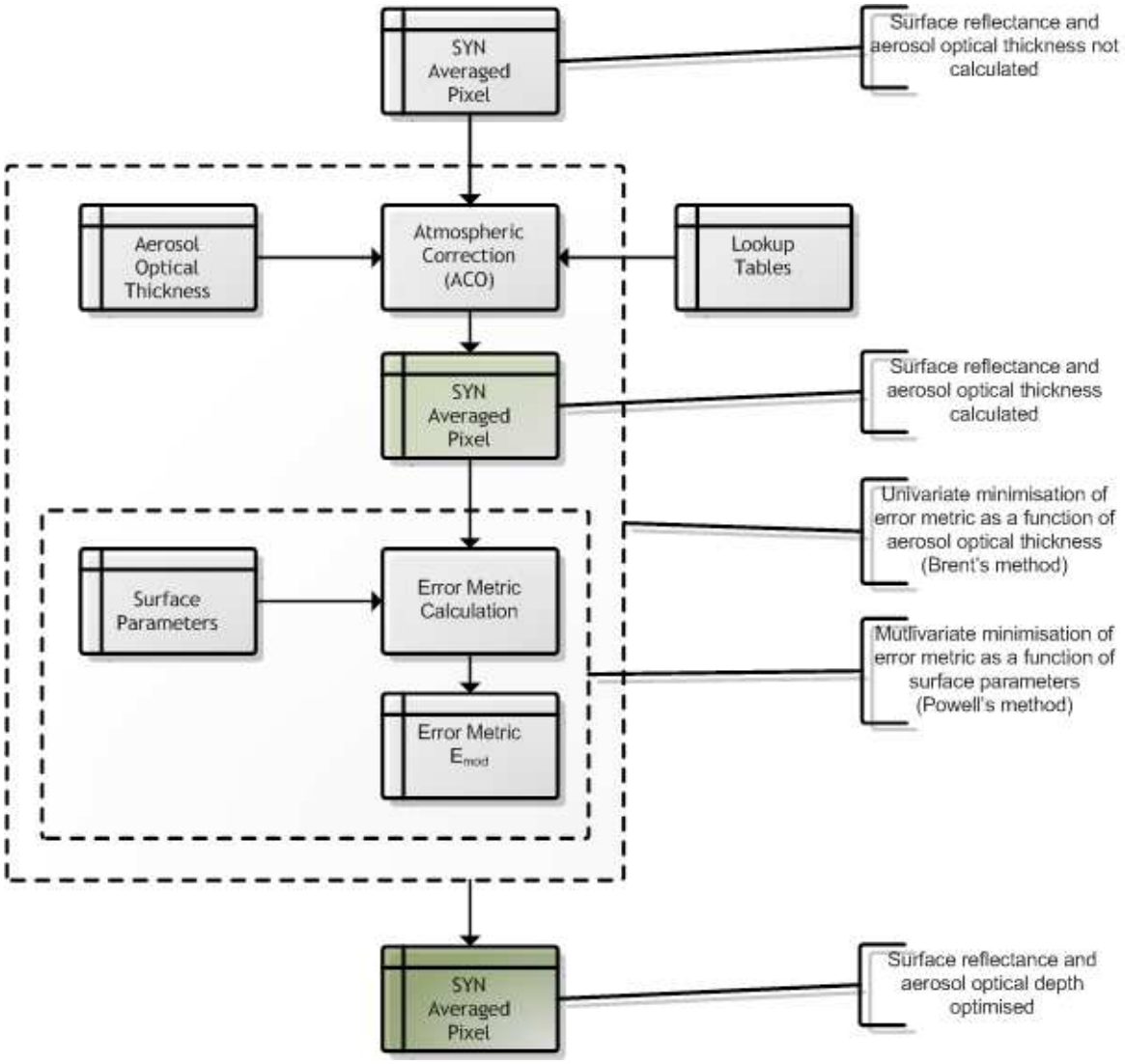


Figure 4-9: Logical flow of the aerosol retrieval and the atmospheric correction scheme. Figure from [SYN_DPMv2.3_2010]

4.5.1 MERIS FR and RR, SPOT VGT P and PROBA-V S1 TOA

The purpose of this paragraph is to provide an overview of the theoretical background of the SDR retrieval, developed by the Institute for Space Sciences, Free University of Berlin, fully documented in [GlobCover_DJFv3.8, 2008] and an improved version documented in [GlobAlbedo_ATBDv4.12, 2013].

The atmospheric correction scheme is designed for the MERIS Level2 data above land surfaces and is based on inverse modelling of radiative transfer simulations by using artificial neural network (ANN) techniques. The inverse model consists of a Multi-Layer-Perceptron with one hidden layer trained by the back-propagation algorithm [Rummelhart and McClelland, 1986]. Figure 4-10 illustrates the flowchart of the aerosol correction scheme, which is divided into two main parts: development and

© UCL-Geomatics 2016
This document is the property of the LAND_COVER_CCI partnership, no part of it shall be reproduced or transmitted without the express prior written authorization of UCL-Geomatics (Belgium).

operation of the algorithm. The development of the algorithm is sub-divided further into the sections for forward and inverse modelling.

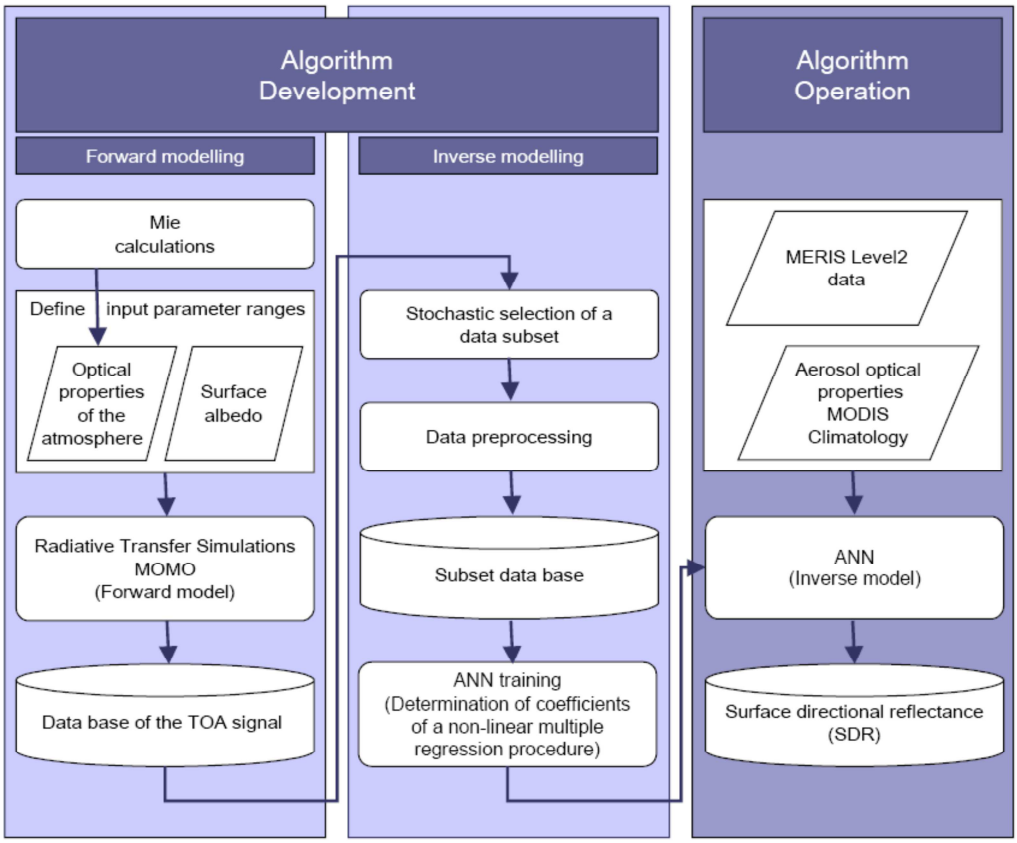


Figure 4-10: Flowchart of the proposed neural network based correction algorithm for the retrieval of the surface directional reflectance (from [GlobCover_DJFv3.8, 2008])

As forward model we used the established radiative transfer code MOMO based on the Matrix-Operator-Method ([Fischer and Grassl, 1984], [Fell and Fischer, 2001]), to simulate a database, describing the functional relationship between the surface reflectance and the Level2 signal at TOA depending on the atmospheric properties and the surface reflectance. The simulated data is then used to adapt the inverse model. The inverse model consists of a Multi-Layer-Perceptron with one hidden layer trained by the backpropagation algorithm [Rummelhart and McClelland, 1986] on a stochastic selected and pre-processed subset of the complete database. The proposed aerosol correction scheme derives the SDR at the Bottom-Of-Atmosphere (BOA) from the cloud screened TOA Level2 reflectance subsequently for each band on a pixel-by-pixel basis. To correct the influence of the aerosols the algorithm requires additional input information like aerosol optical thickness (AOT) at two wavelengths and the associated Angstroem coefficient. In the operational mode these data will be taken from MODIS measurements or from an external database or from the aerosol retrieval. Moreover, the algorithm gives an error estimate of the derived reflectances when introducing the typical uncertainty of the MODIS aerosol retrieval to the ANN input.

The improved version of the SDR retrieval, fully documented in [GlobAlbedo_ATBDv4.12, 2013], should fulfil some requirements

© UCL-Geomatics 2016
This document is the property of the LAND_COVER_CCI partnership, no part of it shall be reproduced or transmitted without the express prior written authorization of UCL-Geomatics (Belgium).

- It must be capable of deriving SDR products from top-of-atmosphere radiance data measured by MERIS, SPOT-VGT and PROBA-V;
- SDR products must include a reliable tracking of uncertainties within the entire processing including error covariance between the different spectral ranges.

The algorithm is designed to produce SDR (including uncertainties) from TOA radiance data. The algorithm requires inputs from the pixel classification and aerosol retrieval.

The TOA reflectance or apparent spectral directional reflectance R_λ^* in the waveband λ of the coupled surface-atmosphere system is related to the radiance L_λ measured by a satellite at the TOA by:

$$R_\lambda^*(\Omega_s, \Omega_v) = \frac{\pi L_\lambda(\Omega_s, \Omega_v)}{\mu_s E_{s,\lambda}}$$

eq. 4-37

where $E_{s,\lambda}$ is the extraterrestrial irradiance at the time of the measurement. The solar and view vectors are denoted by Ω_s and Ω_v respectively, while μ_s and μ_v denote cosines of solar and view zenith.

A uniform, Lambertian surface is normally assumed as a basis for the modelling of the atmosphere-surface radiative transfer for operational atmospheric correction algorithms of single-view instruments. Under that assumption, the relationship between top of atmosphere reflectance R_λ^* and the surface directional reflectance R_λ can be approximated by the equation:

$$R_\lambda^*(\Omega_s, \Omega_v) = R_{atm,\lambda}(\Omega_s, \Omega_v) + \gamma_\lambda(\mu_s)\gamma_\lambda(\mu_v)\frac{R_\lambda}{1 - \bar{\bar{\rho}}_\lambda R_\lambda}$$

eq. 4-38

Where $R_{atm,\lambda}$ means the atmospheric scattering term (TOA reflectance for zero surface reflectance), γ_λ denotes atmospheric transmission for either sensor to ground or ground to sensor for waveband λ, and $\bar{\bar{\rho}}_\lambda$ denotes atmospheric bi-hemispherical albedo with respect to the surface. The solar and view vectors are denoted by Ω_s and Ω_v respectively, while μ_s and μ_v denotes denote cosines of solar and view zenith. Spectral directional reflectance R_λ is derived from TOA reflectance by means of the analytical inversion of eq. 4-39, and the corresponding equation is:

$$R_\lambda(\Omega_s, \Omega_v) = \frac{R_\lambda^*(\Omega_s, \Omega_v) - R_{atm,\lambda}(\Omega_s, \Omega_v)}{\gamma_\lambda(\mu_s)\gamma_\lambda(\mu_v) + \bar{\bar{\rho}}_\lambda\left[R_\lambda^*(\Omega_s, \Omega_v) - R_{atm,\lambda}(\Omega_s, \Omega_v)\right]}$$

eq. 4-39

As discussed in [GlobAlbedo_ATBD/BBDRv1.0, 2010] and in [GlobAlbedo_ATBDv4.12, 2013], the Lambertian equivalent reflectance R_λ derived from eq. 4-39, which is taken as SDR in the GlobAlbedo processing chain, represents a smoothed version of the surface BRDF, with errors up to 15% for turbid atmospheres ([Hu et al., 1999] - see Figure 4-11).

R_λ^* is calculated from TOA radiance with eq. 4-37 and first corrected from gaseous absorption with a look-up table for a set of input AMF, CWV and OZO. AMF and CWV are considered pixel-wise, while a mean value representative of the imaged area is used for OZO. The atmospheric parameters $R_{atm,\lambda}$, γ_λ and $\bar{\bar{\rho}}_\lambda$ are provided by a look-up table per pixel, being the input VZA, SZA, RAA, ELEV

© UCL-Geomatics 2016
This document is the property of the LAND_COVER_CCI partnership, no part of it shall be reproduced or transmitted without the express prior written authorization of UCL-Geomatics (Belgium).

and AOD550 also provided on a per-pixel basis. No correction of adjacency effects ([Mekler and Kaufman, 1982], [Kaufman, 1989]) has been found to be necessary.

The look-up tables intended for aerosol and SDR retrieval and for error propagation have been compiled with the MOMO radiative transfer code ([Fischer and Grassl, 1984], [Fell and Fischer, 2001]). MOMO is a well introduced and widely accepted radiative transfer code which provides all the features required for atmospheric radiative transfer simulations in CCI-LC project. The look-up tables intended for gas correction and also for error propagation for are calculated with the 6S (Second Simulation of the Satellite Signal in the Solar Spectrum) radiative transfer code ([Vermote et al., 1997], [Vermote et al., 1997b]). This code is intended for fast radiative transfer calculations at a relatively coarse internal spectral sampling of 2.5 nm.

Tracking of uncertainties is one of the specific requirements for the CCI-LC processing. The purpose in this part of the processing is to generate a reliable estimation of the errors in the SDR products including the error covariance between the different spectral ranges. Different error sources are considered: instrumental noise, atmosphere and directional reflectance effects.

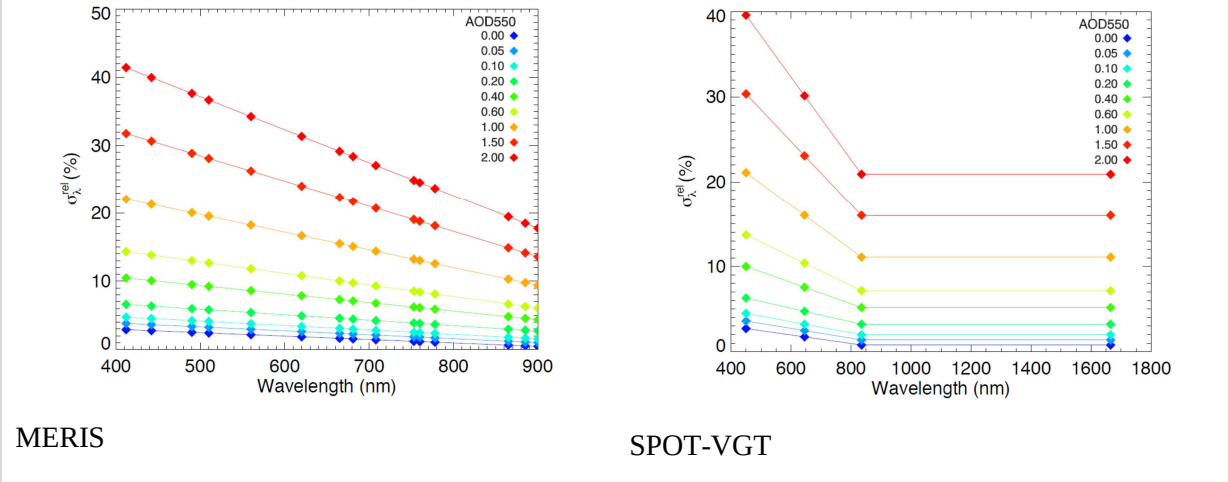


Figure 4-11: Estimation of the relative error in reflectance retrieval caused by the assumption of a Lambertian surface [Lucht, and Strahler, 1999] after resampling to the GlobAlbedo AOD550 grid and the spectral response (from [GlobAlbedo_ATBD/BBDRv1.0, 2010])

4.5.2 AVHRR

In case of AVHRR products, the atmospheric correction scheme consists the following main elements:

- computation of the top of standard atmosphere radiance
- atmospheric correction

The concept of the standard atmosphere with respect to air pressure and ozone column content has been used in order to avoid a LUT with too many parameters and therefore only the standard values for these parameters have been used for the calculation of the LUT. The idea is to put an ozone correction layer and Rayleigh correction layer on top of the standard atmosphere. The first step in the

© UCL-Geomatics 2016
This document is the property of the LAND_COVER_CCI partnership, no part of it shall be reproduced or transmitted without the express prior written authorization of UCL-Geomatics (Belgium).

atmospheric correction is the computation of the top of standard atmosphere (TOSA) radiances with respect to air pressure and ozone column content [Doerffer & Schiller, 2008].

Ozone correction [Doerffer & Schiller, 2008]

The ozone mass for correction is the difference between the standard value ($ozone_{standard}$) and the actual column content ($ozone_{actual}$) in [cm].

$$m_{ozone}^{corr} = ozone_{actual} - ozone_{standard}$$

eq. 4-40

The transmittances for the solar irradiance ($\tau_{TOA\,TOSA}^{ozone}(\lambda, \theta_s)$) and the upward radiance ($\tau_{TOA\,TOSA}^{ozone}(\lambda, \theta_v)$) with the wavelength dependent absorption coefficient ($k_{ozone}(\lambda)$) through the ozone correction layer are given by:

$$\tau_{TOA\,TOSA}^{ozone}(\lambda, \theta_s) = e^{-\left(\frac{k_{ozone}(\lambda) \cdot m_{ozone}^{corr}}{\cos(\theta_s)}\right)}$$

$$\tau_{TOA\,TOSA}^{ozone}(\lambda, \theta_v) = e^{-\left(\frac{k_{ozone}(\lambda) \cdot m_{ozone}^{corr}}{\cos(\theta_v)}\right)}$$

eq. 4-41

Correction of stratospheric aerosol

The transmittance by the stratospheric aerosol for a path under the angle (θ) through the atmosphere can be estimated by using the extinction coefficient and the optical depth ($\hat{\tau}_{modtran}^{ext}$) provided by MODTRAN. The extinction coefficients and the optical depths are given for the different types of stratospheric aerosol types: background, fresh volcanic and aged volcanic stratospheric aerosol.

$$\tau_{background_modtran}^{stratosphere_aerosol}(\lambda, \theta) = \left(e^{-\hat{\tau}_{modtran}^{ext_background}}\right)^{\frac{1}{\cos(\theta)}}$$

$$\tau_{fresh_volcanic_modtran}^{stratosphere_aerosol}(\lambda, \theta) = \left(e^{-\hat{\tau}_{modtran}^{ext_fresh_volcanic}}\right)^{\frac{1}{\cos(\theta)}}$$

$$\tau_{aged_volcanic_modtran}^{stratosphere_aerosol}(\lambda, \theta) = \left(e^{-\hat{\tau}_{modtran}^{ext_aged_volcanic}}\right)^{\frac{1}{\cos(\theta)}}$$

eq. 4-42

The transmittances for the solar irradiance ($\tau_{TOA\,TOSA}^{stratosphere_aerosol}(\lambda, \theta_s)$) and the upward radiance ($\tau_{TOA\,TOSA}^{stratosphere_aerosol}(\lambda, \theta_v)$) through the stratospheric aerosol correction layer which taken into account the difference between the background stratospheric aerosol transmittance ($\tau_{background_modtran}^{stratosphere_aerosol}$) and the actual stratospheric aerosol transmittance ($\tau_{x_modtran}^{stratosphere_aerosol}, x = fresh_vulcanic, aged_vulcanic$) are given by:

$$\tau_{TOA\,TOSA}^{stratosphere_aerosol}(\lambda, \theta_s) = \left(e^{-\left(\hat{\tau}_{modtran}^{ext_x} - \hat{\tau}_{modtran}^{ext_background}\right)}\right)^{\frac{1}{\cos(\theta_s)}} ; \; x = fresh_vulcanic, aged_vulcanic$$

© UCL-Geomatics 2016
This document is the property of the LAND_COVER_CCI partnership, no part of it shall be reproduced or transmitted without the express prior written authorization of UCL-Geomatics (Belgium).

$$\tau_{TOA\,TOSA}^{stratosphere_aerosol}(\lambda,\theta_v) = \left(e^{-\left(\hat{\tau}_{modtran}^{ext_x} - \hat{\tau}_{modtran}^{ext_background}\right)}\right)^{\frac{1}{\cos(\theta_v)}} ;\ x = fresh_vulcanic, aged_vulcanic$$

eq. 4-43

The values for the optical depth ($\hat{\tau}_{modtran}^{ext}$) are given in Table 4-23

Table 4-24 summarizes the selection criteria based on the AOD for different MODTRAN stratospheric aerosol types.

Table 4-23: Optical depth for the different stratospheric aerosols

	$\hat{\tau}_{modtran}^{ext}$ FOR BACKGROUND STRATOSPHERIC AEROSOL	$\hat{\tau}_{modtran}^{ext}$ FOR AGED VOLCANIC STRATOSPHERIC AEROSOL	$\hat{\tau}_{modtran}^{ext}$ FOR FRESH VOLCANIC STRATOSPHERIC AEROSOL
NOAA 11 Band 1	0.0058043	0.0252783	0.0967715
NOAA 11 Band 2	0.0035198	0.0193146	0.0991216
NOAA 14 Band 1	0.0057535	0.0251724	0.0968393
NOAA 14 Band 2	0.0034439	0.0190766	0.0991998

Table 4-24: Selection of stratospheric aerosol type regarding the AOD

MODTRAN STRATOSPHERIC AEROSOL TYPE	CONDITIONS RELATED TO THE AOD
background	$if\ \mathrm{AOD}_{stratosphere} < 0.03\ \ then\ background$
aged volcanic	$if\ 0.03 \leq \mathrm{AOD}_{stratosphere} \leq 0.1\ \ then\ aged\ volcanic$
fresh volcanic	$if\ \mathrm{AOD}_{stratosphere} > 0.1\ \ then\ fresh\ volcanic$

Air pressure correction [Doerffer & Schiller, 2008]

The Rayleigh correction takes into account the differences between the standard ground pressure and the concerning air pressure variations at ground. The actual pressure at ground of the pixel can be calculated from the actual pressure and temperature at altitude and the altitude, according to the barometric formula.

$$p(h_{NN}) = p(\mathrm{h})\left(1 - \frac{a(h_{NN} - h)}{T(h)}\right)^{\frac{Mg}{Ra}}$$

eq. 4-44

© UCL-Geomatics 2016
This document is the property of the LAND_COVER_CCI partnership, no part of it shall be reproduced or transmitted without the express prior written authorization of UCL-Geomatics (Belgium).

Where the constant parameters are:

- earth-surface gravitational acceleration g $= 9.80665\ m/s^2$
- molar mass of dry air M $= 0.0289644$ kg/mol
- universal gas constant R $= 8.31447\ J/(mol\ K)$

Under the assumption that the temperature gradient is 0.0065 K/m, the equation can be written in the form:

$$p(h_{NN}) = p(\mathrm{h}) \left(1 - \frac{0.0065(h_{NN} - h)}{T(h)}\right)^{5.225}$$

eq. 4-45

The relative air mass for the difference TOA-TOSA relevant for the correction is then:

$$m_{ray}^{corr} = \frac{p(h_{NN}) - p_{standard}}{p_{standard}}$$

eq. 4-46

The attenuation coefficient for the Rayleigh scattering is then computed according to the Leckner's 1978 approximate formula [Leckner, 1978]:

$$k_{ray} = 0.008375 \cdot \lambda^{-4.08}\ with\ \lambda[\mu m]$$

eq. 4-47

The transmittances for the downwelling irradiance TOA-TOSA ($\tau_{TOA\,TOSA}^{ray}(\lambda, \theta_s)$) and the upwelling radiance TOSA-TOA ($\tau_{TOA\,TOSA}^{ray}(\lambda, \theta_v)$) can be determined from the following equation:

$$\tau_{TOA\,TOSA}^{ray}(\lambda, \theta_s) = e^{-\left(0.5 \frac{k_{ray}(\lambda) \cdot m_{ray}^{corr}}{\cos(\theta_s)}\right)}$$

$$\tau_{TOA\,TOSA}^{ray}(\lambda, \theta_v) = e^{-\left(0.5 \frac{k_{ray}(\lambda) \cdot m_{ray}^{corr}}{\cos(\theta_v)}\right)}$$

eq. 4-48

The factor 0.5 is used because of the symmetric phase function of Rayleigh scattering. The Rayleigh phase function ($p(cos\Theta)$) is given by:

$$p(cos\Theta) = \frac{3}{4}(1 - cos^2\Theta)$$

eq. 4-49

Where Θ is the scattering angle and the cosine of the scattering angle can be obtained based on the spherical geometry as:

$$cos\Theta = cos\theta_s cos\theta_v + sin\theta_s sin\theta_v cos(\phi_s - \phi_v)$$

eq. 4-50

The path radiance ($L_{TOA\,TOSA}^{path}(\lambda)$) of the layer is given by:

© UCL-Geomatics 2016
This document is the property of the LAND_COVER_CCI partnership, no part of it shall be reproduced or transmitted without the express prior written authorization of UCL-Geomatics (Belgium).

$$L^{path}_{TOA\,TOSA}(\lambda) = \frac{E_{TOA}(\lambda) \cdot k_{ray}(\lambda) \cdot m^{corr}_{ray} \cdot \tau^{ray}_{TOA\,TOSA}(\lambda,\theta_s) \cdot p(cos\Theta)}{(4\pi\, cos\theta_s cos\theta_v)}$$

eq. 4-51

With the considered equations, the downwelling irradiance ($E_{TOA\,TOSA}(\lambda)$) and the upwelling radiance ($L_{TOA\,TOSA}(\lambda)$), can be calculated as follows:

$$E_{TOA\,TOSA}(\lambda) = E_{TOA}(\lambda) \cdot \tau^{ray}_{TOA\,TOSA}(\lambda,\theta_s) \cdot \tau^{ozone}_{TOA\,TOSA}(\lambda,\theta_s) \cdot \tau^{aerosol}_{TOA\,TOSA}(\lambda,\theta_s)$$

$$L_{TOA\,TOSA}(\lambda) = \frac{L_{TOA}(\lambda) - L^{path}_{TOA\,TOSA}(\lambda) \cdot \tau^{ozone}_{TOA\,TOSA}(\lambda,\theta_v) \cdot \tau^{aerosol}_{TOA\,TOSA}(\lambda,\theta_v)}{\tau^{ray}_{TOA\,TOSA}(\lambda,\theta_v) \cdot \tau^{ozone}_{TOA\,TOSA}(\lambda,\theta_v) \cdot \tau^{aerosol}_{TOA\,TOSA}(\lambda,\theta_v)}$$

eq. 4-52

Atmospheric correction [Richter & Schlaepfer, 2012]

Under the assumption of a non-uniform Lambertian surface the relationship between top of atmosphere radiance $L_{sat}(\lambda,\theta_s,\theta_v)$ and the spectral directional surface reflectance $\rho_{surf}(\lambda)$ can be approximated by the equation [Richter, 1992; Richter & Schlaepfer, 2012; Iqbal 1983; Liu 1996]:

$$L_{sat}(\lambda) = L_{p0}(\lambda) + \frac{E^*_g(\lambda)}{\pi} \cdot \rho_{surf}(\lambda)\tau_{dir}(\lambda,\theta_v) + \frac{E^*_g(\lambda)}{\pi} \cdot \overline{\rho}(\lambda)\tau_{diff}(\lambda,\theta_v)$$

eq. 4-53

where $L_p(\lambda,\theta_s,\theta_v)$ means the path radiance, $\tau(\lambda)$ denotes the total atmospheric transmission for ground to sensor for waveband λ (sum of direct $\tau_{dir}(\lambda,\theta_v)$ and diffuse $\tau_{diff}(\lambda,\theta_v)$ transmission), and $E^*_g(\lambda)$ global irradiance on a horizontal surface. The terms in eq. 4-53 can be determined by:

$$E^*_g(\lambda) = E^*_{direct}(\lambda,z) + E^*_{diffuse}(\lambda,z) + E^*_{multiple}(\lambda)$$

$$E^*_{direct}(\lambda,z) = E_s(\lambda)\tau_{dir}(\lambda,\theta_s,z)\,cos\,\theta_s$$

$$E^*_{diffuse}(\lambda,z) = E_{diffuse}(\lambda,z)$$

$$E^*_{multiple}(\lambda,z) = \frac{\left(E^*_{direct}(\lambda,z) + E^*_{diffuse}(\lambda,z)\right)}{1 - s(\lambda)\overline{\rho}(\lambda)} s(\lambda)\overline{\rho}(\lambda)$$

eq. 4-54

where z is the vertical coordinate, $E_s(\lambda)$ is the earth/sun distance-corrected exoatmospheric irradiance, $E_{diffuse}(\lambda,z)$ is the diffuse irradiance for a horizontal surface, θ_s is the solar zenith angle.

© UCL-Geomatics 2016
This document is the property of the LAND_COVER_CCI partnership, no part of it shall be reproduced or transmitted without the express prior written authorization of UCL-Geomatics (Belgium).

The computation of the spectral directional surface reflectance $\rho_{surf}(\lambda)$ is a multi-stage procedure [Richter & Schlaepfer, 2012]:

The reflectance is calculated iteratively and the adjacency effect is neglected at first. The start value for the terrain reflectance is set to $\overline{\rho}_{terrain}(\lambda) = 0.1$ and the reference reflectance is set to $\overline{\rho}_{ref} = 0.15$:

$$L_{TOA\,TOSA}(\lambda) = L_{p0}(\lambda) + \frac{E^*_{dir}(\lambda, z) + E^*_{diff}(\lambda, z)}{\pi} \cdot \rho(\lambda)\tau(\lambda, \theta_v)$$

$$\rho^{(i)}(\lambda) = \frac{\pi\left(d^2 L_{TOA\,TOSA}(\lambda) - L_{p0}(\lambda)\right)}{\tau(\lambda, \theta_v)\left(E^*_{dir}(\lambda, z) + E^*_{diff}(\lambda, z)\right)}$$

eq. 4-55

The term d is the sun earth distance in astronomical units.

Now a correction of the adjacency effect is required. Under the assumption that the direct part of the transmitted radiance comes from the area with a surface reflectance $\rho_{surface}(\lambda)$ and the diffuse part of the transmitted radiance comes from the neighbourhood with a mean reflectance $\overline{\rho}(\lambda)$ the following relationship between the different surfaces reflectances can be assumed [Richter, 1992; Richter & Schlaepfer, 2012].

Therefore the surface reflectance $\rho^*_{surface}(\lambda)$ corrected for the adjacency effect is derived by

$$\rho^*_{surface}(\lambda) = \rho^{(i)}(\lambda) + \frac{\tau_{diff}(\lambda)}{\tau_{dir}(\lambda)}\left(\rho^{(i)}(\lambda) - \overline{\rho}(\lambda)\right)$$

eq. 4-56

The final surface reflectance which includes a correction of the neighbourhood of the global irradiance $E_g(\lambda, \theta_s)$ can be expressed in the form:

$$\rho_{surface}(\lambda) = \rho^*_{surface}(\lambda)\left[1 - s(\lambda)\left(\overline{\rho}(\lambda) - \overline{\rho}_{ref}\right)\right]$$

eq. 4-57

Uncertainty estimation

In case of the uncertainty estimation for the atmospheric correction of AVHRR data, the Monte Carlo simulation, a mostly used modelling approach, has been applied. The uncertainty retrieval scheme consists of the following main elements: [Woolliams et al., 2014; Murphy et al., 2004].

- Ensemble building and AC calculations
    - Computation of the TOA reflectance values using the radiative transfer model with various atmospheric conditions and different surface reflectances (M-times repetitions)

© UCL-Geomatics 2016
This document is the property of the LAND_COVER_CCI partnership, no part of it shall be reproduced or transmitted without the express prior written authorization of UCL-Geomatics (Belgium).

- Applying the atmospheric correction using the atmospheric conditions including the known uncertainty
- N-times repetition of the AC with other atmospheric condition

- Uncertainty estimation

The Table 4-25 summarizes the specification of the parameter and their values using for the uncertainty estimation. The application of the Monte Carlo simulation including the ensemble building allows the estimation of the uncertainties concerning the model output results. The sources of uncertainty in the measurement have been identified and the size of the uncertainty from each source has been estimated. In case of both parameters, model type and aerosol type, no uncertainty has been applied for the building of the ensembles. For all other parameter an uncertainty of 10% has been used for the ensembles building and the uncertainty of the TOA reflectances has been set to 10% also. The resultant uncertainty is then stored in a lookup table regarding the grid nodes and the surface reflectances.

Table 4-25: Specification of the parameter and their values using for the uncertainty estimation

PARAMETER	
Model type	MidLatitude_Summer, MidLatitude_Winter Tropical,Sub-Arctic-Summer Sub-Arctic-Winter 1976 US-Standard
Aerosol type	rural maritime urban desert
Aerosol optical depth	0.05 - 0.5
Water vapour [cm]	0.25 - 5.25 (sealevel)
Ozone content [DU]	200 - 400
Temperature [K]	265 - 320
CO_2 mixing ratio [ppmv]	325 - 400
3 grid nodes sun zenith angles [°].	0 30 60
3 grid nodes view zenith angles [°]	0 30 60

© UCL-Geomatics 2016
This document is the property of the LAND_COVER_CCI partnership, no part of it shall be reproduced or transmitted without the express prior written authorization of UCL-Geomatics (Belgium).

PARAMETER	
3 grid nodes relative azimuth angle [°]	0 90 180
3 grid nodes altitude [km]	0.0 1.0 3.0

4.5.3 SPOT-VGT S1

The atmospheric corrections are based on the use of the SMAC software developed by the Center for the Study of the Biosphere from Space (CESBIO) [Rahman and Dedieu, 1994], which is a simplified implementation of the 6S method ([Vermote et al., 1997], [Vermote et al., 1997b] and [Tanré et al., 1992]). The SMAC software has been tuned for the SPOT-VGT spectral bands. The physical data used as input of SMAC are the following:

- The water vapour data are global short term forecasts, downloaded 4 times/day from Meteo-France. The elementary data cell corresponds to 1.5° x 1.5° in longitude and latitude. A geometrical interpolation is performed to obtain 8/112° x 8/112° cells, and a temporal interpolation is performed between the two nearest measures, taking into account the viewing time.
- A climatology of ozone obtained from the CESBIO
- A simple static models for aerosols obtained from the CESBIO
- A 8/112° resolution DEM for atmospheric pressure estimation

The atmospheric parameters (optical thickness) are calculated on 8km x 8km cells, then interpolated for every pixel, and used for the final reflectance calculation [SPOT-VGT_DataProc, 2011].

4.5.4 Improvements - atmospheric correction

The cloud coverage is one of the limitation factors for the number of available data which had consequences on the quality of the surface reflectance composites and thus, on the CCI-LC maps. As a result, the extension of the atmospheric correction related to semi-transparent clouds could be considered as an additional source for the extraction of more available data. The transfer of radiation through clouds depends on their microphysical and macrophysical properties like stratification, cloud height, particle size and optical thickness [Hünerbein et. al., 2010]. The two following approaches have been identified for the assessment of the suitability and performance:

- Improving the atmospheric correction by extending the LUT for the atmospheric correction to higher optical thicknesses in order to represent semi-transparent clouds.
- The haze removal as an additional step in the pre-processing as proposed by Richter 1996 [Richter, 1996] and Richter and Schläpfer [Richter and Schläpfer, 2012].

© UCL-Geomatics 2016
This document is the property of the LAND_COVER_CCI partnership, no part of it shall be reproduced or transmitted without the express prior written authorization of UCL-Geomatics (Belgium).

These investigations are not yet available.

Haze removal ([Richter, 1996] and [Richter and Schläpfer, 2012])

At this stage of the project, the new proposed algorithm is implemented and could be subjected to a comprehensive assessment. An important aspect is that haze regard as an additive component of the radiance signal measured at the sensor. The haze component can be estimated and removed as described in the following. Furthermore the algorithm only properly works over land and clouds have to be identified and eliminated before the approach can be applied. The algorithm contains four main steps and may be briefly described as follows:

Step 1: Masking of Clear& Haze Area

- applying the Tasseled Cap Haze transformation
- identification of clear and hazy area

Step 2: Regression “ClearLine“

- slope α calculated from scatterplot red channel vs. blue for clear pixels

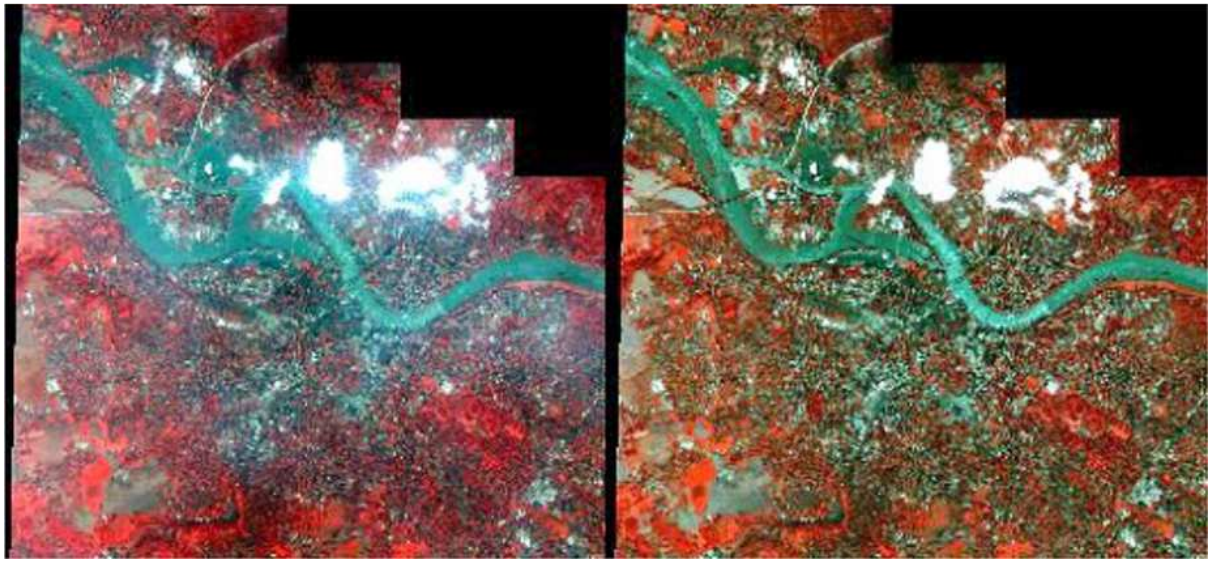
Step 3: Haze optimized transform - HOT

- $HOT = Blue \cdot \sin\alpha - Red \cdot \cos\alpha$

Step 4: Calculation of correction term Δ

- calculation of the histogram of HOT for the haze area
- retrieval of the correction Term Δ as a function of HOT-Level using histograms

A more detailed description can be found by Richter 1996 [Richter, 1996] and Richter and Schläpfer [Richter and Schläpfer, 2012]. The figure shows the result of the haze removal algorithm presenting an example of a subset of an IKONOS scene of Dresden.



© UCL-Geomatics 2016
This document is the property of the LAND_COVER_CCI partnership, no part of it shall be reproduced or transmitted without the express prior written authorization of UCL-Geomatics (Belgium).

Figure 4-12: Subset of IKONOS image of Dresden (Germany), 18. August 2002. ©Space Imaging Europe 2002. Left: original scene, right: after haze removal. Colour coding: RGB= 4,2,1 (NIR/Green/Blue bands) (figure taken from Richter and Schläpfer, 2012 [Richter and Schläpfer, 2012])

Approximate correction of the terrain effect:

Under the assumption of a non-uniform Lambertian surface the relationship between top of atmosphere radiance $L_{sat}(\lambda,\theta_s,\theta_v)$ and the spectral directional surface reflectance $\rho(\lambda)$ can be approximated by the equation ([Richter and Schläpfer, 2012], [Richter, 1996], [Iqbal., 1983], [Liou, 1992]):

$$L_{sat}(\lambda) = L_{p0}(\lambda) + \frac{E_g^*(\lambda)}{\pi} \cdot \rho_{surf}(\lambda)\tau_{dir}(\lambda,\theta_v) + \frac{E_g^*(\lambda)}{\pi} \cdot \overline{\rho}(\lambda)\tau_{diff}(\lambda,\theta_v)$$

eq. 4-58

where $L_p(\lambda,\theta_s,\theta_v)$ means the path radiance, $\tau(\lambda)$ denotes the total atmospheric transmission for ground to sensor for waveband λ (sum of direct $\tau_{dir}(\lambda,\theta_v)$ and diffuse $\tau_{diff}(\lambda,\theta_v)$ transmission), and $E_g^*(\lambda)$ global irradiance on a inclined surface. The global irradiance $E_g^*(\lambda)$ at an inclined surface can be expressed in terms of a sum of the direct irradiance $E_{direct}^*(\lambda,z)$, the diffuse irradiance $E_{diffuse}^*(\lambda,z)$, adjacent slope reflected irradiance $E_{neighbour}^*(\lambda)$ and the irradiance $E_{multiple}^*(\lambda)$ due to the multiple reflection between atmosphere and ground in the form:

$$E_g^*(\lambda) = E_{direct}^*(\lambda,z) + E_{diffuse}^*(\lambda,z) + E_{neighbour}^*(\lambda) + E_{multiple}^*(\lambda)$$

eq. 4-59

The terms in the previous equation can be determined by:

$$E_{direct}^*(\lambda,z) = bE_s(\lambda)\tau_{dir}(\lambda,\theta_s,z)\cos\beta$$

$$E_{diffuse}^*(\lambda,z) = E_{diffuse}(\lambda,z)\left[b\tau_{dir}(\lambda,\theta_s,z)\frac{\cos\beta}{\cos\theta_s} + \left(1 - b\tau_{dir}(\lambda,\theta_s,z)\right)V_{sky}\right]$$

$$E_{neighbour}^*(\lambda,z) = 0.5\,\overline{\rho}(\lambda)\left(E_{direct}^*(\lambda,z) + E_{diffuse}^*(\lambda,z)\right)(1-\cos\alpha)$$

$$E_{neighbour}^*(\lambda,z) = \overline{\rho}_{terrain}(\lambda)\left(E_{terrain}^*(\lambda,z)\right)\left(1 - V_{sky}\right)$$

$$E_{multiple}^*(\lambda,z) = \frac{\left(E_{direct}^*(\lambda,z) + E_{diffuse}^*(\lambda,z) + E_{neighbour}^*(\lambda,z)\right)}{1 - s(\lambda)\overline{\rho}(\lambda)} s(\lambda)\overline{\rho}(\lambda)$$

$$\cos\beta = \cos\theta_s\cos\theta_n + \sin\theta_s\sin\theta_n\cos(\phi_s - \phi_n)$$

eq. 4-60

where z is the vertical coordinate, b is a binary factor taken into account the shadow pixel, $E_s(\lambda)$ .the earth/sun distance-corrected exoatmospheric irradiance, $E_{diffuse}(\lambda,z)$ is the diffuse irradiance for a horizontal surface, α is the slope of the terrain, V_{sky} is the sky view factor The terms θ_s, θ_n, ϕ_s, ϕ_n, β denote solar zenith angle, terrain slope, solar azimuth and topographic azimuth and the illumination angle (angle between the solar ray and the surface normal).

© UCL-Geomatics 2016
This document is the property of the LAND_COVER_CCI partnership, no part of it shall be reproduced or transmitted without the express prior written authorization of UCL-Geomatics (Belgium).

4.5.5 Pseudo-code representation

This subsection provides an overview of the atmospheric correction including aerosol retrieval from the software development point of view. A more detailed description of the logical flow and individual processing steps can be found in the CCI Land Cover DPM [Ph1_DPMv2.2, 2013]. Furthermore the input and output products being used within the LC-CCI processing modules are described in the CCI Land Cover IODD [Ph1_IODDv1.0, 2013] in more detail.

```
algorithm AER is
    input: Pixel p with input properties, e.g pixel identification flag
    output: Pixel q containing the aerosol parameters:
                aerosol model index i,
                aerosol Angstrom exponent a,
                aerosol optical depth τ,
                uncertainty in aerosol optical depth Δτ
                aerosol retrieval flags f
        return q(i, a, d, dErr, f)
```

Algorithm 4-26: Aerosol retrieval

```
algorithm API is
    input: Raster of samples for the 8x8 coarse grid, S
    output: Raster of samples for the original grid, T
    return T
```

Algorithm 4-27: Interpolation of aerosol parameters (API)

```
algorithm ACO is
    input: Pixel p with input properties obtained from AER algorithm, i.e.
           Aerosol model index i,
           Aerosol optical depth d
    output: Pixel q containing the properties
                aerosol optical depth d,
                surface reflectance r(b) for each band b in p
    return q(d,r)
```

Algorithm 4-28: Atmospheric correction

```
algorithm ERR is
    input: Pixel q with properties; here:
              surface reflectance r_surf(b) for each band b in q,
```

© UCL-Geomatics 2016
This document is the property of the LAND_COVER_CCI partnership, no part of it shall be reproduced or transmitted without the express prior written authorization of UCL-Geomatics (Belgium).

```
            aerosol optical depth d
        Spectral mixing coefficient C_soil,
        Spectral mixing coefficient C_veg,
        Structural parameters for model of surface reflectance v_1, v_2,
        Spectral parameters for model of surface reflectance w_1, …, w_6
    output:Error metric e
    return e
```

Algorithm 4-29: Error metric calculation

```
algorithm SDR is
    input: Pixel q with input properties; here:
        1) TOA reflectance R_λ*(b) for each band b in q,
        2) lookup table for atmospheric transmissions γ_λ(−μ_s) , γ_λ(μ_v) ,
           and the atmospheric scattering term R_atm as a function of
           aerosol optical depth τ_550, elevation h, and
           view and solar vectors, LUT-1(τ_550, h, Ω_v, Ω_s)
        3) lookup table for gaseous transmittance T_g as a function of
           air mass factor, water vapour and ozone, LUT-3(AMF, CWV, OZO)
        4) atmospheric bi-hemispherical albedo ρ̄_λ
    output:  SDR R_λ(b) for each band b in q
    return q(R_λ; R_λ*, γ_λ(−μ_s), γ_λ(μ_v), R_atm T_g)
```

Algorithm 4-30: SDR retrieval

```
algorithm SDR_ERR is
    input: Pixel q with input properties; here:
        1) the SDR R_λ(b) retrieved for each band b in q,
        2) lookup table for gradient J_AOD as a function of R_λ ,
           aerosol optical depth τ_550, elevation h, and
           view and solar vectors, LUT-2(τ_550, h, Ω_v, Ω_s)
        3) lookup table for gradients J_CWV and J_OZO as a function of R_λ ,
           air mass factor, water vapour and ozone, LUT-4(AMF, CWV, OZO)
        4) the AOT uncertainty, Δτ_550
        5) the CWV uncertainty, σ²_CWV (from auxdata file, see
           [GlobAlbedo_ATBD/BBDRv3.0, 2011]
        6) the OZO uncertainty, σ²_OZO (from auxdata file, see
           [GlobAlbedo_ATBD/BBDRv3.0, 2011]
```

© UCL-Geomatics 2016
This document is the property of the LAND_COVER_CCI partnership, no part of it shall be reproduced or transmitted without the express prior written authorization of UCL-Geomatics (Belgium).

output: SDR error $\sigma_\lambda^2(i,j)$ for each band combination (b_i,b_j) in q

return $q(\sigma_\lambda^2;\ R_\lambda,\ J_X,\ \sigma_x^2)$

Algorithm 4-31: SDR error retrieval

4.6 L3-Processing

The processing steps to retrieve the final Level 3 products from an input set of single satellite observations (i.e., SDR and pixel classification data as derived in the previous sections) are (i) the reprojection of the input products onto a Plate Carrée grid, (ii) the aggregation of the single satellite observations for given binning cells (tiles), and (iii) the mosaicing of the binning cells to a (usually global) Level 3 product with the aggregation results. This processing flow is illustrated in Figure 4-13. The Level 3 product will in return serve as input for the classification algorithms to derive a final landcover map [Ph1_DPMv2.2, 2013].

4.6.1 Plate-Carrée projection

The plate carrée projection or geographic projection or equirectangular projection, is a very simple map projection that has been in use since the earliest days of spherical cartography. The name is from the French for "flat and square". It is a special case of the equidistant cylindrical projection in which the horizontal coordinate is the longitude and the vertical coordinate is the latitude.

The spherical earth can only be mapped onto a developable surface by allowing distortion, so certain geometric properties on the sphere are not preserved. The Platte Carrée projection is a cylindrical projection but unlike the Mercator projection, the entire sphere, including the poles can be represented on a finite sized map. The projection is not a conformal map so angles are not preserved.

Because of the distortions introduced by this projection, it has little use in navigation or cadastral mapping and finds its main use in thematic mapping. It has also become a de-facto standard for computer applications that process global maps, such as Celestia, because a given co-ordinate is very easily identifiable in an image file.

The following equations describe the mapping of geographic coordinates in terms of latitude φ and longitude λ onto the x and y coordinates of a point on the map. From its latitude φ and longitude λ (with φ_0 and λ_0 being the latitude and longitude in the centre of map) and k being an appropriate scale factor at the equator:

$$x = k(\lambda - \lambda_0)$$
$$y = k(\varphi - \varphi_0)$$

eq. 4-61

For the CCI-LC products, the geoid WGS84 is used.

© UCL-Geomatics 2016
This document is the property of the LAND_COVER_CCI partnership, no part of it shall be reproduced or transmitted without the express prior written authorization of UCL-Geomatics (Belgium).

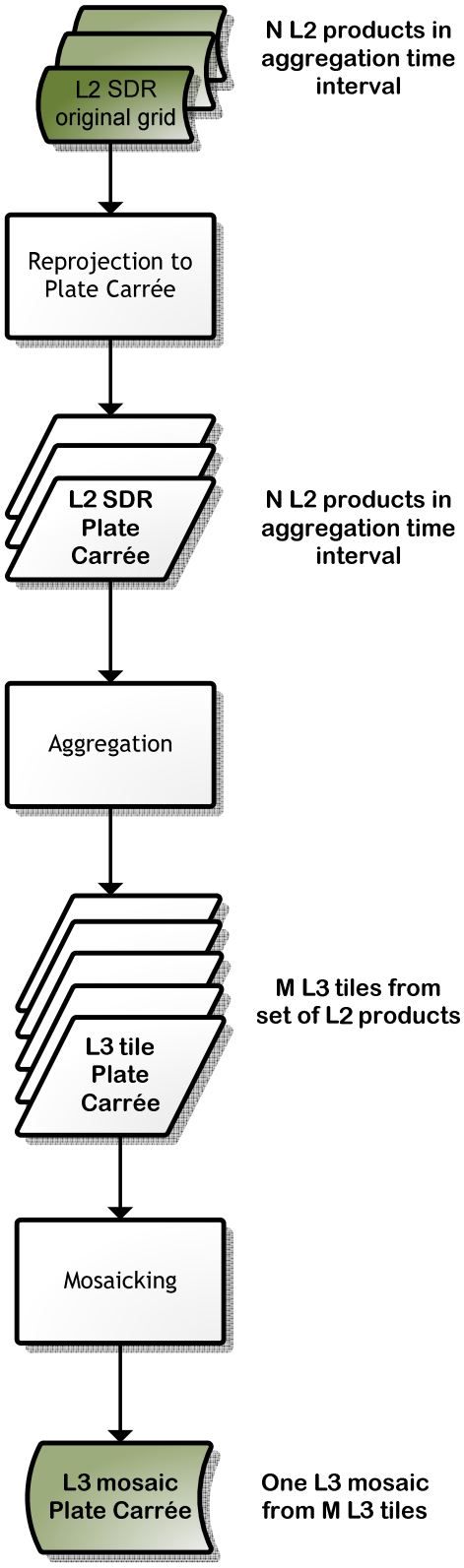


Figure 4-13: Overall logical flow of the CCI-LC L3 processing as final step of the pre-processing part (from [Ph1_DPMv2.2, 2013])

© UCL-Geomatics 2016
This document is the property of the LAND_COVER_CCI partnership, no part of it shall be reproduced or transmitted without the express prior written authorization of UCL-Geomatics (Belgium).

4.6.2 Resampling

If a product is projected it comes up that the pixel centres of the target product generally not correspond to the centres of the pixels of the input product. Resampling entitles the process of determination and interpolation of pixels in the source product for computation of the pixel values in the target product. The effects of resampling will especially be visible if the pixels in the target product are larger than the source pixels. Three different resampling methods for this computation are described here.

4.6.2.1 *Nearest neighbour*

Every pixel value in the output product is set to the nearest input pixel value.

Table 4-26: Advantages and disadvantages of the nearest neighbour

PROS	CONS
Very simple, fast	Some pixels get lost and others are duplicated
No new values are calculated by interpolation	Loss of sharpness
Fast, compared to Cubic Convolution resampling	

Figure 4-14 demonstrates the calculation of the new pixel value.

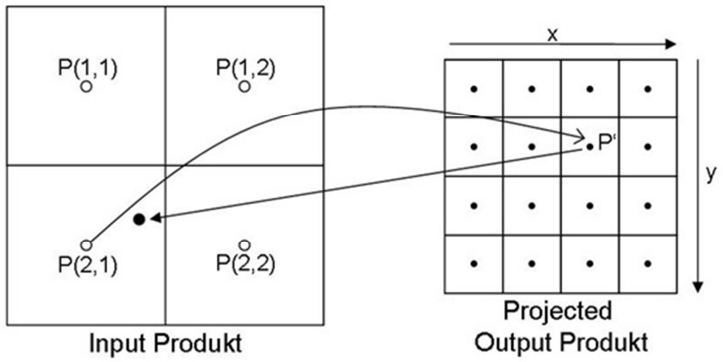


Figure 4-14: Nearest Neighbour

4.6.2.2 *Bi-linear interpolation*

Calculation of the new pixel value is performed by the weight of the four surrounding pixels.

Table 4-27: Advantages and disadvantages of the bilinear interpolation

PROS	CONS
Extremas are balanced	Less contrast compared to Nearest Neighbour
Image losses sharpness compared to Nearest Neighbour	New values are calculated which are not present in the input product

Figure 4-15 demonstrates the calculation of the new pixel value.

© UCL-Geomatics 2016
This document is the property of the LAND_COVER_CCI partnership, no part of it shall be reproduced or transmitted without the express prior written authorization of UCL-Geomatics (Belgium).

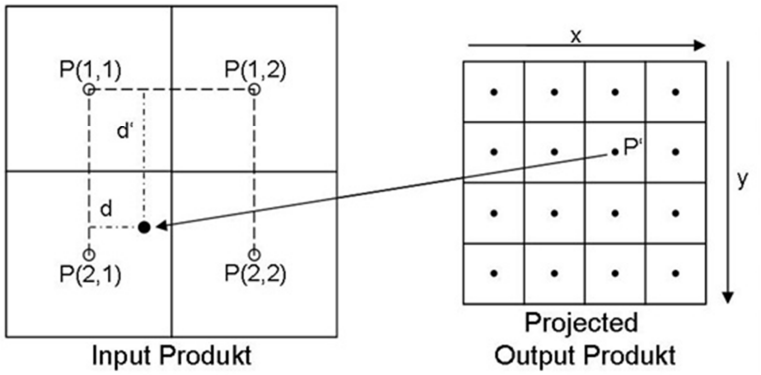


Figure 4-15: Bilinear Interpolation

The bilinear interpolation is performed by the following equation:

$$P'(x,y) = P(1,1)(1-d)(1-d') + P(1,2)(d)(1-d') + P(2,1)(d')(1-d) + P(2,2)d\,d'$$

eq. 4-62

4.6.2.3 *Cubic convolution*

Calculation of the new pixel value is performed by weighting the 16 surrounding pixels.

Table 4-28: Advantages and disadvantages of the cubic convolution

PROS	CONS
Extremas are balanced	Less contrast compared to Nearest Neighbour
Image is sharper compared to Bi-linear Interpolation	New values are calculated which are not present in the input product
	Slow, compared to Nearest Neighbour resampling

Figure 4-16 demonstrates the calculation of the new pixel value.

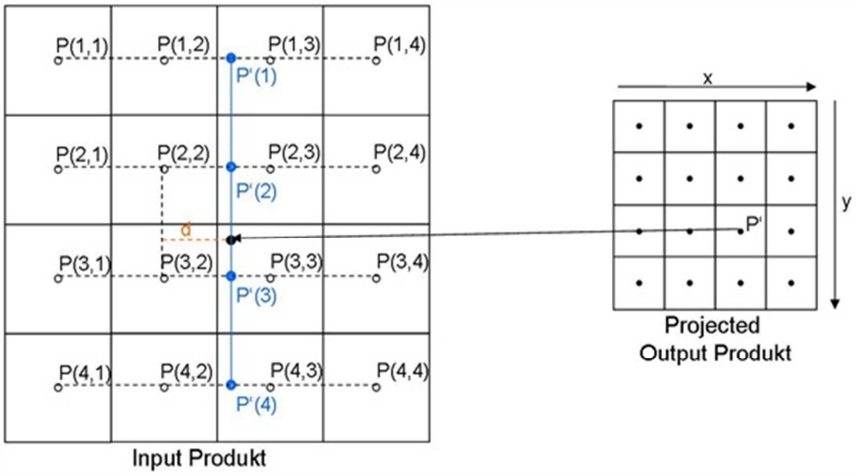


Figure 4-16: Cubic Convolution

© UCL-Geomatics 2016
This document is the property of the LAND_COVER_CCI partnership, no part of it shall be reproduced or transmitted without the express prior written authorization of UCL-Geomatics (Belgium).

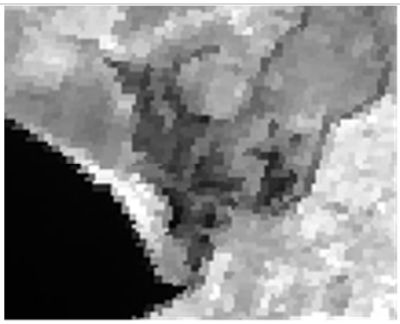
The cubic interpolation is performed by the following equation:

$$P'(k) = P(k,1)[4 - 8(1+d) + 5(1+\mathrm{d})^2 - (1+\mathrm{d})^3] + P(k,2)[1 - 2d^2 + d^3] + P(k,3)[1 - 2(1-d)^2 + (1-d)^3] + P(k,4)[4 - 8(2-d) + 5(2-d)^2 - (2-d)^3]$$

eq. 4-63

In the first step the average value for each line is calculated, afterwards the new pixel value is calculated with the four new average values P'(1) - P'(4) similar to the preceding calculation.

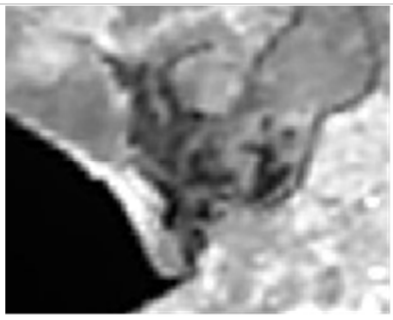
4.6.2.4 *Visual comparison of the resampling methods*



Nearest Neighbour



Bi-linear Interpolation



Cubic Convolution

Figure 4-17: Visual comparison

Nearest Neighbour

Each output cell value in the nearest neighbour method is the unmodified value from the closest input cell. Less computation is involved than in other methods, leading to a speed advantage for large input raster files. Preservation of the original cell values can also be an advantage if the resampled raster will be used in later quantitative analysis, such as automatic classification. However, nearest neighbour resampling can cause feature edges to be offset by distances up to half of the input cell size. If the raster is resampled to a different cell size, a blocky appearance can result from the duplication (smaller output cell size) or dropping (large cell size) of input cell values.

Bilinear Interpolation

An output cell value in the bilinear interpolation method is the weighted average of the four closest input cell values, with weighting factors determined by the linear distance between output and input cells. This method produces a smoother appearance than the nearest neighbour approach, but it can diminish the contrast and sharpness of feature edges. It works best when resampling to a smaller output cell size.

Cubic Convolution

The cubic convolution method calculates an output cell value from a 4 X 4 block of surrounding input cells. The output value is a distance-weighted average, but the weight values vary as a nonlinear function of distance. This method produces sharper, less blurry images than bilinear interpolation, but

© UCL-Geomatics 2016
This document is the property of the LAND_COVER_CCI partnership, no part of it shall be reproduced or transmitted without the express prior written authorization of UCL-Geomatics (Belgium).

it is the most computationally intensive resampling method. It is the preferred method when resampling to a larger output cell size.

However, the nearest neighbour method has been selected as resampling method for the projection caused by its preservation of the original physical values.

4.6.3 Temporal sample aggregation

Basically, the temporal sample aggregation is, for a given pixel in a given aggregation grid cell (a spatial tile), an integration over all input data, providing aggregated values of SDR and SDR uncertainties, the number of counts from all observations for each possible status, and a final status flag derived from a scheme which analyses these number of counts. Finally, SDR and SDR uncertainties are normalized by the number of occurrences of the "final status" for the given pixel. Table 4-29 summarizes the types of final status flag [Ph1_DPMv2.2, 2013].

Table 4-29: Final status flag

FLAG NAME	DESCRIPTION
CURRENT_PIXEL_STATE	final pixel classification after aggregation (one of the following flags)
CLEAR_LAND	pixel was classified as land
CLEAR_WATER	pixel was classified as water
CLEAR_SNOW_ICE	pixel was classified as cloudy
CLOUD	pixel was classified as cloud or pixel was classified as 'temporal' cloud (a posteriori cloud check within the aggregation scheme)
CLOUD_SHADOW	pixel was classified as cloud shadow
INVALID	pixel was classified as invalid or cosmetic

The temporal sample aggregation sums up all measurements to the intermediate variables and saved different status counts for a pixel. The 7-day compositing period is adapted on a fixed basis: every January 1st as starting point and a continuous 7 day intervals for each year has been proposed. The last composite of each year and the last February composite of a leap year include 8 days instead 7days.

Figure 4-18 and the following pseudo-code (eq. 4-2) describe and illustrate the temporal sample aggregation [Ph1_DPMv2.2, 2013].

© UCL-Geomatics 2016
This document is the property of the LAND_COVER_CCI partnership, no part of it shall be reproduced or transmitted without the express prior written authorization of UCL-Geomatics (Belgium).

pixel classification status **after** aggregation (X=LAND, CLOUD etc.)

STATUS_X

surface reflectances for N_λ wavelengths of given sensor

for j=1 … N_λ and $N_{obs} := N_{obs,STATUS_X}$

$$S_{agg(j,i)} := \overline{SDR_j}(i) = \frac{1}{N_{obs}(i)} \sum_{m=1}^{N_{obs}(i)} SDR_j(i,m)$$

NDVI

for $Nobs := Nobs_{,STATUS_X}$

$$Sagg(N\lambda + 1, i) := \overline{NDVI}(i) = \frac{1}{N_{obs}(i)} \sum_{m=1}^{Nobs(i)} NDVI(i,m)$$

error in surface reflectances for N_λ wavelengths of given sensor

for j=N_λ +2 … 2*N_λ +2 and $N_{obs} := N_{obs,STATUS_X}$

$$S_{agg(j,i)} := \overline{\Delta SDR_j}(i) = \frac{1}{N_{obs}(i)} \sum_{m=1}^{N_{obs}(i)} \Delta SDR_j(i,m)$$

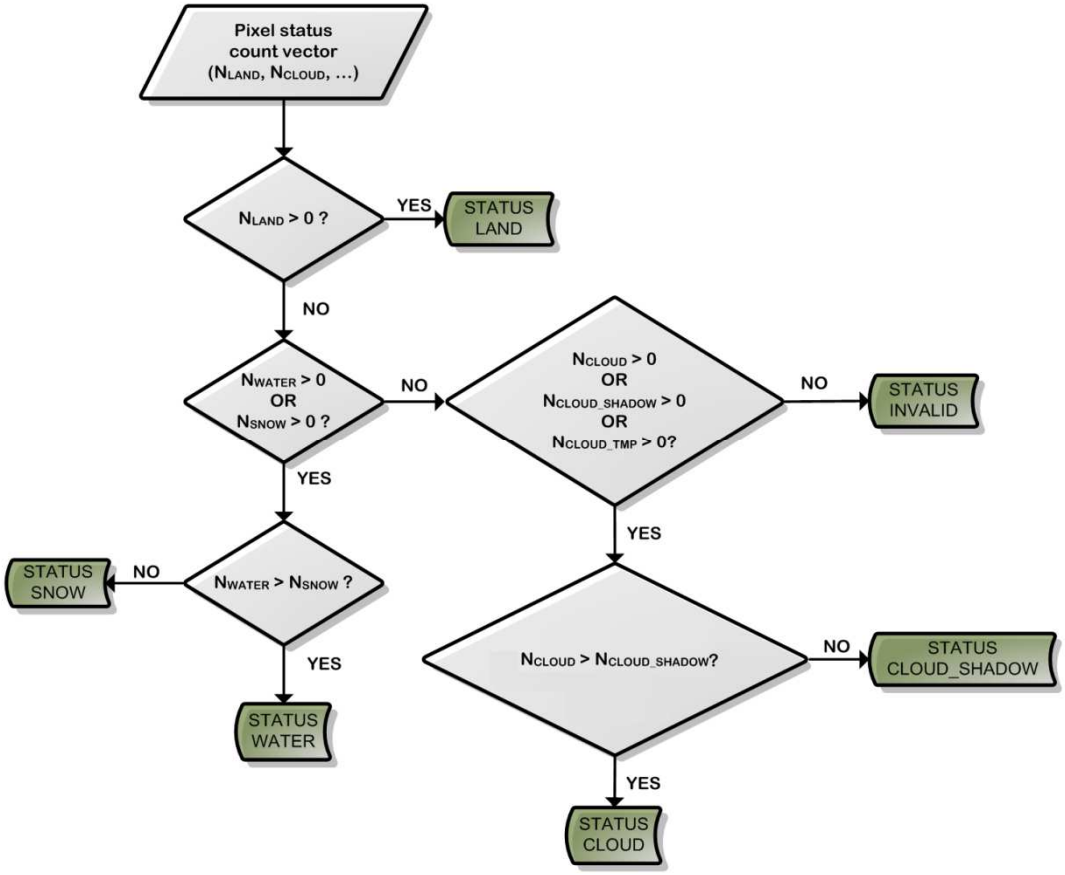


Figure 4-18: Logical flow of the pixel classification after aggregation. NX (with STATUS_X from Table 4-29) represents the number of single observations of a pixel Pi with status X, the green boxes show the final (taken from [Ph1_DPMv2.2, 2013]).

© UCL-Geomatics 2016
This document is the property of the LAND_COVER_CCI partnership, no part of it shall be reproduced or transmitted without the express prior written authorization of UCL-Geomatics (Belgium).

4.6.4 Clear land filtering

4.6.4.1 *Clear land feature of IdePix*

An important step before or in the compositing algorithm is the application of the clear land feature, which was developed to deal with a significant amount of residual clouds and haze not detected by the other IdePix features and which are thus present in the L2 products. The clear land feature is applied to all pixels classified as "clear land" by IdePix. The steps of this clear land pixel filter applied to each pixel of the SDR image can be summarized as follow:

- Conversion from RGB to HSV
- Retrieving of probability of land and cloud based on prior probability densities of each class
- Applying of threshold to a combination of the retrieved probability of land and cloud

This algorithm is based on surface reflectance values (i.e. on the final L2 products, just before the re-projection and compositing steps).

To convert from RGB to HSV, the values of H (hue), S (saturation) and V (value) could been computed from the values of R (red), G (green) and B (blue) for each pixel by applying the following equations:

$$V = MAX(R,G,B)$$

$$S = \begin{cases} 0 & if\ R = G = B = 0 \\ \dfrac{MAX(R,G,B) - MIN(R,G,B)}{MAX(R,G,B)} & \end{cases}$$

$$H = \begin{cases} 0^{\circ} & if\ R = G = B \\ 60^{\circ} \cdot \left(0 + \dfrac{G - B}{MAX(R,G,B) - MIN(R,G,B)}\right) & if\ MAX(R,G,B) = R \\ 60^{\circ} \cdot \left(2 + \dfrac{B - R}{MAX(R,G,B) - MIN(R,G,B)}\right) & if\ MAX(R,G,B) = G \\ 60^{\circ} \cdot \left(4 + \dfrac{R - G}{MAX(R,G,B) - MIN(R,G,B)}\right) & if\ MAX(R,G,B) = B \end{cases}$$

$$if\ H < 0^{\circ}\ then\ H = H + 360^{\circ}$$

eq. 4-64

The clear land filter uses the following bands coding the false colour RGB.

- R = SDR of MERIS band 7
- G = SDR of MERIS band 14
- B = SDR of MERIS band 3

The computed values of hue, saturation and value of each pixel allows determining the probability of cloud, town and land on each pixel. The value of the probabilities is determined for this purpose by the prior probability density. This prior probability density can be derived from manually classified cloud, town and land pixel in satellite images. Here different MERIS FR L2 SDR pre-processing

© UCL-Geomatics 2016
This document is the property of the LAND_COVER_CCI partnership, no part of it shall be reproduced or transmitted without the express prior written authorization of UCL-Geomatics (Belgium).

products has been used. The Figure 4-19 shows the exemplified prior probability density for cloud, town and land.

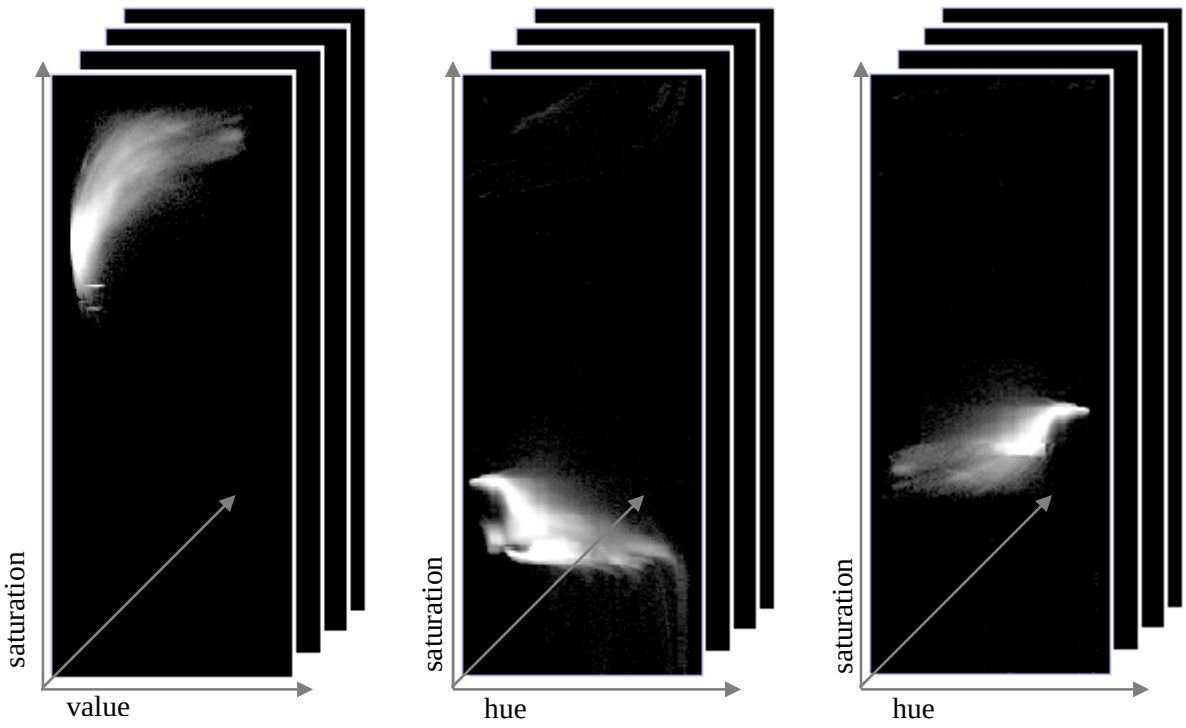


Figure 4-19: Exemplified prior probability density for cloud, town and land derived from MERIS FR L2- SDR pre-processing products

Based on the probability of clear land (land+ town) and cloud pixel, the final status for each pixel has been defined by the following conditions:

$$p_{cloud} = NaN \; and \; p_{land} = NaN \; and \; p_{town} = NaN \Longrightarrow status_{final} = cloud$$
$$p_{cloud} = NaN \; and \; p_{land} \neq NaN \; and \; p_{town} \neq NaN \Longrightarrow status_{final} = land$$
$$p_{cloud} \neq NaN \; and \; p_{land} = NaN \; and \; p_{town} = NaN \Longrightarrow status_{final} = cloud$$
$$p_{cloud} \neq NaN \; and \; p_{land} \neq NaN \; and \; p_{town} = NaN \Longrightarrow status_{final} = \begin{cases} land & if \; p_{cloud} < p_{land} \\ cloud & if \; p_{cloud} \geq p_{land} \end{cases}$$
$$p_{cloud} \neq NaN \; and \; p_{land} = NaN \; and \; p_{town} \neq NaN \Longrightarrow status_{final} = \begin{cases} land & if \; p_{cloud} < p_{town} \\ cloud & if \; p_{cloud} \geq p_{town} \end{cases}$$

© UCL-Geomatics 2016
This document is the property of the LAND_COVER_CCI partnership, no part of it shall be reproduced or transmitted without the express prior written authorization of UCL-Geomatics (Belgium).

$$p_{cloud} \neq NaN \; and \; p_{land} \neq NaN \; and \; p_{town} \neq NaN \Longrightarrow status_{final} = \begin{cases} cloud \;\; if \; p_{cloud} \geq p_{town} \; and \; p_{cloud} \geq p_{land} \\ land \;\; otherwise \end{cases}$$

eq. 4-65

The combination of the other IdePix feature and clear land feature leads to a balancing of their strengths and weaknesses. Although it does not completely solve the problem of remaining clouds, it allows significant improvement of the quality of the detection of clouds.

4.6.4.2 *Temporal filtering*

An important step in the compositing algorithm is the temporal pixel classification, which was developed to deal with a significant amount of residual clouds and haze not detected by IdePix and the clear land filter and which are thus present in the L2 products. The temporal pixel classification amounts to a temporal filtering. It is applied to all pixels classified as "clear land" by IdePix and consists in computing the mean μ and standard deviation σ of the MERIS band 8 ρ_8 or of SPOT VGT/ P band B3 ρ_{B3} or PROBA-V band B3 ρ_{B3} or AVHRR band 2 ρ_{B2} over a certain time interval. This time interval does not only consist of the compositing period but has been extended by 10 days before and after the compositing period, thus corresponding to 27 days for the compositing periods of 7. Such enlargement was found to be necessary to ensure statistic values (μ and σ) computed based on a sufficient amount of data. Based on these μ and σ values, the three following thresholds τ_1, τ_2 and τ_3 have been defined:

$$\tau_1 = \frac{\sigma}{\mu}$$

$$\tau_2 = \mu + \sigma$$

$$\tau_3 = 1.35\,\mu$$

eq. 4-66

The threshold τ_3 has been inferred from investigations about BRDF achieved in this project, in which a "variability" of the SDR measurements between 5 to 31% was found. The threshold value was defined using the maximum variability (i.e. 31%) plus an additional safety factor. The following additional threshold has been assessed for an improvement of the efficiency of the temporal filtering:

$$\tau_4 = \rho_{band}^{MAX_NDVI} + 2\sigma \; e.g. \; band = 8 \; (MERIS), B3 \; (SPOT \; VGT/PROBA-V) \text{ and b2 (AVHRR)}$$

eq. 4-67

A pixel would be now flagged as cloud (i.e. not clear land) if it satisfies the following conditions:

$$\tau_1 > 0.075 \; (\text{MERIS}, SPOT \; VGT, PROBA-V, \text{AVHRR})$$

$$\rho_{band} > MIN(\tau_2, \tau_3, \tau_4)$$

eq. 4-68

In case of SPOT VGT and PROBA-V, an additional temporal filter is applied to all pixels classified as "clear land" and as "cloud shadow" by IdePix with the idea of identification and removing of cloud shadow pixels. Based on the μ and σ values, the two following thresholds τ_5 and τ_6 have been defined:

© UCL-Geomatics 2016
This document is the property of the LAND_COVER_CCI partnership, no part of it shall be reproduced or transmitted without the express prior written authorization of UCL-Geomatics (Belgium).

$$\tau_5 = \mu - \sigma$$

$$\tau_6 = 0.65\,\mu$$

eq. 4-69

The threshold τ_6 has been also inferred from investigations about BRDF achieved in this project. A pixel would be now flagged as cloud shadow if it satisfies the following conditions:

$$\rho_{band} < MIN(,\tau_5,\tau_6)$$

eq. 4-70

Accordingly, the number of clear land of observation in the L3 products are a combined function of the composite period but also of the temporal filter efficiency. The temporal filter efficiency depends on three main factors: (i) the length of the filter interval, (ii) the quality of IdePix results and (iii) the pixels seasonality.

With regard to the length of the filter interval (first factor), it is related to the statistic values computation: a longer filter interval will allow more robust mean and standard deviation values (μ and σ) and hence, a higher efficiency of the filter. The IdePix performance (second factor) is also important since it will influence the proportions of correct and misclassified clear land pixels in the set of clear land pixels to reclassify through the temporal filter. If the fraction of misclassified clear land pixel is high, the corresponding SDRs lead to an increasing of the standard deviation of the calculated threshold respective and prevent an effective filtering. Finally, the pixels seasonality (third factor) also plays a role in decreasing the robustness of the mean value (μ).

The Figure 4-20 shows the dependence of temporal filtering on the distribution of the SDRs for 3 possible cases:

- **ideal case**: a lot of correct classified clear land pixels and only a few misclassified pixels leads to the following result after applying the temporal filter: only correct classified clear land pixels exist;
- **seasonal case**: only correct classified clear land pixels, but with a seasonal characteristic leads to the following result after applying the temporal filter: a lot of correct classified clear land pixels are reclassified as cloud;
- **worst case**: a lot of misclassified clear land pixels and only a few correct classified pixel leads to the following result after applying the temporal filter: a lot of misclassified clear land pixels still remain.

© UCL-Geomatics 2016
This document is the property of the LAND_COVER_CCI partnership, no part of it shall be reproduced or transmitted without the express prior written authorization of UCL-Geomatics (Belgium).

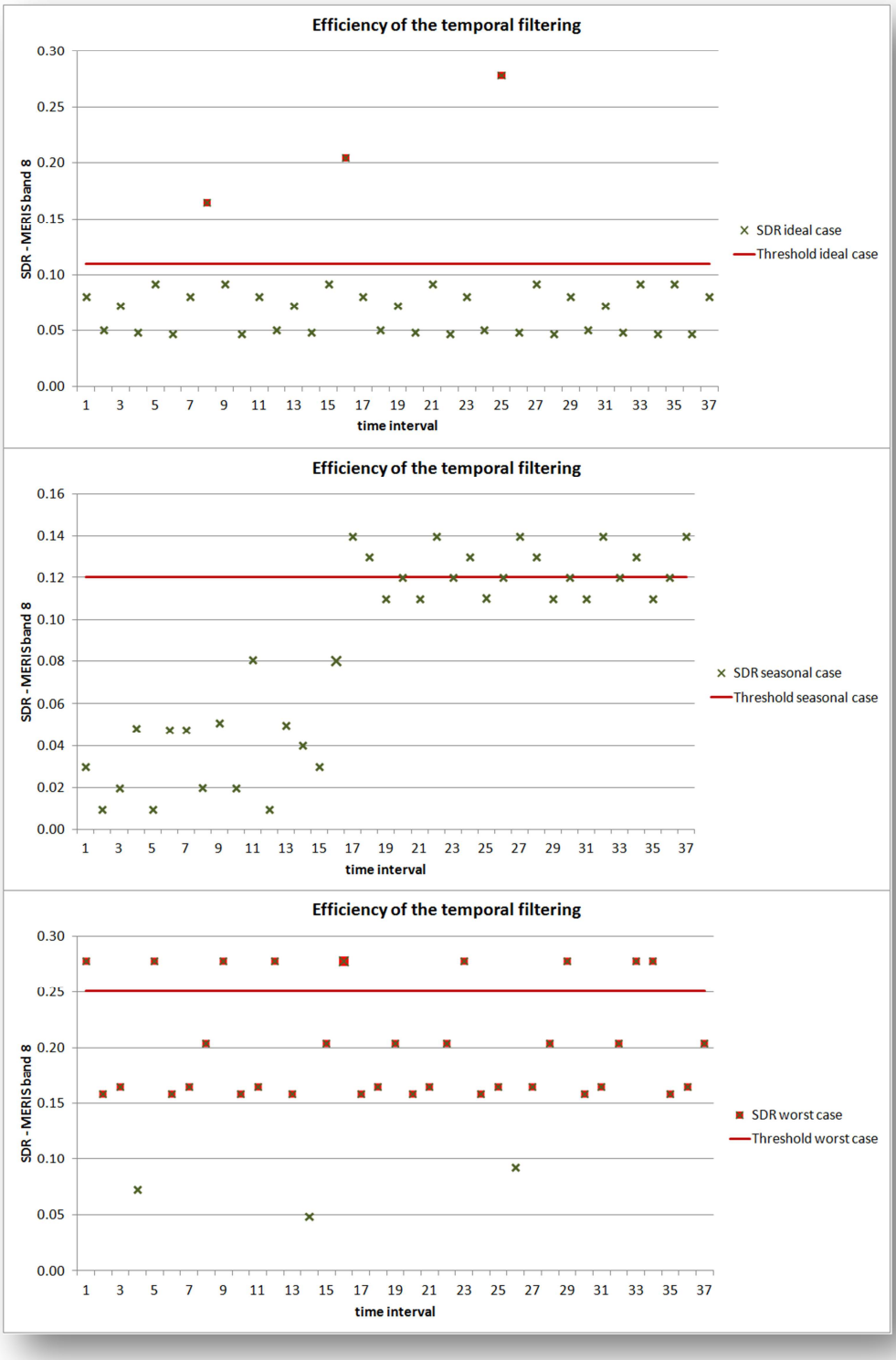


Figure 4-20: Efficiency of temporal filtering depends on the quality of the classification by IdePix and seasonal variability of the surface

© UCL-Geomatics 2016
This document is the property of the LAND_COVER_CCI partnership, no part of it shall be reproduced or transmitted without the express prior written authorization of UCL-Geomatics (Belgium).

4.6.5 BRDF - Correction - averaging of the surface directional reflectances

To produce sensor composited images corrected for angular effects (so called L3A), the base line is to start from the atmospherically corrected daily images and through an appropriate compositing technique, at the same time actually produce composited images at various time steps, and correct the reflectances for sun and view directions. The temporal frequency of these composites is variable according to various needs. The classification module needs "fundamental" composites which could be averaged over dedicated periods according to each equal reasoning area.

Three methods were implemented, tested and intercompared during the GlobCover project: the BISE method [Viovy et al., 1992], the Mean Compositing algorithm [Vancutsem et al., 2004] and an algorithm developed by [Hagolle et al. 2004]. These methods and the results and conclusions of the analysis (which are still applicable), are summarized below in the section. In addition, during the Round Robin phase of the CCI-LC project phase I, a fourth method [Vermote et al., 2009] has been tested and this method is presented in the section 4.6.5.1.4 and its performance is pointed out in the Product Validation and Algorithm Selection Report of the CCI-LC project [Ph1_PVASRv2.0, 2012].

The simple averaging is applied for the current LC-CCI pre-processing. In parallel we will continue with the investigation but also with regard to other sensors. If we decide reprocessing the input data, we will include any knowledge gained meanwhile. A main point for the decision regarding to repeating the pre-processing is the ensuring of the consistency of its chain and products for all used sensors.

For example, the AVHRR sensor as an across-track scanning system has a field of view (FOV) of ~ ±55° with respect to the nadir direction. Therefore the different methods regarding the BRDF correction has to be assessed again. Due to the fact that the 7-day TOA cloud-free composite is the deliverable of phase II year 1 no dedicated BRDF correction has to be applied.

4.6.5.1 *GlobCover experience*

4.6.5.1.1 Method 1: BISE algorithm

A widely used technique is that of the Best Index Slope Extraction (BISE) [Viovy et al., 1992]. It has been used for the generation of LASUR (LAnd SUrface Reflectance) data set [Berthelot et al., 1997] that includes top of atmosphere and « surface » (atmospherically corrected) reflectances, temperatures and NDVI, viewing and sun angles, plus a channel (flag channel) at 1/7° x 1/7° and 1° x 1° spatial resolution. The BISE algorithm is therefore well suited for residual noise removal on NDVI temporal series. But the need here is to produce noise free reflectance time series, in addition to NDVI time series. The noise associated with reflectance time series has therefore to be carefully assessed with this method.

From the first date of the NDVI time series, for a given pixel, the BISE algorithm searches forward and considers the succeeding point if it is of higher value than the preceding point. When the NDVI value decreases from one day to the next, this decrease is accepted only if there is no point ahead in a pre-defined period of time (called a sliding period, typically 30 days) with a value greater than a percentage threshold of the difference between the two days in consideration. If such a high value is encountered it is selected and the low point is ignored. The original threshold (20%) has been empirically determined for West African conditions.

© UCL-Geomatics 2016
This document is the property of the LAND_COVER_CCI partnership, no part of it shall be reproduced or transmitted without the express prior written authorization of UCL-Geomatics (Belgium).

The drawback of such method lies in the fact that the first point of the series can be kept even if it is cloudy. We have therefore used a slightly modified version allowing reducing the errors generated at the beginning of the cycle. In this version (Figure 4-21), the date of the maximum NDVI value is firstly searched. From this date, the temporal profile is divided in two parts: one corresponding to the growing vegetation phase and another corresponding to the senescence phase.

For each part, BISE scans the points searching if the previous point is greater than the current point. To do that, the slope between two successive points is processed. If this slope is lower than a predefined percentage (20%) then the points are kept. Moreover, some irregularities may still be present (considered as errors) in the shape of the NDVI profile. To detect at best these errors, it is supposed than in each sliding window, the difference between two kept points do not exceed a threshold following the relationship ([NDVI (t) – NDVI (t+ti)]/NDVI (t) < 0.15). Following the Figure 4-21, the low NDVI value (shown by the red triangle) is not kept. Therefore, the smaller the sliding window is the larger the number of kept points is.

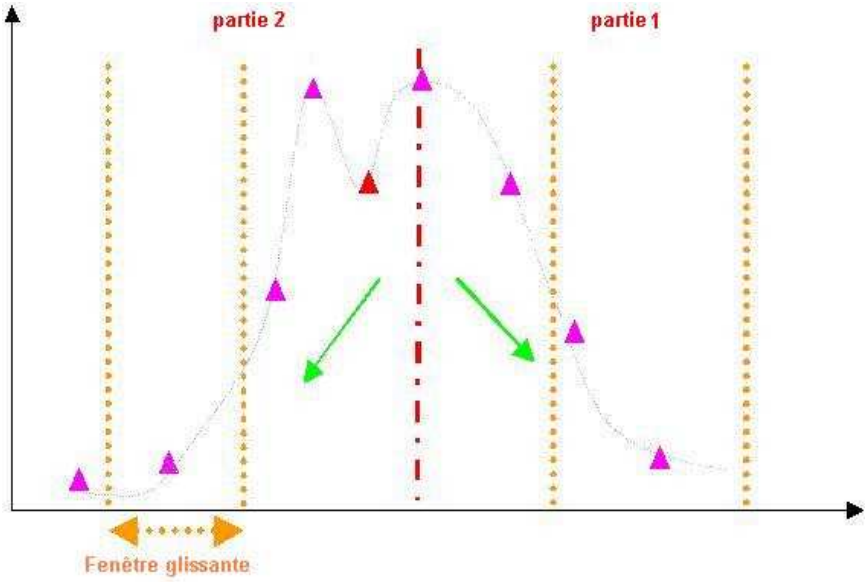


Figure 4-21: Scheme for the BISE method. The triangles represent points of a standard profile. The profile is divided in two parts from the point where NDVI is maximal. In each part (part 1 and part 2), successive iterations on the NDVI points start from the highest point of the profile (green arrows). The time period of the sliding window is draw in vertical dashed points (figure taken from [GlobCover_DJFv3.8, 2008])

4.6.5.1.2 Method 2: Vancutsem algorithm

Another way to avoid the inconsistencies due to geometric and atmospheric variations while being flexible enough is to use a statistical approach. We propose to consider here the Mean Compositing (MC) method [Vancutsem et al., 2004]. The methodology (Figure 4-22) consists of averaging for each pixel and in each spectral band all the valid reflectance values acquired during the chosen compositing period. Vegetation indices are computed on the basis of these reflectance averages.

© UCL-Geomatics 2016
This document is the property of the LAND_COVER_CCI partnership, no part of it shall be reproduced or transmitted without the express prior written authorization of UCL-Geomatics (Belgium).

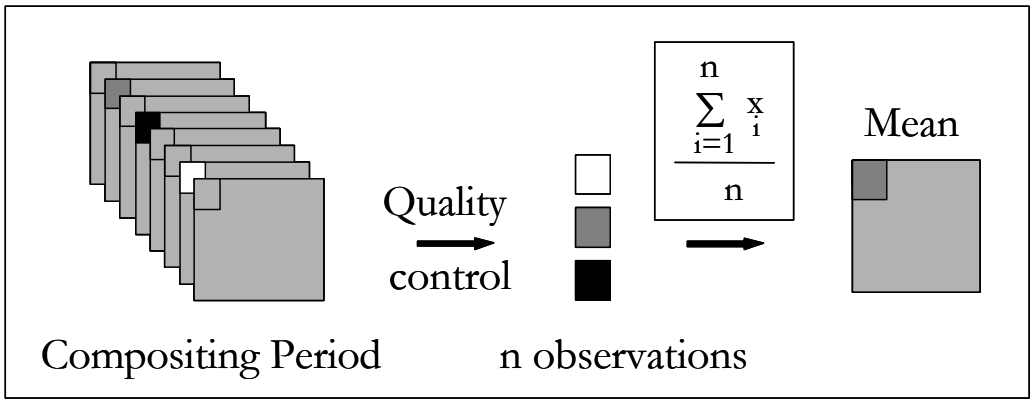


Figure 4-22: Quality control of all reflectance values and mean estimation for each band (figure taken from [GlobCover_DJFv3.8, 2008])

This compositing strategy requires two conditions to be applicable. First, the daily images have to be superimposed with an accuracy corresponding to the sub-pixel level, which is the case for the SPOT-VGT images and which will be the case for MERIS images after the geometric corrections. Second, in case of a cyclic variation of the viewing zenith angle, the compositing period must be a multiple of this cycle. In this way, the different compositing periods will have a similar distribution of the viewing angle.

The first step of the work consists in determining the sub-cycle of the viewing angle which a factor independent from the pixel location. It has been determined plotting a temporal profile of MERIS RR L2 reflectances for two sites extracted from the BELMANIP database (see Figure 4-23). A sub-cycle of around 17 days has been found leading to a temporal period synthesis of around 34 days or 51 days.

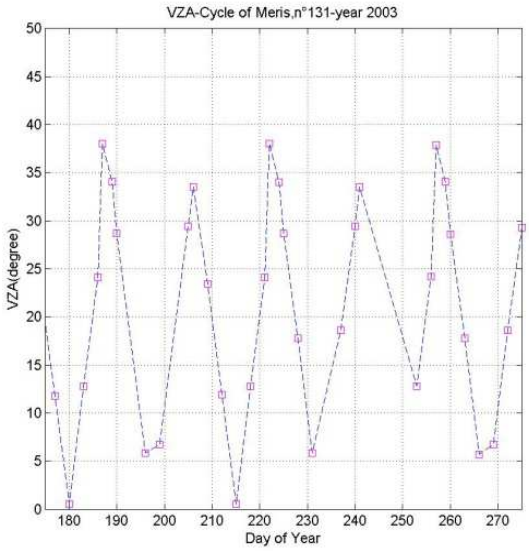


Figure 4-23: Subcycle of the viewing zenith angle (figure taken from [GlobCover_DJFv3.8, 2008])

© UCL-Geomatics 2016
This document is the property of the LAND_COVER_CCI partnership, no part of it shall be reproduced or transmitted without the express prior written authorization of UCL-Geomatics (Belgium).

4.6.5.1.3 Method 3: Hagolle algorithm

The Hagolle algorithm (CYC) is based on an improvement of the method called BDC ([Duchemin and Maisongrande, 2002], [Duchemin et al., 2002]) has been tested and applied so far on SPOT-VGT data.

Its principle is to fit a linear bidirectional reflectance model on the atmospherically corrected reflectance data over a temporal window, then use the model to retrieve a reflectance corrected for sun and view effects (see Figure 4-24). The BRDF model used is that proposed in [Roujean et al., 1992]. It encompasses three unknown coefficients, $k_{i=0,1,2}$, weighting the Lambertian (or isotropic) component, a geometric kernel, and a volume-scattering kernel. The inversion of the BRDF model is operated on a pixel-per-pixel basis for each of the spectral bands of the sensor, provided that at least 3 cloud-free scenes are available within the temporal window. The three unknown coefficients $k_{i=0,1,2}$ are retrieved by minimizing the cost function C defined by:

$$C = \left(\sum_{i=1}^{N} \frac{(\rho_i - \hat{\rho}_i)^2}{\sigma_i^2} \right) + \frac{\left(k_1 - C1(\lambda)\right)^2}{\sigma_{k1}^2} + \frac{\left(k_2 - C2(\lambda)\right)^2}{\sigma_{k2}^2}$$

eq. 4-71

In that equation, $C1(\lambda)$ and $C2(\lambda)$ are constants for a given spectral band. They do not depend on the pixel not on the date. They have been determined by prior experiments from the inversion of the model for various types of landscapes, which has provided averaged k_1 and k_2 values. $C1(\lambda)$ and $C2(\lambda)$ have then been assigned to these averaged k_1 and k_2 values. N is the number of observations available in the temporal window, ρ_i are the measured reflectance data, and $\hat{\rho}_i$ are modelled reflectances. $1/\sigma_i^2$ are the weights of the observations and $1/\sigma_{k1}^2$and $1/\sigma_{k2}^2$ are the weights of the constraints, they have been determined by previous work [Geiger et al., 2003].

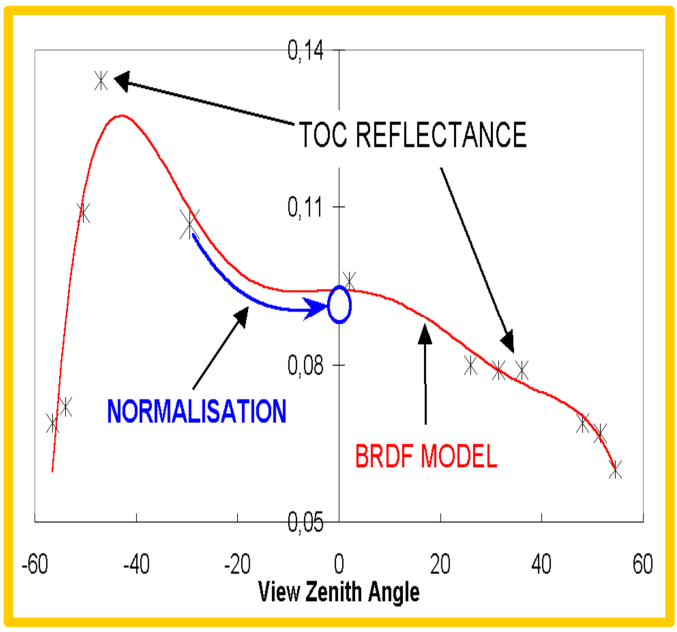


Figure 4-24: Scheme of the angular effects normalization procedure (figure taken from [GlobCover_DJFv3.8, 2008])

© UCL-Geomatics 2016
This document is the property of the LAND_COVER_CCI partnership, no part of it shall be reproduced or transmitted without the express prior written authorization of UCL-Geomatics (Belgium).

The use of $C1(\lambda)$ and $C2(\lambda)$ in the cost function brings some a priori information in the system, which constrains and influences the result (Figure 4-25). This makes easier to detect and discard residual cloud contaminated pixels. The detection is operated using the blue band because it enables the best distinction between clouds and continental surfaces. If the standard deviation of errors σ of the model fit is above a threshold, our algorithm discards all the observations that are greater that the adjusted model values plus σ. At this stage, many previously undetected cloudy pixels are discarded. Then a second fit and a new σ value is computed (smaller than the previous one); all the pixels with a difference to the fitted model greater than $1.5 \cdot \sigma$ are discarded whatever the sign of the difference is. This last step is iterated until no pixels are discarded anymore, or until the number of remaining pixels is lower than 3

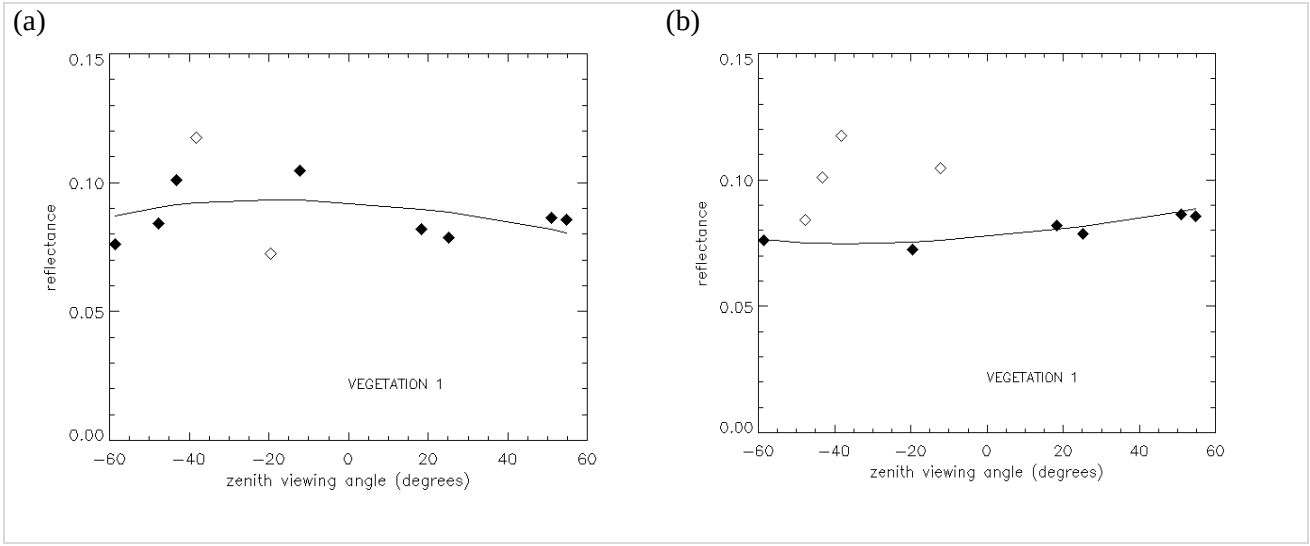


Figure 4-25: BRDF model fit for VEGETATION data with (a) no a priori information and (b) a priori information. Unfilled diamonds are discarded pixels, only filled diamonds are used for the BDRF estimate (from [GlobCover_DJFv3.8, 2008])

The 3 coefficients $k_{i=0,1,2}$ are used to normalize the cloudless reflectance dataset entering the 10-day period to nadir view and solar observation observed at 10h00 local time for the median day of the compositing period. Besides, the method supplies for each composite product the following information for each pixel and each spectral band: the normalized reflectance, the number of observations used to assess the BRDF and a quality flag including information about the processed pixel. This algorithm has been tested and evaluated with a method described at the end of this Section. It is really efficient when there are a sufficient number of valid observations during the temporal compositing period (Figure 4-26). As for the Vancutsem et al. algorithm, the fact that MERIS data are about three times less frequent than SPOT-VGT data may induce some limitations of the method.

© UCL-Geomatics 2016
This document is the property of the LAND_COVER_CCI partnership, no part of it shall be reproduced or transmitted without the express prior written authorization of UCL-Geomatics (Belgium).

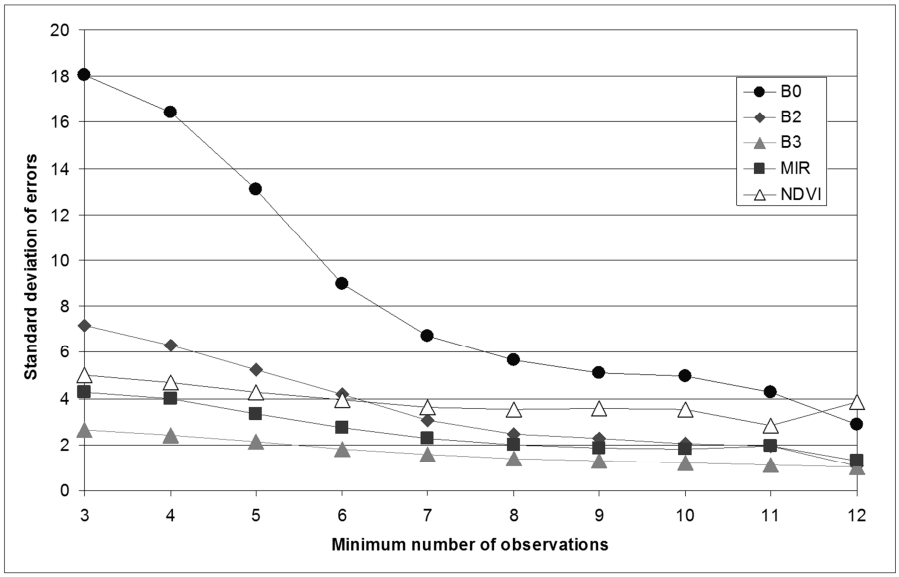


Figure 4-26 : Standard deviation of the errors calculated as a function of the minimum number of observations used in the BRDF model inversion (from [GlobCover_DJFv3.8, 2008])

4.6.5.1.4 GlobCover analyses and decisions for the BRDF correction

The work of the GlobCover project has addressed the problem of estimating the performance of global reflectance composited products of land surfaces. Two criteria were used to perform such estimations: a qualitative criterion relying on temporal MERIS RR profile over pixels extracted from BELMANIP sites. A quantitative criterion providing a way to estimate the standard deviation of the noise added to time series of reflectance data [GlobCover_DJFv3.8, 2008].

The qualitative criteria have allowed observing that all the methods were able to reproduce the temporal trends of the temporal vegetation evolution. They presented rather similar behaviours. Using the quantitative criterion, two situations may be distinguished. When the number of input data is relatively sufficient (favourable cases), the performances of BISE, MC, CYC are rather similar. When this number of data is low (unfavourable conditions but a regular case for MERIS), the BISE method is not so efficient as MC or CYC. The MC method restores a mean of the values observed during the temporal period of acquisition. The values derived from BISE are directly linked to the chosen sliding window. The selection of this sliding window is a function of the phenological stage of the vegetation. Therefore, this method requires having complementary information on this phenology. To have better results with BISE, a geographical mapping of this parameter should be applied. This dependence makes this method non generic at the global scale. A further investigation was done to assess the performance of MC and CYC. Both methods have very similar results but with always a slight advantage for MC.

The GlobCover project finally selected the MC algorithm as BRDF correction and compositing method. However, a slight modification was adopted, which consisted in coupling the MC method with the filtering module of the CYC algorithm. The MC method was first applied on the observations present in a 51-day compositing period (defined as a good trade off between a small temporal period suitable for monitoring the temporal evolution of the vegetation and a large period to be able to produce composites). Then, the filtering module of the CYC method was performed to remove

© UCL-Geomatics 2016
This document is the property of the LAND_COVER_CCI partnership, no part of it shall be reproduced or transmitted without the express prior written authorization of UCL-Geomatics (Belgium).

outliers. This method was applied on the 51 days period to flag "valid" observations which were used to perform composites over reduced time period (15-day composites in GlobCover).

4.6.5.2 *Method 4: improved BRDF inversion developed by Vermote et al. 2009 [Vermote et al., 2009]*

The fourth method for the estimation and the correction of directional effects on satellite derived surface reflectance time series based on the BRDF inversion technique is used for the MODIS BRDF/albedo product ([Vermote et al., 2009], [Strahler et al., 1999], [Bréon et al., 2002], [Maignan et al., 2004] and [Snyder and Wan, 1998]) with the objective of minimisation the differences between the observed and modelled directional reflectances over a given time period. The fundamental BRDF model, the Ross-Li-Maignan model, computes the surface reflectances as the sum of three terms, which describe the isotropic, volumetric and geometric parts:

$$\rho(\theta_s,\theta_v,\phi) = k_0 + k_1F_1(\theta_s,\theta_v,\phi) + k_2F_2(\theta_s,\theta_v,\phi) = k_0\left[1 + \frac{k_1}{k_0}F_1(\theta_s,\theta_v,\phi) + \frac{k_2}{k_0}F_2(\theta_s,\theta_v,\phi)\right]$$
$$= k_0[1 + VF_1(\theta_s,\theta_v,\phi) + RF_2(\theta_s,\theta_v,\phi)]\ where\ V = \frac{k_1}{k_0}\ and\ R = \frac{k_2}{k_0}$$

eq. 4-72

where θ_s, θ_v, ϕ are the solar zenith, view zenith and the relative azimuth angles, F_i are the kernel and the k_i are the free weighting parameter. The kernel F_1 as the volumetric scattering kernel accounting for the hot spot and F_2 as the geometric scattering kernel, are function of the observation geometry and given by:

$$F_1(\theta_s,\theta_v,\phi) = \frac{4}{3\pi}\frac{1}{\cos\theta_s + \cos\theta_v}\left[\left(\frac{\pi}{2} - \xi\right)\cos\xi + \sin\xi\right]\left[1 + \frac{1}{1+\frac{\xi}{\xi_0}}\right] - \frac{1}{3}$$

$$F_2(\theta_s,\theta_v,\phi) = \frac{m}{t}(t - \sin t\cos t\ - \pi) + \frac{1+\cos\xi}{2\cos\theta_s\cos\theta_v}$$

$$m = \frac{1}{\cos\theta_s} + \frac{1}{\cos\theta_v}$$

$$\xi = \cos^{-1}(\cos\theta_s\cos\theta_v + \sin\theta_s\sin\theta_v\cos\phi)$$

$$\xi_0 = \frac{LD}{H}\frac{(\cos\theta_s + \cos\theta_v)^2}{4\cos\theta_s\cos\theta_v} \approx \frac{LD}{H}$$

$$\Delta(\theta_s,\theta_v,\phi) = \sqrt{tan^2\theta_s\ + tan^2\theta_{sv} - 2\tan\theta_s\tan\theta_v\cos\phi}$$

$$\cos t = \frac{2}{m}\sqrt{\Delta^2 + (\tan\theta_s\tan\theta_v\cos\phi)^2}$$

eq. 4-73

where ξ is the scattering angle, ξ_0 is a characteristic angle that can be related to the ratio of scattering element size and the canopy vertical density, H is the canopy depth, L is the leaf area index and D

© UCL-Geomatics 2016
This document is the property of the LAND_COVER_CCI partnership, no part of it shall be reproduced or transmitted without the express prior written authorization of UCL-Geomatics (Belgium).

define the typical scale of the leaves. To avoid the addition of a free parameter, Maignan et al [Maignan et al., 2004] suggest taking a constant value of $\xi_0 = 1.5°$.

The alternative BRDF inversion technique assumes no temporal variation of shape of the BRDF, but allows the change of target reflectances during the compositing period in the contrast to the MODIS standard algorithm. Based on this hypothesis and on a set of N observations the parameter V and R are retrieved by minimizing the merit function M on the classical way of computation of the first derivation of the merit function, which is defined by:

$$\frac{\partial M}{\partial V} = \frac{\partial M}{\partial R} = 0$$

$$M = \sum_{i=1}^{N-1} \frac{\left(\rho_{i+1}\left[1 + VF_1^i + RF_2^i\right] - \rho_i\left[1 + VF_1^{i+1} + RF_2^{i+2}\right]\right)^2}{day^{i+1} - day^i + 1}$$

$$\begin{pmatrix} \sum_{i=1}^{N-1} \Delta^i\rho F_1 \Delta^i\rho F_1 & \sum_{i=1}^{N-1} \Delta^i\rho F_1 \Delta^i\rho F_1 \\ \sum_{i=1}^{N-1} \Delta^i\rho F_1 \Delta^i\rho F_1 & \sum_{i=1}^{N-1} \Delta^i\rho F_1 \Delta^i\rho F_1 \end{pmatrix} \begin{pmatrix} V \\ R \end{pmatrix} = \begin{pmatrix} \sum_{i=1}^{N-1} \Delta^i\rho F_1 \Delta^i\rho F_1 \\ \sum_{i=1}^{N-1} \Delta^i\rho F_1 \Delta^i\rho F_1 \end{pmatrix}$$

where

$$\Delta^i d = day^{i+1} - day^i + 1$$

$$\Delta^i \rho = \frac{\rho_{i+1} - \rho_i}{\sqrt{\Delta^i d}}$$

$$\Delta^i \rho F_1 = \frac{\rho_{i+1} F_1^i - \rho_i F_1^{i+1}}{\sqrt{\Delta^i d}}$$

$$\Delta^i \rho F_2 = \frac{\rho_{i+1} F_2^i - \rho_i F_2^{i+1}}{\sqrt{\Delta^i d}}$$

eq. 4-74

A further refinement accounting for a change of the BRDF shape with the vegetation cover based on the clustering of the data with respect to the NDVI. For each of these classes the parameter R and V were retrieved and the relationship to the NDVI can be derived by a linear fit among the different classes.

Therefore, the full BRDF correction process includes the following steps

- first guess estimate of V and R by inverting the model using the method described before
- correction of the reflectances with these estimates of V and R
- computation of the NDVI
- clustering based on the NDVI

© UCL-Geomatics 2016
This document is the property of the LAND_COVER_CCI partnership, no part of it shall be reproduced or transmitted without the express prior written authorization of UCL-Geomatics (Belgium).

- inversion of the model for each class to get V and R
- linear fit between NDVI and the parameter V and R
- final BRDF-correction

The method doesn't assume an invariance of the surface during the compositing period and allows the monitoring of the vegetation with a period smaller than the compositing method. Therefore the correction can be performed with the same frequency as the observation. The used parameter V and R can be derived from previous observations, which avoids the limitation by data availability.

The important step of the work consists in the verification of the proposed algorithm for the CCI-LC project and its requirements by a study based on synthetic data. Because the approach was evaluated on a global MODIS data set at a 0.05° resolution for two channels and the NDVI. Therefore the widely used PROSPECT/SAIL model has been implemented and different BRDF could be retrieved [Jacquemoud et al., 2009]. The following Figure 4-27 shows an example of the retrieved BRDF.

Based on these modelled BRDF's the retrieval of the parameter V and R has been investigated for MERIS. The typical observation und illumination geometry is derived from the MERIS Round Robin database of the CCI_LC project phase I. It has been determined plotting a temporal profile of MERIS FSG L1 viewing and sun angles for six sites (see Figure 4-28 and Figure 4-29). A sub cycle of viewing zenith angle of around 17 days has been found.

The BRDF correction scheme developed by Vermote et al [Vermote et al., 2009] has been prototyped and compared with simple averaging (GlobCover method). The assessment on simulated and measured ground data, and on MERIS data has shown:

- Synthetic and measured BRDF measurements are generally well retrieved (under realistic MERIS observation geometry during a yearly cycle, and assumption of 365 observations);
- When applied to MERIS, results are not (yet) satisfactory;
- Disturbance by residual clouds may become of lesser importance if improvements are brought to the cloud detection step;
- The performance is impacted by the low number of observations characteristic of the MERIS sensor (less than 365 per year).

© UCL-Geomatics 2016
This document is the property of the LAND_COVER_CCI partnership, no part of it shall be reproduced or transmitted without the express prior written authorization of UCL-Geomatics (Belgium).

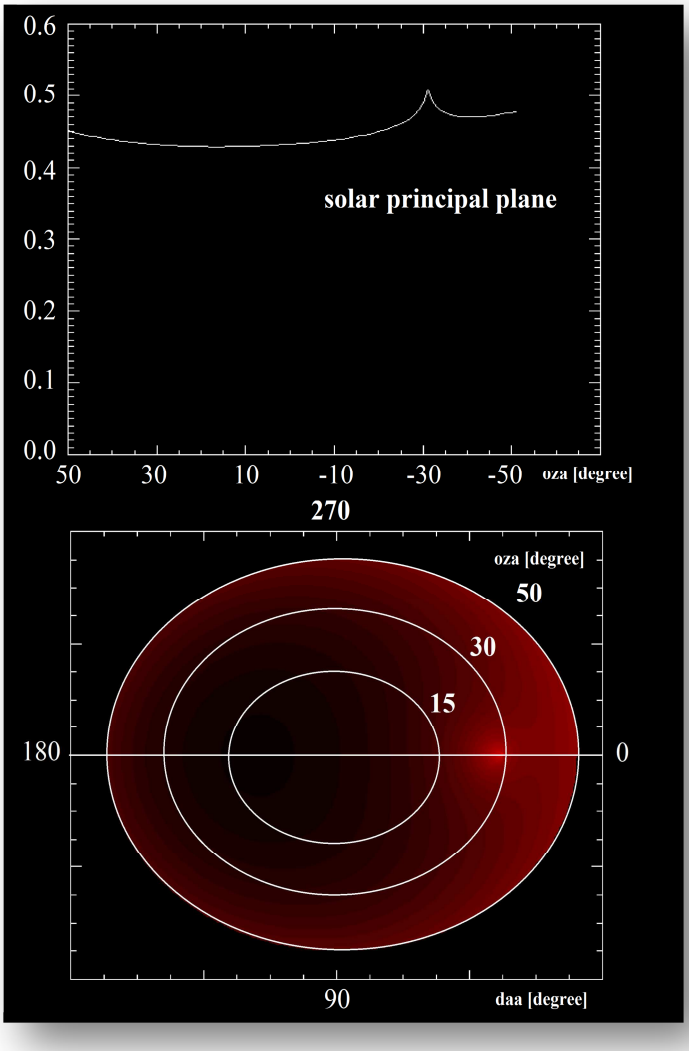


Figure 4-27: Example of modelled BRDF using PROSPECT/SAIL model (parameter: Cab = 30.0 (chlorophyll content [µg cm-2]); Car = 10.0 (carotenoid content [µg cm-2]); Cbrown = 0.0 (brown pigment content [arbitrary units]; Cw = 0.015 (equivalent water thickness EWT [cm]); Cm = 0.009 (leaf mass per area LMA [g.cm-2]); N = 1.5 (structure coefficient); LAI = 4 (leaf area index); angl = 50.0 (average leaf angle [degree]); psoil = 1(soil coefficient); skyl = 70 (% diffuse/direct radiation); hspot = 0.05 (hot spot - leaf size relative to canopy height)); ihot = 1.0 (hot spot flag); tts = 30.0 (solar zenith angle [degree])). daa: difference azimuth angle [degree]; oza: observer zenith angle [degree]

© UCL-Geomatics 2016
This document is the property of the LAND_COVER_CCI partnership, no part of it shall be reproduced or transmitted without the express prior written authorization of UCL-Geomatics (Belgium).

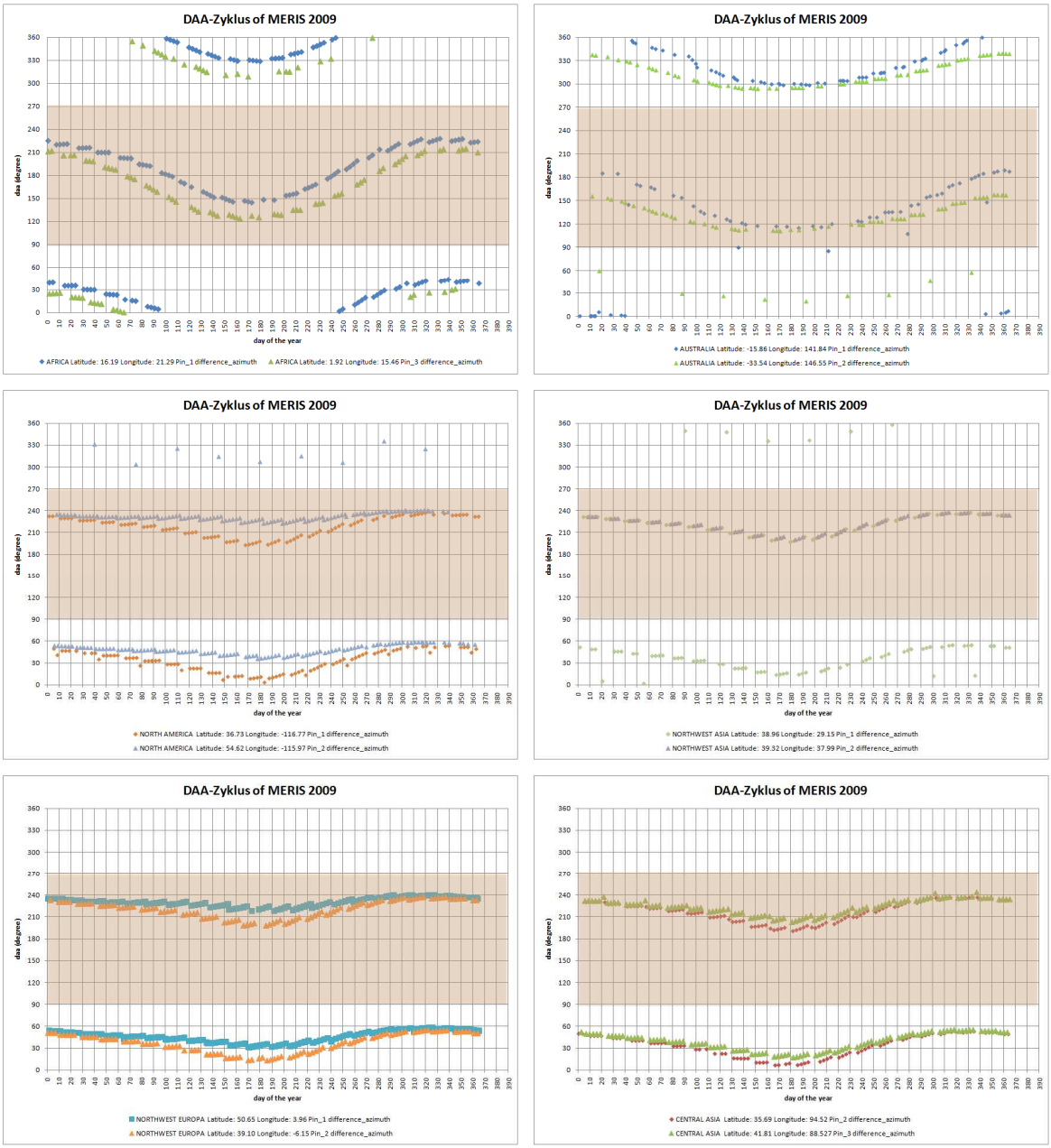


Figure 4-28: Sub cycle of the difference azimuth angle

© UCL-Geomatics 2016
This document is the property of the LAND_COVER_CCI partnership, no part of it shall be reproduced or transmitted without the express prior written authorization of UCL-Geomatics (Belgium).

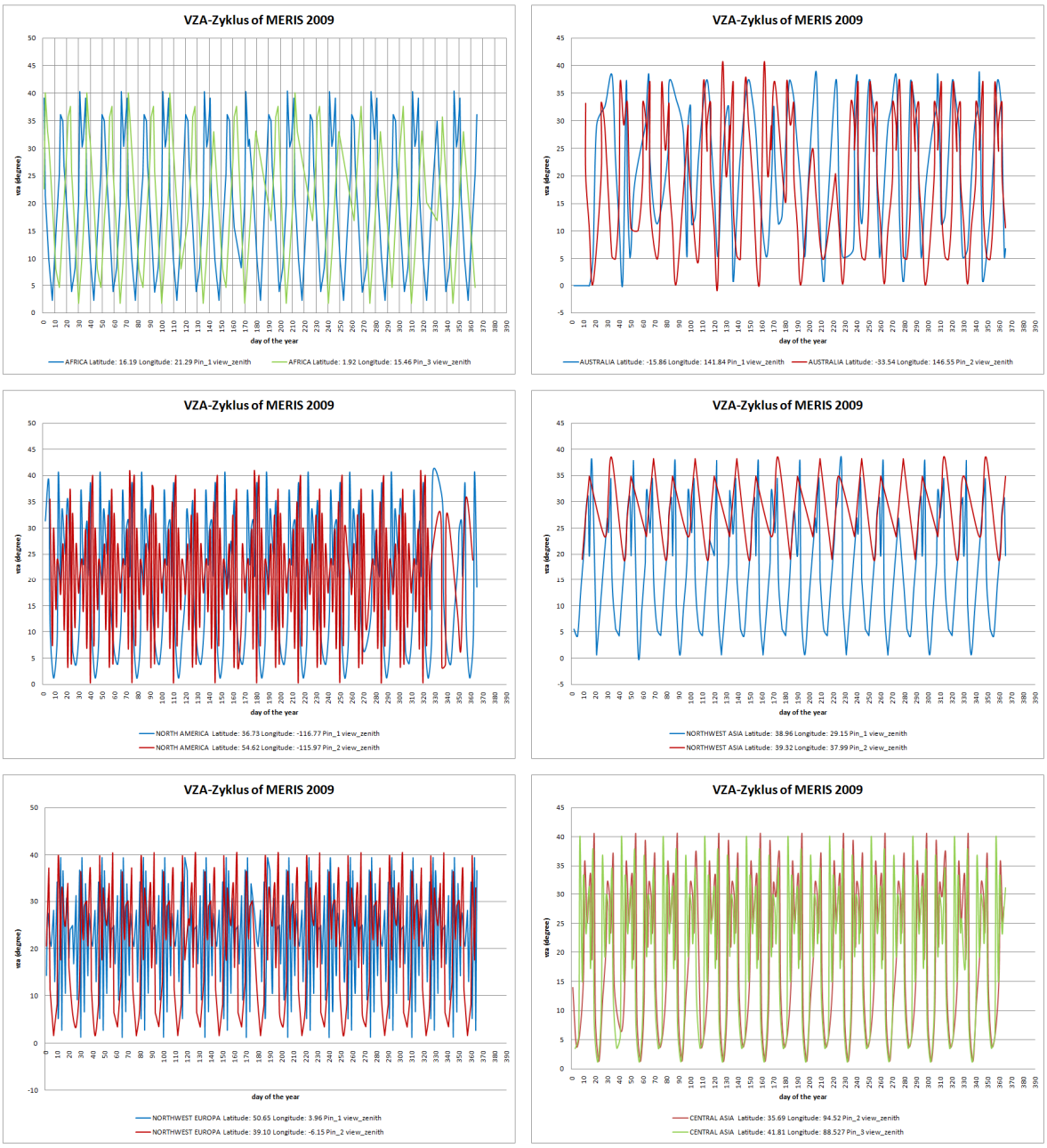


Figure 4-29: Sub cycle of the viewing zenith angle

© UCL-Geomatics 2016
This document is the property of the LAND_COVER_CCI partnership, no part of it shall be reproduced or transmitted without the express prior written authorization of UCL-Geomatics (Belgium).

4.6.6 Generation of mosaics

As final step, all grid cells (tiles) which were part of one or more input products for the aggregation and which were processed as described above are merged into a single Level 3 result product. Usually, this product shall be a global mosaic. The Table 4-30 summarizes the bands, which will be included in the final L3 pre-processing products for MERIS, SPOT VGT P and AVHRR [Ph1_DPMv2.2, 2013].

Table 4-30: Variables used in Level 3 mosaicing for MERIS, SPOT VGT P and AVHRR

PARAMETER	DESCRIPTION
SR of band x_{sensor}; x_{MERIS} = 1 ... 10,12 ... 14 $x_{SPOT\ VGT\ P}$ = B0, B2, B3 and MIR $x_{SPOT\ AVHRR}$ 2 = B1, B2, B3b, B4, and B5	surface reflectance of band x_{sensor}; x_{MERIS} = 1 ... 10,12 ... 14 $x_{SPOT\ VGT\ P}$ = B0, B2, B3 and MIR $x_{SPOT\ AVHRR}$ 2 = B1, B2, B3b, B4, and B5
ε_{SR} of band x_{sensor}; x_{MERIS} = 1 ... 10,12 ... 14 $x_{SPOT\ VGT\ P}$ = B0, B2, B3 and MIR $x_{SPOT\ AVHRR}$ 2 = B1, B2, B3b, B4, and B5	uncertainties of the surface reflectance of band x_{sensor}; x_{MERIS} = 1 ... 10,12 ... 14 $x_{SPOT\ VGT\ P}$ = B0, B2, B3 and MIR $x_{SPOT\ AVHRR}$ 2 = B1, B2, B3b, B4, and B5
Ndvi	NDVI
Status	current pixel status classified by IdePix, clear land filter and temporal filter
Status_counts of status y; y=land, snow/ice, water, cloud, etc.	number of observation over pixel covered by clear land clear snow/ice clear water cloud cloud shadow

Finally, it is worth noting that since the BRDF correction is linked with the compositing process, the pre-processing module does not deliver daily products but global surface reflectance “fundamental” composites 7-day composite (i.e. generated over a “fundamental” period). The 7-day compositing period is adapted on a fixed basis. So every January 1st as starting point and a continuous 7 day intervals for each year has been proposed. The last composite of each year and the last February composite of a leap year include 8 days instead 7days.

These “fundamental” composites has been served as input to the classification module, and thus for the generation of longer (seasonal and annual) composites. This articulation is illustrated in Figure 4-30.

© UCL-Geomatics 2016
This document is the property of the LAND_COVER_CCI partnership, no part of it shall be reproduced or transmitted without the express prior written authorization of UCL-Geomatics (Belgium).

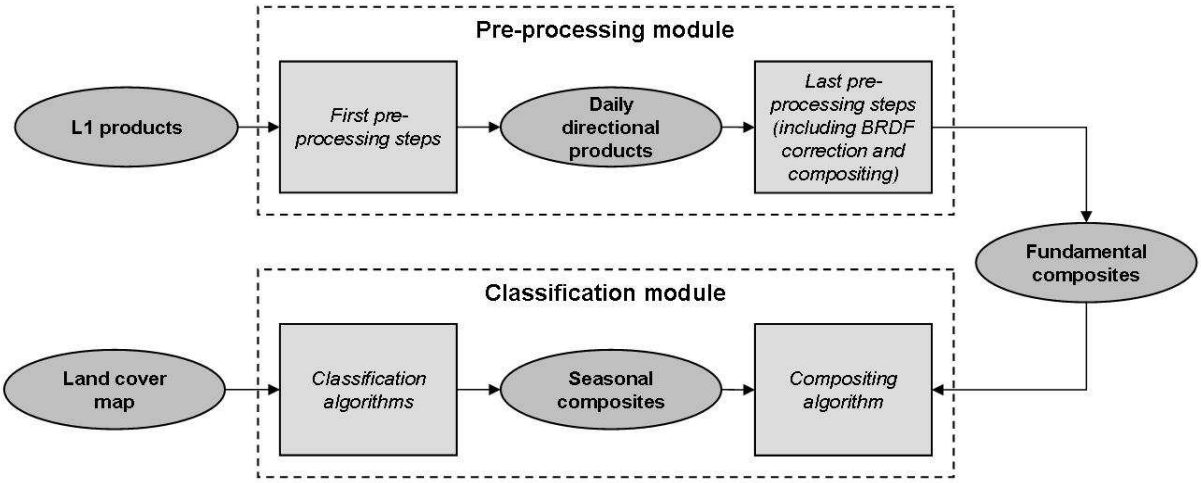


Figure 4-30: Articulation between the fundamental composites delivered by the pre-processing module and the seasonal composites used in the classification algorithms

4.6.7 Pseudo-code representation

This subsection provides an overview of the L3 processing from the software development point of view. A more detailed description of the logical flow and individual processing steps can be found in the CCI Land Cover DPM [Ph1_DPMv2.2, 2013]. Furthermore the input and output products being used within the LC-CCI processing modules are described in the CCI Land Cover IODD [Ph1_IODDv1.0, 2013] in more detail.

```
algorithm DGL is
    input: Pixel position (x, y) on product grid
           Longitude and latitude coordinates (λi, φi) on tie point grid
    output: Longitude and latitude coordinates (λ, φ) corresponding to (x, y)
    return (λ, φ)
```

Algorithm 4-32: Direct geo-location (DGL)

```
algorithm IGL is
    input: Longitude and latitude coordinates (λ, φ)
           Pixel position accuracy goals σl and σm
    output: Pixel position (x, y) corresponding to input coordinates
    return (x, y)
```

Algorithm 4-33: Inverse geo-location (IGL)

© UCL-Geomatics 2016
This document is the property of the LAND_COVER_CCI partnership, no part of it shall be reproduced or transmitted without the express prior written authorization of UCL-Geomatics (Belgium).

```
algorithm PLATE_CARREE is
    input: Raster of pixels in source grid, I
    output: Raster of pixels on Plate-Carrée grid, I'
    return I'
```

Algorithm 4-34: Plate Carrée projection

```
algorithm clear_land_filtering is
    input:  per pixel, the MERIS SDR for band 14, 7, 3, representing R, G, B values
            probability density from LUT for 'cloud' pixels, p_cloud
            probability density from LUT for 'land' pixels, p_land
            probability density from LUT for 'town' pixels, p_town
    output: status_final., the final pixel classification status (either LAND or CLOUD)
    return status_final
```

Algorithm 4-35: Clear land filtering

```
algorithm SAMPLE_AGGREGATION_SDR8 is
    input: Aggregation grid cell AGC with input properties; here:
                1) SDR for each observation OBS in MERIS band 8 (681nm)
                   in each pixel q_i, SDR(b=681, q_i, OBS)
                2) SDR error for each observation OBS in MERIS band 8 in
                   each pixel q_i, ΔSDR(b=681, q_i, OBS)
                3) status of q_i for each observation OBS as obtained from
                   pixel classification, status(q_i, OBS)
           Number of pixels (samples) in this AGC for aggregation, N_pixels
           Number of observations of this AGC, N_obs
    output: status flag for each observation and each pixel q_i in given AGC,
            array STAT
    return STAT
```

Algorithm 4-36: Temporal filtering (e.g. Level 3 sample aggregation for MERIS band 8)

© UCL-Geomatics 2016
This document is the property of the LAND_COVER_CCI partnership, no part of it shall be reproduced or transmitted without the express prior written authorization of UCL-Geomatics (Belgium).

algorithm SAMPLE_AGGREGATION **is**

input: Aggregation grid cell AGC with input properties; here:

1) SDR for each observation OBS in band b in each pixel q_i, $SDR(b,q_i,OBS)$
2) SDR error for each observation OBS in band b in each pixel q_i, $\Delta SDR(b,q_i,OBS)$
3) NDVI for each observation OBS in each pixel q_i, $NDVI(q_i,OBS)$
4) status of q_i for each observation OBS as obtained from pixel classification, $status(q_i,OBS)$

Number of pixels (samples) in this AGC for aggregation, N_{pixels}

Number of observations of this AGC, N_{obs}

Threshold for cloud classification in MERIS 681nm band, CLOUD_THRESH_681

output: aggregation samples for given AGC, S_{agg}

return S_{agg}

Algorithm 4-37: Level 3 Sample Aggregation

algorithm PIXEL_STATUS_AGGREGATION **is**

input: Counts of given pixel q classified as LAND, $S_{agg}(j_{LAND},q)$

Counts of given pixel q classified as WATER, $S_{agg}(j_{WATER},q)$

Counts of given pixel q classified as SNOW, $S_{agg}(j_{SNOW},q)$

Counts of given pixel q classified as CLOUD, $S_{agg}(j_{CLOUD},q)$

Counts of given pixel q classified as CLOUD_SHADOW, $S_{agg}(j_{CLOUD_SHADOW},q)$

output: status of given pixel q after aggregation, $S_{agg}(0,q)$

return $S_{agg}(0,q)$

Algorithm 4-38: Retrieval of aggregated pixel classification

algorithm L3_MOSAIC **is**

input: list of all AGCs with aggregation sample results for all of its pixels, $L(S_{agg}(AGC_i,q_j))$

output: L3 mosaic product with all AGCs merged, MP

return MP

Algorithm 4-39: L3 generation of mosaics

© UCL-Geomatics 2016
This document is the property of the LAND_COVER_CCI partnership, no part of it shall be reproduced or transmitted without the express prior written authorization of UCL-Geomatics (Belgium).

5 VALIDATION OF ALGORITHMS

Validation is needed in order to assess the effectiveness and quality of the different algorithms. Several mathematical and other empirical methods of validation are available. However, the validation of an algorithm is fairly complex and the validation procedure proposed for the pre-processing algorithms is to run through an iterative process with following major points:

- Testing the algorithms on (real) remote sensing data for the use cases
- Comparison between independent in situ data and outputs created by the algorithms if possible

The validation plan [Ph1_PVPv1.3, 2011] provides the different factors influencing the requirements and the selection process for suitable validation methods should be examined.

Therefore in the following steps the influence of several disturbances as noise and clouds are analysed and the sensitivity due to the choice of thresholds is determined. The validation and optimisation of the algorithms will be an iterative process and consists of:

- Testing the algorithm with remote sensing data using case studies
- Validation of intermediate products with in-situ data if possible
- Analysing the dependency of thresholds used in the algorithms
- Quality measure
- Documentation
- At the end we get an overview about the individual thresholds and quality measure of pre-processing intermediate products.

The results of the validation of the pre-processing algorithm and products from CCI-LC project phase I are presented in the Product Validation and Intercomparison Report (PVIRv2.0, 2013) and in the Product Validation and Algorithm Selection Report (PVASRv2.0, 2013).

For the CCI-LC project Phase II the validation of the pre-processing products and the new developed pre-processing algorithms will be part of the phase II Product Validation and Intercomparison Report of Phase II PVIR.

© UCL-Geomatics 2016
This document is the property of the LAND_COVER_CCI partnership, no part of it shall be reproduced or transmitted without the express prior written authorization of UCL-Geomatics (Belgium).